



HAL
open science

Ocean- atmosphere variability over the Indo- Pacific basin

Jérôme Vialard

► **To cite this version:**

Jérôme Vialard. Ocean- atmosphere variability over the Indo- Pacific basin. Ocean, Atmosphere. Université Pierre et Marie Curie - Paris VI, 2009. tel-00755963

HAL Id: tel-00755963

<https://theses.hal.science/tel-00755963>

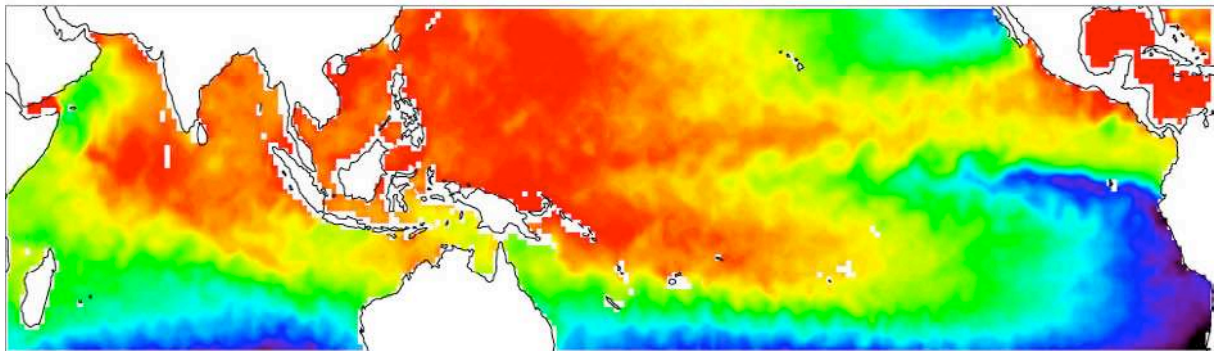
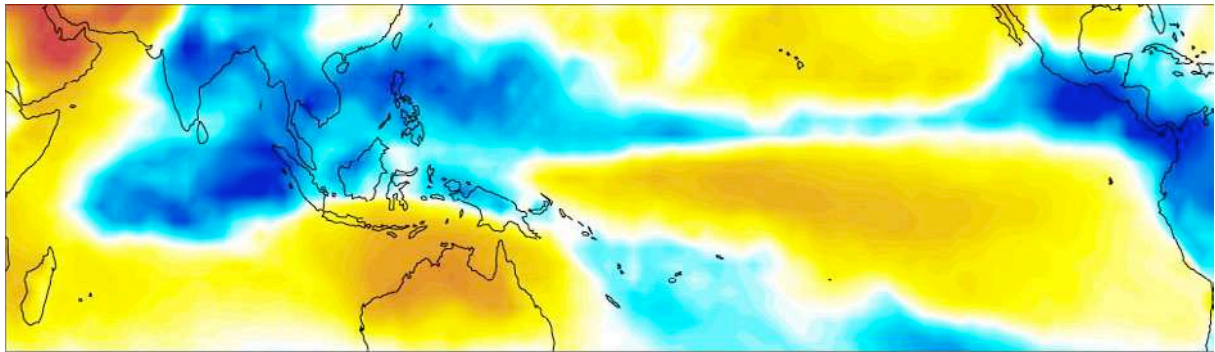
Submitted on 23 Nov 2012

HAL is a multi-disciplinary open access archive for the deposit and dissemination of scientific research documents, whether they are published or not. The documents may come from teaching and research institutions in France or abroad, or from public or private research centers.

L'archive ouverte pluridisciplinaire **HAL**, est destinée au dépôt et à la diffusion de documents scientifiques de niveau recherche, publiés ou non, émanant des établissements d'enseignement et de recherche français ou étrangers, des laboratoires publics ou privés.

Habilitation à diriger des Recherches
Université Pierre et Marie Curie

Ocean-atmosphere variability over the Indo-Pacific basin



Jérôme Vialard

Chargé de Recherche à l'Institut de Recherches pour le Développement

Laboratoire d'Océanographie et du Climat: Expérimentation et
Approches Numériques (LOCEAN)
UMR 7159 CNRS/IRD/UPMC/MNHN
Institut Pierre Simon Laplace (IPSL)

Soutenue le 26 juin 2009 devant le jury composé de :

*Claude Frankignoul
Jean-Luc Redelsperger
Yves Gouriou
Bach-Lien Hua
Jean-Philippe Duvel
Thierry Delcroix
Yves du Penhoat*

*Professeur (Université Paris 6)
Directeur de recherches (CNRS)
Directeur de recherches (IRD)
Directeur de recherches (Ifremer)
Directeur de recherches (CNRS)
Directeur de recherches (IRD)
Directeur de recherches (IRD)*

*Président du Jury
Rapporteur
Rapporteur
Rapporteur
Examineur
Examineur
Examineur*

Contents

RÉSUMÉ	4
ABSTRACT	5
1. INTRODUCTION	6
1.1. GENERAL INTRODUCTION AND STRUCTURE OF THIS DOCUMENT	6
1.2. THE INDO-PACIFIC WARM POOL	7
1.3. SEASONAL CYCLE	10
1.3.1. PACIFIC BASIN	10
1.3.2. INDIAN BASIN	11
1.4. TIMESCALES AND CENTRES OF ACTION	15
1.4.1. INTRASEASONAL VARIABILITY	16
1.4.2. INTERANNUAL VARIABILITY	19
2. PACIFIC BASIN	22
2.1. INTRODUCTION	22
2.2. TROPICAL INSTABILITY WAVES	23
2.2.1. BACKGROUND INFORMATION	23
2.2.2. SELECTED RESULTS	24
2.3 EL NIÑO	31
2.3.1. BACKGROUND INFORMATION	31
2.3.2. SELECTED RESULTS	33
3. INDIAN BASIN	40
3.1. BACKGROUND	40
3.1.1. INTERANNUAL VARIABILITY OF THE INDIAN OCEAN	40
3.1.2. MJO AND ITS OCEANIC SIGNATURE	44
3.1.3. THE RAMA ARRAY	48
3.1.4. THE CIRENE CRUISE	49
3.2. RESULTS: MJO OCEANIC SIGNATURE	51
3.2.1. DYNAMICAL RESPONSE	51
3.2.2. THERMODYNAMIC RESPONSE AND AIR SEA COUPLING	54
3.3. RESULTS: THE INDIAN OCEAN DIPOLE	60
3.3.1. CIRENE: INTERANNUAL ANOMALIES IN THE THERMOCLINE RIDGE REGION	60
3.3.2. THE IOD: A TRIGGER TO EL NIÑO?	64
4. WHAT'S NEXT?	67
4.1. NEW AREAS TO EXPLORE...	67
4.1.1. TROPICAL CYCLONES	67
4.1.2. QUESTIONS ABOUT THE MJO	68
4.1.3. THE NORTH-WESTERN AUSTRALIAN BASIN (NWAB)	69
4.1.4. INDO-PACIFIC AS A SINGLE BASIN	69
4.2. OBSERVATIONAL PROGRAMS	70
4.2.1. THE TRIO PROGRAM	70
4.2.2. FRENCH CONTRIBUTION TO THE RAMA ARRAY	72
4.3. CONCLUDING REMARKS	72
ABBREVIATIONS	74
REFERENCES	76
APPENDIX A. SCIENTIFIC OUTPUT AND TRAINING	84
A.1 PUBLICATIONS	84
A.2 SCIENTIFIC ADVISORY AND TRAINING ACTIVITIES	87
A.3 RESEARCH PROJECTS / CRUISES	89
A.4 CURRICULUM VITÆ	90
APPENDIX B. SELECTION OF ARTICLES	91

Résumé

Variabilité océan-atmosphère du secteur Indo-Pacifique tropical

Les océans Pacifique et Indien tropicaux se partagent la plus grande étendue d'eau chaude et de convection profonde de la planète. Cette région est le siège de la branche ascendante de la circulation de Walker, circulation atmosphérique d'échelle planétaire parfois décrite comme la « machine thermique » de la Terre. Cette région, dont les répercussions sur le climat sont importantes, est aussi source de variabilité océanique et atmosphérique aux échelles *intrasaisonniers* et *interannuelles*. En effet, la variabilité interannuelle associée à *El Niño*, dans l'océan Pacifique, et – dans une moindre mesure – au *dipôle de l'Océan Indien* (DOI) ont des conséquences climatiques marquées sur les pourtours de ces bassins et à l'échelle du globe. La variabilité intrasaisonnière liée à l'oscillation de Madden-Julian (OMJ) a également des conséquences climatiques marquées : modulations des moussons indiennes et australiennes et un rôle potentiellement important dans le déclenchement d'ENSO.

Dans ce mémoire, je vais décrire mes travaux de recherche sur la variabilité océanique et atmosphérique aux échelles intrasaisonnière et interannuelle dans les Océans Indien et Pacifique. *El Niño* ou le DOI sont des modes *couplés* : c'est la rétroaction positive découlant des interactions océan-atmosphère qui est source de variabilité (le « Bjerknes feedback »). À l'échelle intrasaisonnière, le rôle du couplage océan-atmosphère semble moins primordial, et modifie seulement des modes de variabilité essentiellement atmosphériques ou océaniques. Par exemple, les *ondes d'instabilité* dans le Pacifique Est sont le résultat d'une instabilité interne océanique. Cependant, elles affectent la stabilité atmosphérique, les vents de surface, et cela tend à réduire légèrement leur activité. À l'inverse, l'OMJ est un phénomène dont la source est atmosphérique, naissant du couplage entre dynamique et convection dans les tropiques. Toutefois, nous verrons que ce phénomène a une réponse océanique forte dans l'Océan Indien, à la fois en termes de dynamique et de thermodynamique. Le degré d'influence du couplage dans les propriétés de l'OMJ reste toutefois une question largement ouverte.

Nous nous intéresserons aussi à la question des *interactions* entre ces différents modes de variabilité. Nous verrons par exemple comment la variabilité intrasaisonnière atmosphérique peut déclencher un *El Niño*, comment *El Niño* peut supprimer l'activité des ondes tropicales d'instabilité et l'effet retour, comment le DOI module l'activité de l'OMJ et enfin, quelles sont les interactions entre DOI et *El Niño*. Je présenterai alors une région de l'Océan Indien assez emblématique de ces interactions d'échelle, et dans laquelle j'ai développé une activité d'observations (campagnes océanographiques Cirene de 2005 à 2008 et projet de campagne TRIO). La bande 5°S-10°S dans l'Océan Indien est une région très particulière. En raison de la structure des vents, la thermocline y est proche de la surface et la couche de mélange est peu profonde, ce qui induit une forte réactivité de la température de surface aux sollicitations de l'atmosphère. De plus, la température de surface en hiver boréal est proche du seuil de convection, impliquant une sensibilité accrue de l'atmosphère à de petites variations de température. Ces deux facteurs augmentent le couplage océan atmosphère dans cette région qui a une variabilité très marquée aux échelles synoptiques (cyclones), intrasaisonniers (OMJ) et interannuelle (réponse à *El Niño*, mais aussi au DOI). Cette région a enfin des conséquences climatiques marquées (sur l'intensité des pluies de la mousson suivante, sur le nombre de cyclones dans le secteur La Réunion-Madagascar, sur la convection au-dessus du continent maritime, et même sur l'Amérique du Nord).

Pour conclure, je présenterai ma réflexion sur mes axes de recherches futurs, ainsi que mes projets en termes de campagnes et réseaux d'observations.

Abstract

The tropical Indian and Pacific oceans share the largest span of warm water and deep atmospheric convection on our planet, which is also the ascending part of the Walker circulation, an essential component of the climate system. This region is also home to strong atmospheric and oceanic *intraseasonal* to *interannual* variability, with strong climatic consequences. *The El Niño* phenomenon, and, to a lesser extent, the *Indian Ocean dipole* (IOD) indeed have strong climatic consequences around these two basins, but also at global scale. Intraseasonal variability linked to the *Madden-Julian oscillation* (MJO) is also important, with its modulation of Indian and Australian monsoons and its potentially important role in triggering El Niño.

In this document, I describe my research on intraseasonal to interannual oceanic and atmospheric variability in the Indian and Pacific basins. El Niño or the IOD are by essence coupled ocean-atmosphere phenomena: they result from positive feedbacks arising from air-sea interactions (the “Bjerknes feedback”). At intraseasonal timescale, the coupling seems less important and only partially modifies the characteristic of a dominantly atmospheric or oceanic mode of variability. For example, *Tropical Instability Waves* in the eastern Pacific are the results of internal oceanic instabilities. However, they influence the stability of the atmospheric boundary layer and the surface windstress, and this feedback tends to reduce slightly their variability. On the other hand, the MJO is predominantly an atmospheric process, resulting from the coupling between atmospheric dynamics and deep atmospheric convection. But I will show that this phenomenon induce a strong oceanic response in the Indian ocean, both in terms of dynamics and surface temperature. The degree to which air-sea coupling influences properties of the MJO however remains an open question.

I will also discuss interactions between those various modes of variability. I will for example illustrate how intraseasonal atmospheric variability can trigger an El Niño; how an El Niño can suppress tropical instability waves and be affected in return; how the IOD modulates the MJO activity and the interactions between the IOD and El Niño. I will then discuss a region of the Indian ocean which is emblematic of these scale interactions and in which I have developed past (Cirene cruises from 2005 and 2008) and hopefully future (TRIO cruise) observational programs. The 5°S-10°S band in the Indian Ocean has an elevated thermocline and shallow mixed layer due to climatological Ekman pumping, but high SST close to the threshold of deep atmospheric convection. These two factors increase air-sea coupling in this region, which has clear variability at synoptic (cyclones), intraseasonal (MJO) and interannual (IOD) timescales. This region has strong climatic consequences and impacts the quality of the following Indian monsoon, the number of cyclones in the Madagascar-La Réunion area and even atmospheric patterns over the Maritime continent and Northern Pacific ocean.

I will conclude by presenting my future research plans and my projects in terms of cruises and observational networks.

1. Introduction

1.1. General introduction and structure of this document

Most countries from the rim of the Indian Ocean or from South America still have an economy that is strongly based on Agriculture, and hence vulnerable climate variability. There is, for example, a clear correlation between the annual rice production in India and the quality of the monsoon (e.g. Gadgil and Gadgil, 2006). Another example of dependency of economical activity on climate variability is the sensitivity of fish catches to *interannual* variability in the Indian Ocean (e.g. Marsac and Leblanc, 1999; Lehodey et al., 1997).

In addition to year-to-year variability, there is also considerable variability at *intraseasonal* timescales in the tropics, with associated modulation of e.g. the monsoon rainfall (e.g. Goswami, 2005) or cyclonic activity (e.g. Bessafi and Wheeler, 2006). The intraseasonal modulation of rain can also have a considerable impact on agriculture. Indeed, when interviewed, groups of African farmers indicated that a prior knowledge of “active” and “break” phases of the monsoon would benefit them (seeds planted before a break phase are generally lost, Ingram et al. 2002). Because of less developed infrastructures and housing, the countries from the south are also highly vulnerable to extreme events like cyclones, as the dramatic impact of Cyclone Nargis on Myanmar is a recent example (Webster, 2008).

In the examples above, I singled out two types of variability of the tropical region: *interannual* and *intraseasonal* variability. Variability at these timescales appears prominently in both the ocean and the atmosphere in the tropical band. In some cases, this variability clearly arises from air-sea coupling. It is the case for, e.g., *interannual* variability of the Pacific Ocean (the famous “El Niño”) or the Indian Ocean (the less famous and less poetically named “Indian Ocean Dipole”, hereafter IOD). At *intraseasonal* timescale, the coupling is less obvious. For example, the “Madden Julian Oscillation” (hereafter MJO¹) is the leading mode of atmospheric intraseasonal variability in the tropics. The origin of the MJO is clearly the coupling between large scale convection and atmospheric dynamics, but its large oceanic signature can leave us wondering if air-sea interactions don’t influence it as well. Similarly, “Tropical instability waves” (hereafter TIWs) which modulate the Sea Surface Temperature (hereafter, SST) in the eastern Atlantic and Pacific Oceans are clearly the result of oceanic internal instabilities. But they also have an atmospheric signature: does it feedback on them?

Most my work since my PhD has revolved around investigating tropical oceanic and atmospheric variability at *intraseasonal* to *interannual* timescales. My main focus has been on the Pacific and Indian Oceans. In this document, I’ll try to brush a picture of the various phenomenons I have looked into, and to highlight my contribution to their study. To ease that, I have highlighted in blue any quoted article for which I am a co-author. I’ll also generally separate a “Background” from a “Selected results” section.

I have assumed in this text that the reader is familiar with the basic concepts of simple geophysical fluid dynamics (e.g. planetary waves in particular in the tropical waveguide, instabilities in a rotating stratified fluid, vertical modes of the stratification, etc...). In case of need, I suggest the reader to refer to one of the holy books in our field: Gill (1982). He describes all of these concepts with far more clarity and details than I’d be able to do.

The rest of this introductive section will aim at giving the larger picture of the themes investigated here. I will start with some description of the Indo-Pacific warm pool and its importance, and then give an overview of the seasonal cycle of the surface winds and ocean in the Indo-Pacific region. I will finally introduce the main characters we’ll be concerned with (El Niño, the IOD, the MJO and TIWs!) by precisising their timescales and centers of action.

¹ See the list of abbreviations at the end of the document: climate scientists are fond of them.

Section 2 is concerned with the Pacific Ocean. I will first introduce in more details the basic processes of TIWs, and then zoom on some selected results. I will then give more details on the current understanding of El Niño, and highlight my contributions to its study.

Section 3 is concerned with the Indian Ocean. I will start by giving some background information on variability in the Indian Ocean, and describe some observing programs (RAMA and Cirene). I will then present some selected results on intraseasonal and interannual variability over the Indian Ocean basin, with highlights on some recent contributions from the Cirene program.

Section 4 is entitled “What’s next?”. I will describe the new science areas in which I want to invest myself in the next few years. I will also describe my aims in terms of observational programs in the Indian Ocean, and conclude.

1.2. The Indo-Pacific warm pool

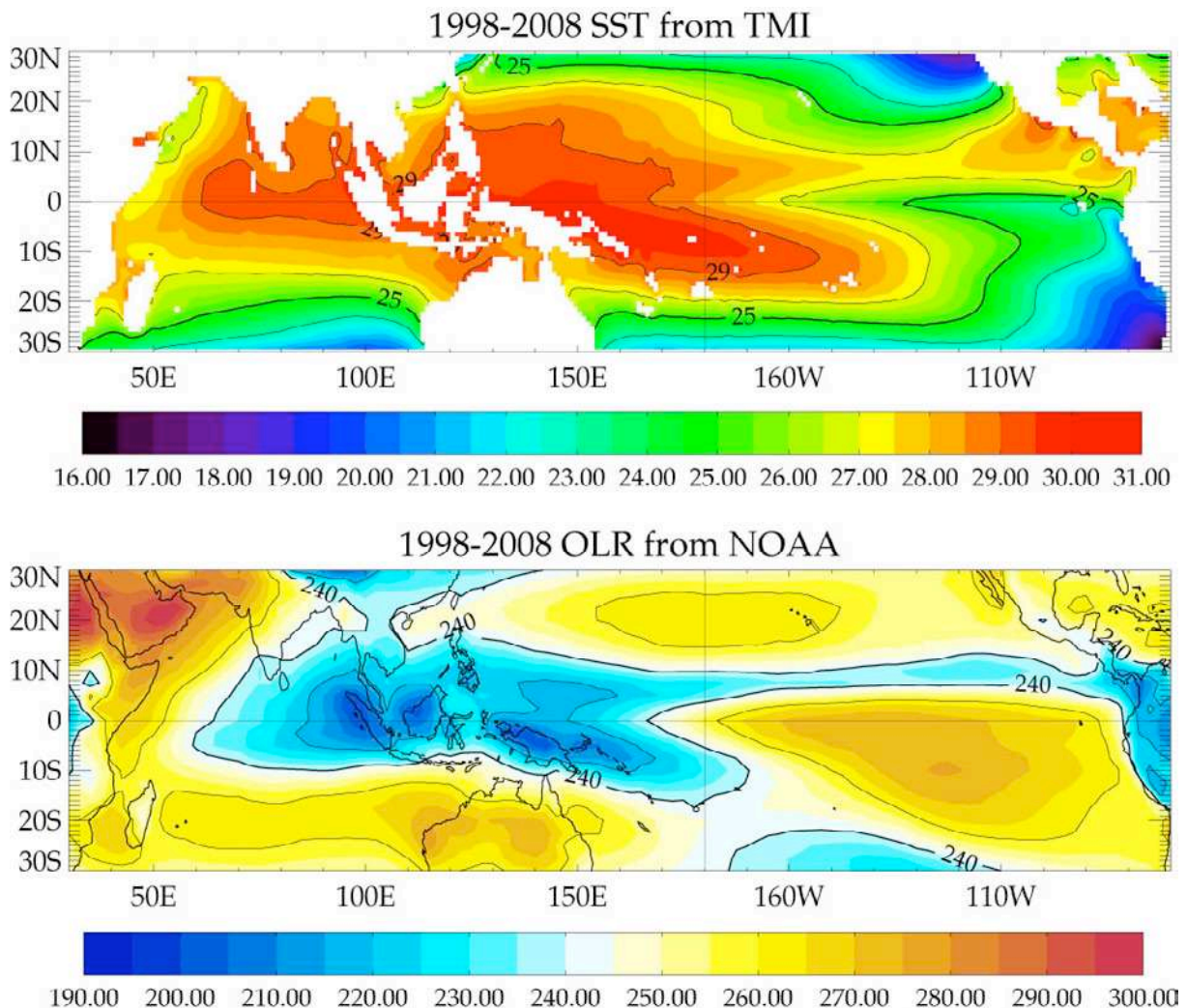


Figure 1. Climatological SST ($^{\circ}\text{C}$, 1998-2008 average from TMI, Wentz et al. 2000) and outgoing longwave radiation (OLR) at the top of the atmosphere ($\text{W}\cdot\text{m}^{-2}$, 1979-2008 average from NOAA, Liebmann and Smith, 1996). The OLR is an indicator of the temperature of the top of the clouds, and has low values associated with deep atmospheric convection. There’s a sharp increase of convective activity above $26\text{-}27^{\circ}\text{C}$, with deep convection occurring generally above 28.5°C (high SSTs are a necessary, but not sufficient condition for deep convection to occur: Graham and Barnett, 1987; Gadgil et al., 1986).

The tropical Indian and Pacific ocean basins are separated by a series of Islands (Indonesia and Papua-New Guinea) most generally referred to as “the maritime continent”,

but also by the South-East Asian landmass to the North, and by Australia to the South. In view of this geographical evidence, one will indeed be tempted to consider those two oceans as separate entities. On the other hand, these two oceans have in common what is probably the largest atmospheric circulation pattern on earth, and one of importance for our climate, related to the largest span of warm water on earth.

The surface of water above 28.5°C in the Indo Pacific warm pool exceeds 35 millions of square kilometers (Fig. 1). A necessary condition for atmospheric convection to occur over the oceans is sufficiently high SST (Gadgil et al. 1986; Graham and Barnett, 1987). While the threshold for deep atmospheric convection can vary from an ocean to the other, 28.5°C is a generally accepted critical threshold for allowing deep atmospheric convection. As the result, there is a strong almost permanent region of deep atmospheric convection anchored to the western Pacific warm pool and maritime continent (Fig. 1).

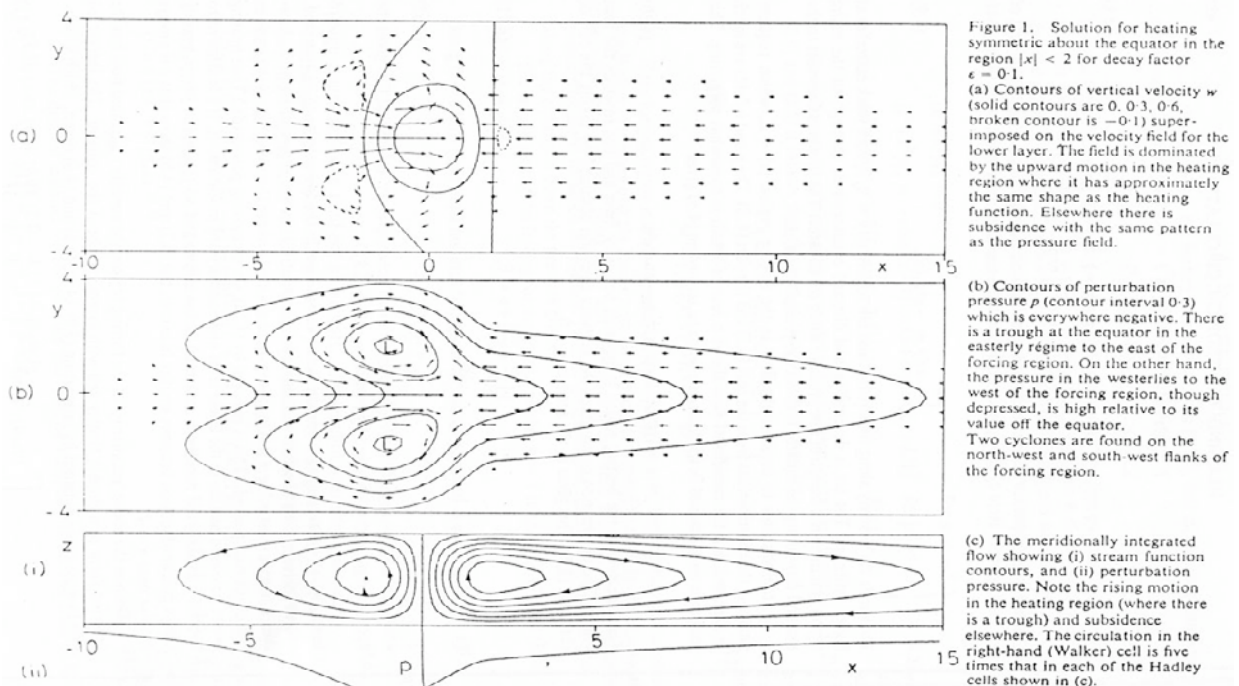


Figure 2. Atmospheric response to tropospheric heating as predicted by the Gill model (Gill, 1980). This very simple model explains many aspects of the mean circulation over the Indo-Pacific ocean and, as we will see later, of the surface wind perturbations associated with the MJO or ENSO.

The tropospheric heating associated to deep atmospheric convection drive easterly winds along the equator in the Pacific Ocean (Fig. 2ab). Those winds moisten progressively along the way, providing one of the sources of moisture to maintain convection in the western Pacific. Parcel of winds rise and release latent heat that maintain the convection and circulation pattern. The dry air returns eastward and subsides over the eastern Pacific Ocean and western Indian Ocean, where it tends to suppress convection (Fig 2c). This image is simplified, because the tropospheric heating associated with the deep convection in the western Pacific is coupled at the same time with the Walker (zonal) and Hadley (meridional) circulations through angular momentum conservation.

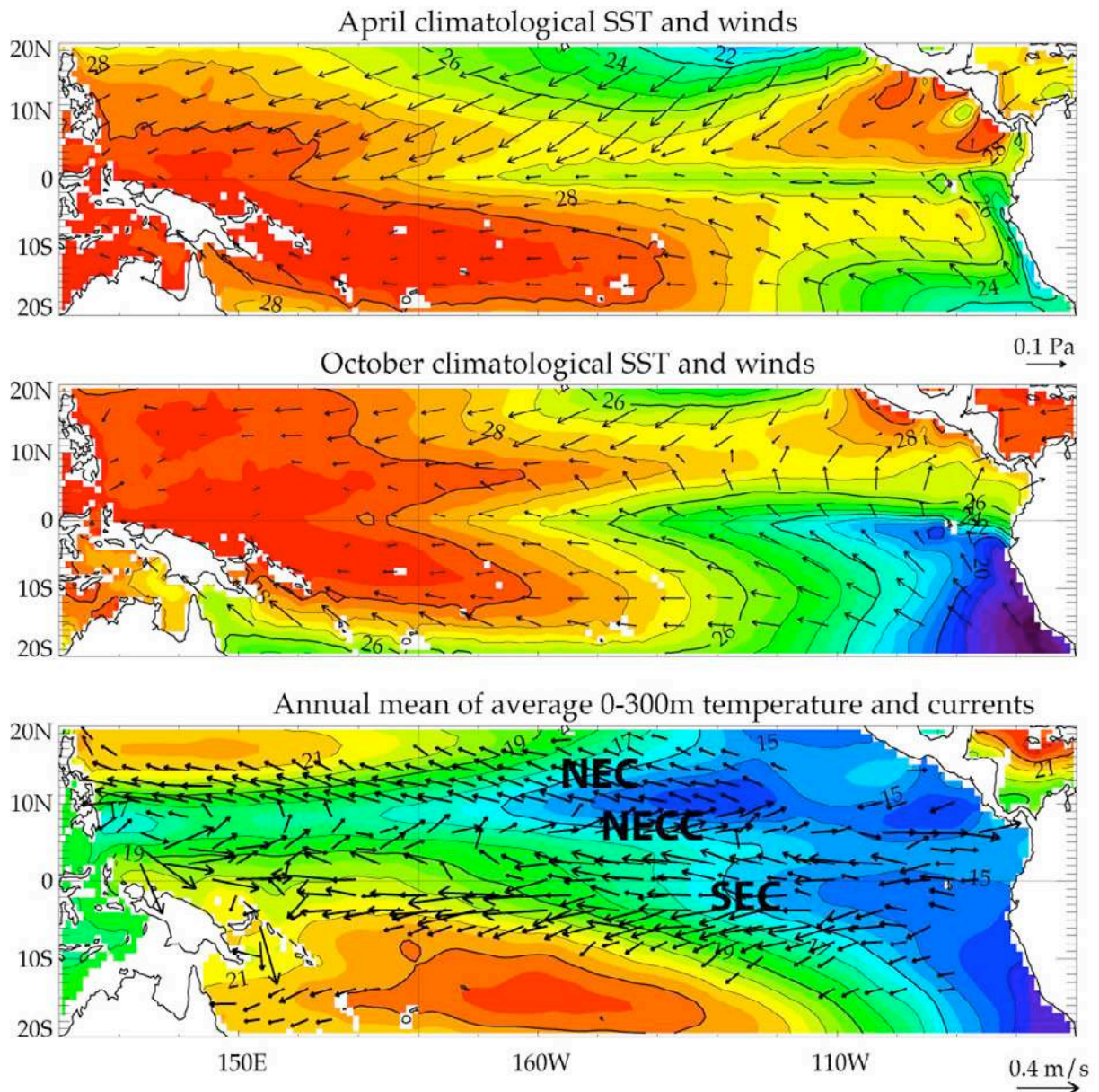


Figure 3. Mean state and seasonal cycle in the Pacific Ocean. Top panel shows the wind stress (Quickscatt 1999-2008 average) and SST (TMI 1999-2008 average, Wentz et al. 2000) for April. Next panel shows the same fields for October. The third panel shows the 0-300m averaged ocean climatological temperature (from World Ocean Atlas 2005, Locarnini et al., 2006) and 1993-2006 average of surface current estimates (Oscar product, Bonjean and Lagerloef, 2002). The surface current systems are indicated: the South Equatorial Current (SEC), North Equatorial Counter-Current (NECC) and North Equatorial Current (NEC).

I don't want to discuss the detailed processes of the Walker and Hadley circulation here, but want to convey that the Indo-Pacific warm pool is associated to an atmospheric circulation pattern that extends zonally over ~29000 km, has remote influences, and ties the Pacific and Indian ocean together. The Walker circulation is sometimes referred to as the "heat engine" of the earth and we'll see later that zonal displacements of the warm pool associated to e.g. El Niño induce worldwide consequences because of the planetary scale of the Walker circulation.

1.3. Seasonal cycle

In this section, I will give a brief overview of the mean state and seasonal cycle of the Indian and Pacific Oceans, since this background information will be useful for some of the interpretations in the following sections. While the seasonal cycle of the Pacific and southern Indian Ocean (south of 10°S) are roughly similar (dominated by easterlies), the Indian Ocean north of 10°S has a strikingly different response, because of the powerful monsoon annual cycle.

1.3.1. Pacific Basin

Fig. 3 gives an overview of the mean state and seasonal cycle in the tropical Pacific Ocean. First, there is an obvious asymmetry in the SST and wind distribution, with the Inter-Tropical convergence Zone (ITCZ) and warmest SSTs being located north of the equator. The easterlies drive Ekman divergence along the equator and coastal upwelling along the coasts of South America, resulting in the formation of the east Pacific “cold tongue” and Peruvian coastal upwelling.

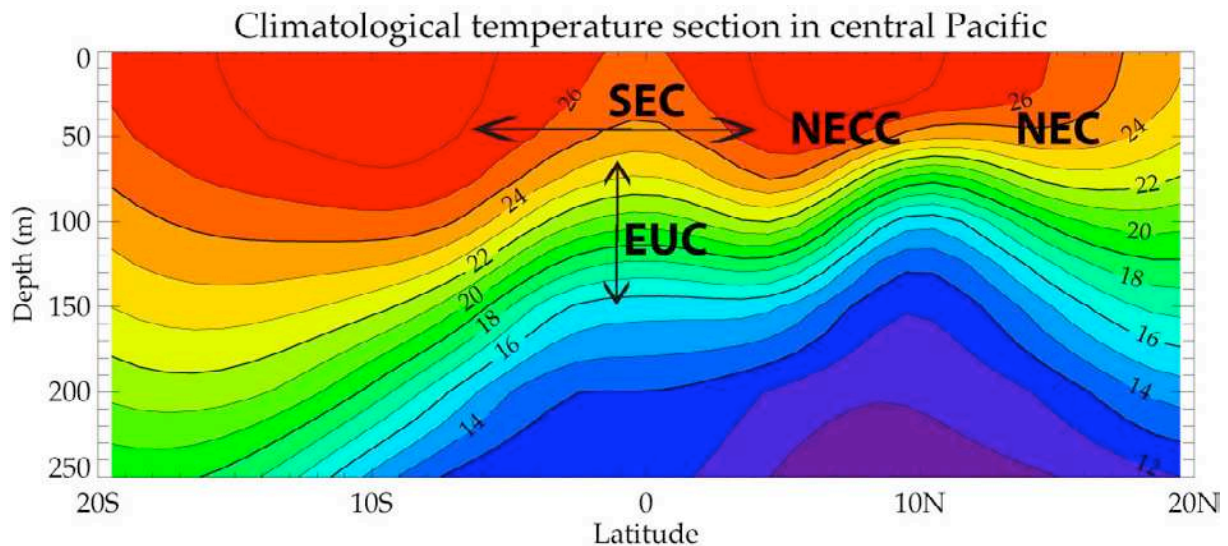


Figure 4. Meridional section of temperature in the central Pacific. The various current systems associated with this stratification are indicated: the South Equatorial Current (SEC), Equatorial Under-Current (EUC), North Equatorial Counter-Current (NECC) and North Equatorial Current (NEC).

The equatorial divergence results in a sea level minimum at the equator, which drives the South Equatorial Current (Figs. 3 and 4.). The ITCZ at 10°N is associated with wind convergence that induces another sea level minimum with the North equatorial Counter current on its equatorward flank and North equatorial current on its poleward flank. The easterlies along the equator need to be balanced by a zonal pressure gradient: this results in a tilt of the thermocline, with shallow thermocline in the eastern Pacific and a deep thermocline in the western Pacific warm pool. The wind stress forcing does not penetrate enough into the subsurface to balance the westward pressure gradient in the thermocline, resulting in an eastward subsurface return flow: the equatorial under current.

Contrary to the Indian ocean, where the seasonal cycle of winds results in very contrasted distributions of the currents and sea level, the seasonal cycle in the Pacific ocean is just a more subtle modification of the patterns discussed above. In april (the end of boreal winter), the ITCZ has migrated south because of the annual march of the sun, and stands close to the equator. It thus bringing the “doldrums” (weak winds in the convergence region) to the

equatorial strip, and easterly stress at the equator is then weakest. In September-October (at the end of Boreal summer) the ITCZ reaches its northernmost position, in response to the annual march of the sun, and easterlies along the equator are then strongest. The most striking response to this change in strength of easterlies is a cold tongue, which is most developed in September-October. There are also changes in the strength of various currents (e.g. the SEC is stronger, etc...) but they are more subtle.

1.3.2. Indian Basin

The Indian Ocean basin is a peculiar basin. It is the only tropical basin to be bounded by a continental landmass to the north. This is one of the reasons (together with elevated heating on the Tibetan plateau and Himalayas) why the Indian monsoon is so strikingly energetic. The southwest monsoon starts in June, and is associated with a strong low level jet over the eastern Arabian Sea (the Findlatter jet, see Fig. 5). In winter, the Asian landmass has cooled and the ITCZ stands south of the equator, following the annual march of the sun. This results in northeasterly winds over the Northern Indian from roughly November to March.

There are two “intermediate” seasons between the northeast and southwest monsoons, generally referred to as the two inter monsoons (April-May and October-November). During these two seasons, the monsoonal (highly meridional) circulation weakens, and the Walker circulation becomes more obvious along the equator. At these seasons, equatorial westerlies can be seen along the equator, whereas easterlies or near-zero winds exist along the equator at other seasons.

A natural separation line can be drawn to separate the Northern Indian ocean from the southern Indian Ocean. Indeed, while the wind field north of $\sim 10^\circ\text{S}$ is dominated by the strong annual cycle linked to the monsoons, there is no seasonal wind reversal south of 10°S . Instead, there are year-long easterlies in the Southern Indian Ocean, which only exhibit varying strength, and are strongest during the southwest monsoon (Fig 5.).

I will first describe the Southern Indian Ocean, putting some emphasis on the peculiar thermocline structure that emerges at the meeting point of the Easterly and Monsoon wind regimes. I will then proceed to an overview of the intricacies of the North Indian Ocean circulation.

1.3.2.1. Thermocline ridge

South of 10°S , the northward termination of the easterlies is associated with Ekman pumping. This Ekman pumping is strengthened in winter when northwesterly winds associated with the winter monsoon induce northward transport to the north of 10°S . It results in the formation of a thermocline ridge, between 5°S and 10°S , to the east of 50°E in the Indian Ocean (e.g McCreary et al. 1993, Fig. 6a). This year-round feature is more pronounced in boreal winter. A more detailed explanation of the formation of this ridge and its annual cycle can be found in (Hermes and Reason 2008; Yokoi et al 2008).

The Seychelles-Chagos thermocline ridge marks the limit between two current systems: the westward “South Equatorial Current” (Fig. 7) south of 10°S and the eastward “South Equatorial Counter-Current”, most marked in boreal winter, to the north of the ridge.

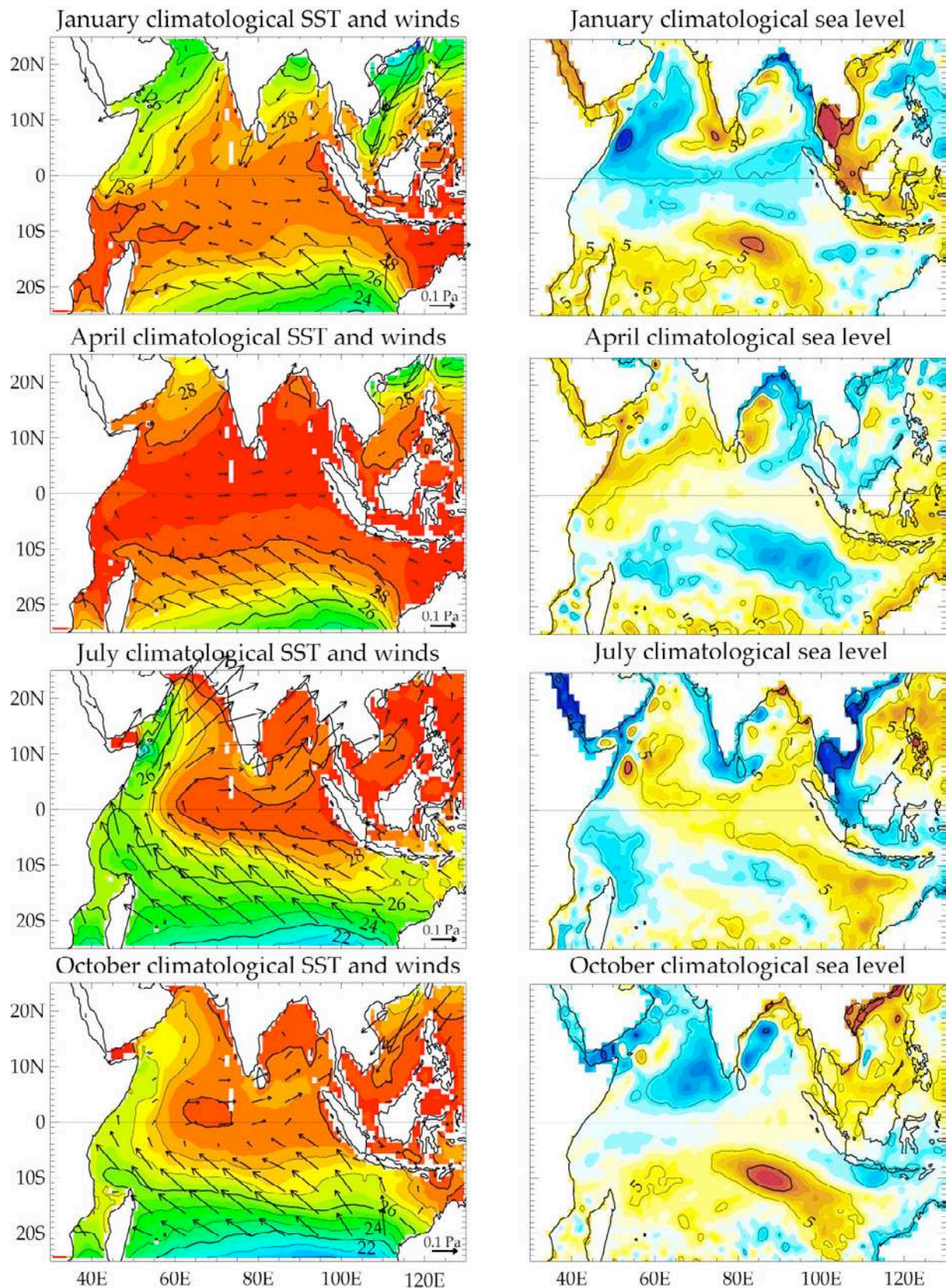


Figure 5. Seasonal cycle of Quickscat wind stress and TMI SST (left) and sea level (right) over the Indian Ocean. Note the complete seasonal reversal of the winds north of 10°S, associated with the Indian monsoon.

The thermocline ridge has a shallow thermocline and high SST, thus making it a potentially important region for air-sea interactions (Xie et al., 2002; Vialard et al., 2009a), as we will see in section 3. This region has attracted attention since it is home to distinct oceanic and atmospheric variability at multiple timescales, each time with significant climatic consequences. Anomalously high heat content in the ridge region is associated with increased cyclonic activity near Madagascar and La Réunion (Jury et al. 1999; Xie et al. 2002). Anomalously warm SST in this region also induces above-average rainfall along the Western Ghats of India during the following monsoon (Vecchi and Harrison 2004; Izumo et al. 2008). Atmospheric model experiments suggest that these SST anomalies force a substantial fraction of interannual precipitation anomalies over the west Pacific and maritime continent (Annamalai et al. 2005b) and influence the northern hemisphere extratropical circulation during boreal winter (Annamalai et al. 2007). These numerous climatic consequences are an incentive to better understand the various climate phenomena that affect SST in this region.

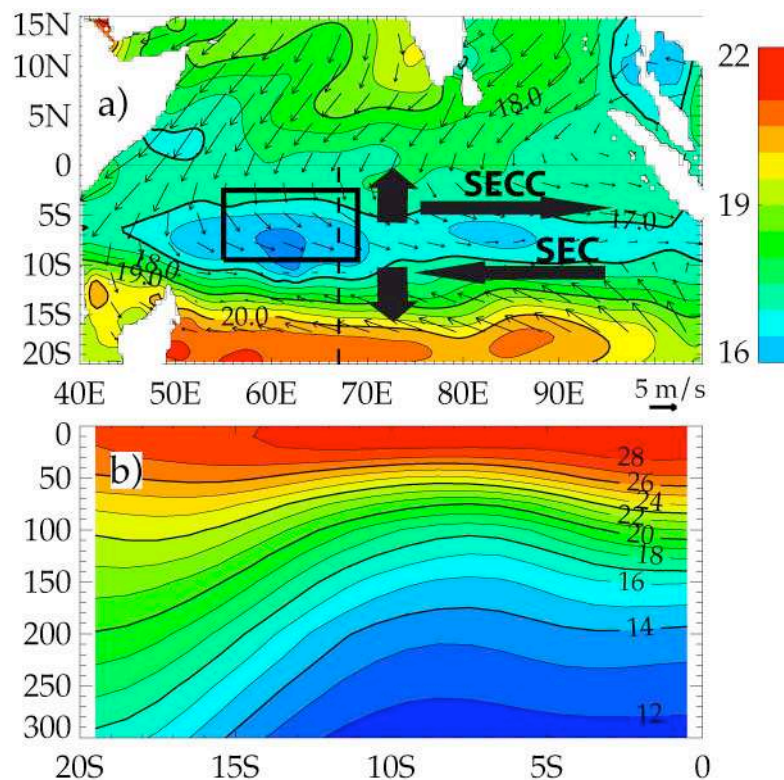


Figure 6. a) Climatological surface winds and 0-300m average ocean temperature in January-February. The thick black arrows indicate the surface flow induced by wind that promotes upwelling and leads to the SCTR formation. The arrows marked SEC and SECC indicate the South Equatorial Current and South Equatorial Counter-Current. b) Meridional section of the ocean temperature along 67°E, indicated by a dashed line in a). The climatological temperature data comes from world Ocean Atlas 2005 (Locarnini et al. 2006), while the wind is the Quikscat wind grided product produced by CERSAT.

The most prominent seasonal signal between 5°S and 15°S is the strong seasonal signal in sea level in the eastern half of the Indian Ocean (Fig. 5). Surprisingly the strong signals that develop in the eastern Indian Ocean seem to vanish as they reach ~75°E. This is the result of destructive interference between the local and remote forcing in the western half of the basin (Wang et al, 2001).

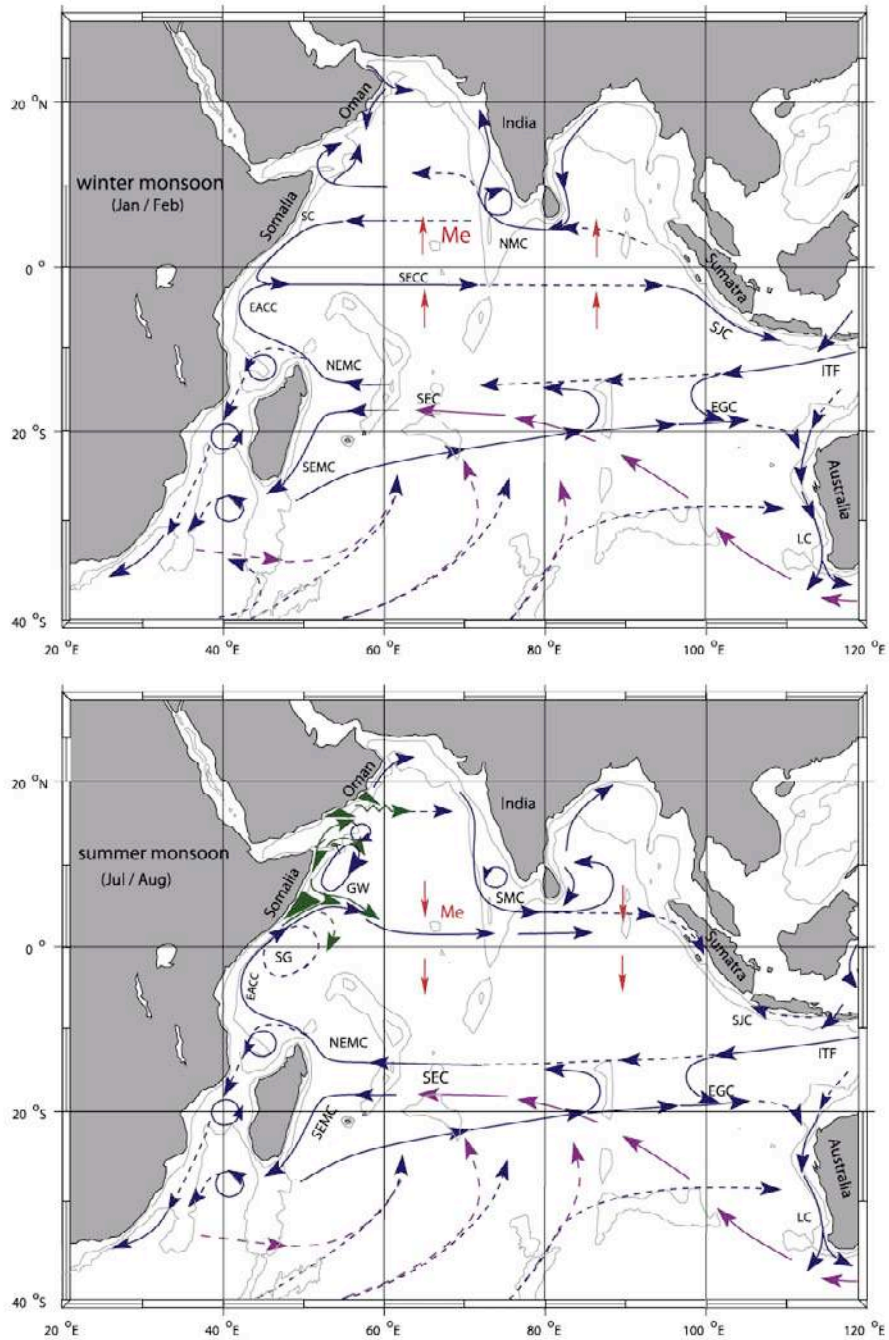


Figure 7. From Schott et al. (2009). Schematic representation of identified current branches during the summer (southwest) and winter (northeast) monsoons. Current branches indicated are the South Equatorial Current (SEC), South Equatorial Countercurrent (SECC), Northeast and Southeast Madagascar Current (NEMC and SEMC), East African Coastal Current (EACC), Somali Current (SC), Southern Gyre (SG) and Great Whirl (GW) and associated upwelling wedges (green shades), Southwest and Northeast Monsoon Currents (SMC and NMC), South Java Current (SJC), East Gyral Current (EGC), and Leeuwin Current (LC). The subsurface return flow of the supergyre is shown in magenta. Depth contours shown are for 1000 m and 3000 m (grey). Red vectors (Me) show directions of meridional Ekman transports. ITF indicates Indonesian Throughflow.

1.3.2.2. North Indian Ocean

Contrary to the south Indian Ocean, where currents do not reverse but only vary in strength annually, the Northern Indian ocean is home to very energetic seasonally reversing currents and strong seasonal upwellings. I won't give an exhaustive description of North Indian Ocean circulation here (see Schott and McCreary, 2001 for that), but will only focus on some features, which will be of relevance for the rest of the text.

First, the SST in the northern Indian Ocean has a strong semi annual cycle, with coldest temperatures during both monsoons (the coldest being actually during the winter monsoon), and warm SST in between. While those changes are almost entirely driven by air-sea fluxes (and primarily shortwave and latent fluxes) in the Bay of Bengal and eastern Arabian Sea, there is a strong contribution of Oceanic processes during the southwest monsoon in the western Arabian Sea (Shenoi et al., 2002; de Boyer Montégut et al., 2007). Indeed, the strong alongshore wind stress component associated with the Findlater jet drives two localized upwellings during the summer monsoon: the Somalia and Oman upwellings (Figs. 5, 7). There are also fascinating dynamical features associated with the rise of the Findlater jet (the great whirl, the Socotra eddy, the reversing and very intense Somali Current but I defer the interested reader to Shott and McCreary, 2001 for a review of those).

The northern Indian Ocean also displays a strong dynamical response to the changing monsoon winds. The most striking example of this strong dynamical response is the Wyrtki jet (Wyrtki 1973). As I mentioned earlier, the zonal wind stress along the equator in the Indian Ocean is near zero or slightly easterly during both monsoons, and switches to stronger easterlies during the two Inter-monsoon seasons (April-May and October-November). The strong imbalance during the wind stress and zonal pressure gradient thus forces a strong eastward jet at the equator with zonal velocities frequently in excess of 1 m/s. As we shall see later (section 3.3), this zonal jet, and currents along the equator in general, are strongly modulated at intraseasonal timescale.

The last point of relevance here is the dynamical response of the equatorial and coastal waveguides of the Northern Indian Ocean to the monsoon winds. Currents sometimes flow against the direction suggested by local wind forcing in the Northern Indian Ocean. This is for example the case for currents off the west coast of India during the winter monsoon (the southward wind stress would tend to force coastal upwelling Kelvin waves, negative sea level anomalies at the coast and southward currents offshore, but the opposite actually occurs: Figs. 5 and 7). This is because remote forcing is very important in the Northern Indian Ocean. The alternating southwest/northeast monsoons provide a strong annual forcing that drives a basin-scale sea-level response involving both equatorial wave dynamics and coastal wave propagation around the perimeter of the northern Indian Ocean (McCreary et al., 1993). The East India Coastal Current (EICC), for example, is largely influenced by remote wind forcing from the equatorial region (through the equatorial and coastal waveguides) and from the interior of the Bay of Bengal (through planetary waves) (McCreary et al., 1996). Coastal Kelvin waves then travel around Sri Lanka and the southern tip of India to impact the West India Coastal Current (WICC) (McCreary et al., 1993; Shankar and Shetye, 1997). I will discuss in section 3.3 how this picture is modified when considering intraseasonal rather than seasonal propagation of signals in the equatorial and coastal waveguides of the Northern Indian Ocean.

1.4. Timescales and centres of action

Now that I have given a quick overview of the mean state and seasonal cycle of the tropical Pacific Ocean, let me introduce the main timescales of variability that I will investigate in this manuscript: intraseasonal and interannual variability. I won't discuss the

processes in detail here (I'll give more precise description in the “background” sections of chapters 2 and 3) but just give an overview of the timescales and of the regions affected by intraseasonal variability in the Indo-Pacific region.

1.4.1. Intraseasonal variability

Fig. 8 gives an overview of the amplitude of SST and convection interannual variability over the Indo-Pacific. There is a strong modulation of convective variability in this frequency band over the Indo-Pacific warm pool. We will see below that this is largely associated with the Madden-Julian oscillation, the dominant mode of atmospheric intraseasonal variability in the tropics. For SST, the most striking feature is a region of strong intraseasonal variability, slightly shifted to the north of the equator, close to the cold tongue in the Eastern Pacific. We will see that this variability is associated with oceanic internal instabilities known as “Tropical Instability Waves” (hereafter TIWs). The more modest SST variability outlined in the tropical ocean corresponds to the oceanic signature of the MJO (except in the western Arabian Sea, where there's also a contribution from meso-scale eddies) and has potentially important climatic significance, which I will discuss in section 3.3.

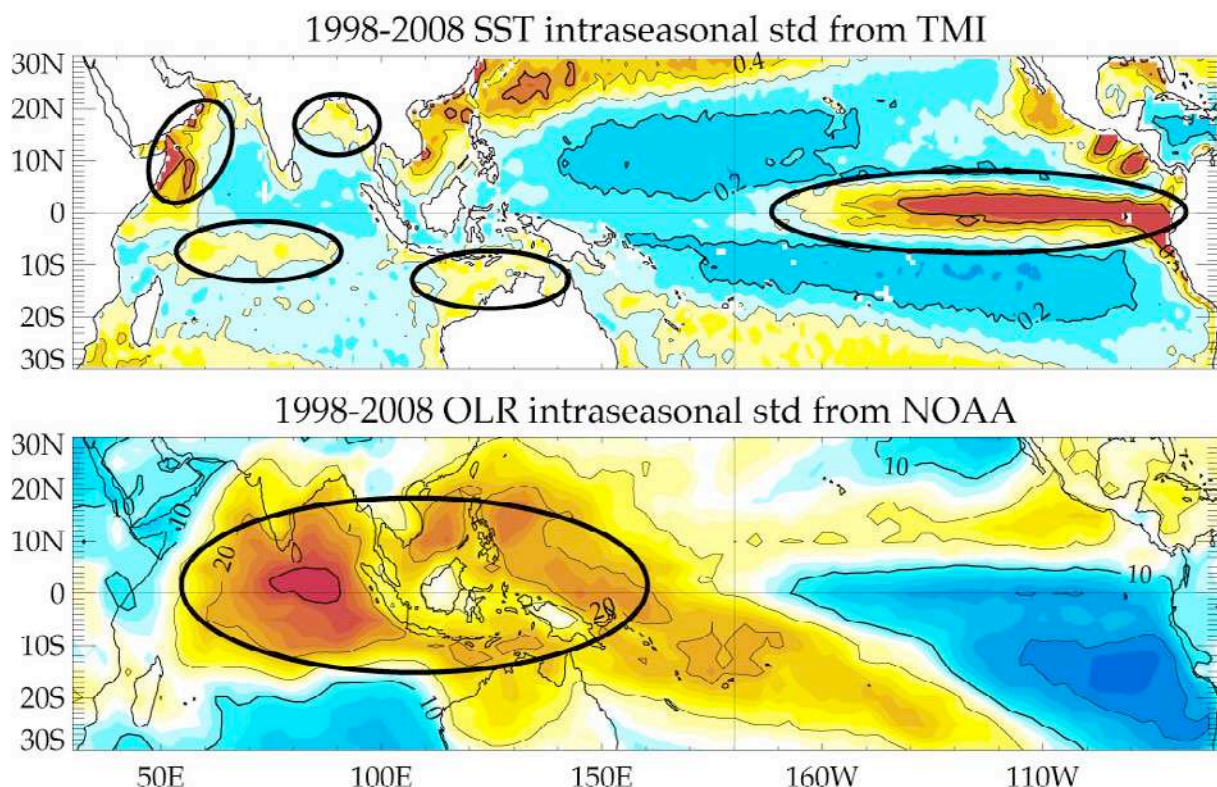


Figure 8. Intraseasonal amplitude of the SST ($^{\circ}\text{C}$, TMI product, Wentz et al. 2000) and OLR (W.m^{-2} , NOAA interpolated OLR, Liebmann and Smith, 1996) variability. This was estimated as the standard deviation of daily interannual anomalies these two fields in the 20-100 days band. Regions of strong variability that will be discussed later in the manuscript have been outlined.

1.4.1.1. MJO

Linear equatorial wave theory has proven to be a powerful tool for describing the oceanic or atmospheric response in near equatorial regions. Figure 9 shows that convection over the Indo Pacific warm pool indeed has modes of variability that match well the theoretical dispersion relation for equatorial waves. Mixed Rossby-Gravity waves are antisymmetric, can propagate either east- or west-ward but with eastward group velocity (Fig. 9). At planetary scale, they have short timescales (6 days or less). The symmetric solution

include the eastward propagating Kelvin waves, with timescales of ~ 15 day or shorter. At lowest frequencies (say periods longer than 15 days), there are two sources of variability of convection. The first is the westward propagating long Rossby waves (zonal wavenumbers 2-6, periods ~ 15 -40 days). The second one is not predicted by the linear equatorial wave theory and corresponds to the MJO (zonal wavenumbers 1-4, ~ 30 -80 day periods).

The MJO is a large-scale organised perturbation of the atmospheric deep convection, with energetic fluctuations of tropospheric winds at periods of 30-90 days (e.g. Zhang, 2005). The MJO originates from the Indian Ocean and propagates eastward at $\sim 5 \text{ m s}^{-1}$ into the western Pacific. Because of the strong coupling with deep atmospheric convection, the MJO surface signature becomes much weaker beyond the eastern edge of the Pacific warm pool (Figure 8).

Note that a distinction is generally made between the “MJO” (which was originally seen as an essentially equatorial, eastward propagating phenomenon) and the “summer Tropical Intraseasonal Oscillation” (the active and break phases of the Indian and south-east Asian monsoon, which is shifted to the northern Hemisphere and displays northward phase propagation) (e.g. Goswami 2005, Wang 2005). In this document, we have chosen to collectively name the summer and winter oscillations “MJO”, irrespective of the fact that they might have slightly different physics: they are in any case closely associated (e.g. Wheeler and Hendon 2004).

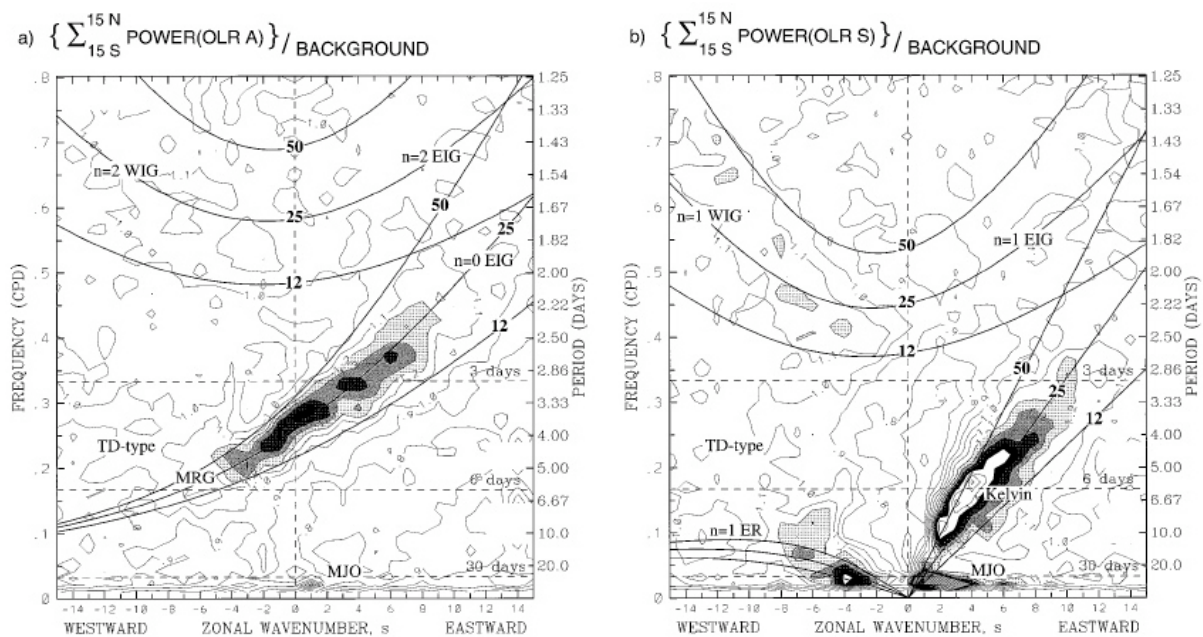


Figure 9. From (Wheeler and Kiladis, 1999). Spectrum of the OLR field in the frequency-zonal wavenumber space for the antisymmetric (left) and symmetric (right) parts. Curves corresponding to the theoretical dispersion diagram of equatorial waves have been added for three equivalent depths (12, 25 and 50m). In addition to the modes predicted by linear equatorial wave theory (mixed Rossby-gravity waves, Kelvin and Rossby waves), there's a planetary scale eastward propagating mode: the MJO.

I will present the main theories for explaining the MJO briefly in section 3.3. I underline here its basic timescale (30-90 day) and spatial distribution (over the Indo-Pacific warm pool). Because MJO is modulating convection, it is associated with perturbations of surface fluxes. Those perturbations include primarily momentum (surface wind response to the tropospheric heating associated with convection), latent heat flux (increased evaporation due to stronger winds) and shortwave flux (decreased solar radiation due to increased cloudiness). The MJO is hence associated with SST perturbations over most of the Indo-Pacific warm pool (e.g.

Duvel and Vialard, 2007). I will discuss in more details the processes of these SST perturbations and their potential feedbacks on the MJO in section 3.3.

1.4.2.2. TIWs

We saw above that the MJO is intrinsically an atmospheric phenomenon, with an oceanic signature. For TIWs, it is largely the opposite. As we will see in section 2.2, TIWs arise from instabilities developing within the eastern Pacific currents and cold tongue systems. TIWs also exist in the eastern Atlantic Ocean. There are no TIWs per se in the Indian Ocean, but there some related variability in the *western* equatorial Indian Ocean (e.g. Luyten and Roemmich, 1982; Reverdin and Luyten, 1986; Tsai et al., 1992). I will focus in this document on equatorial Pacific TIWs.

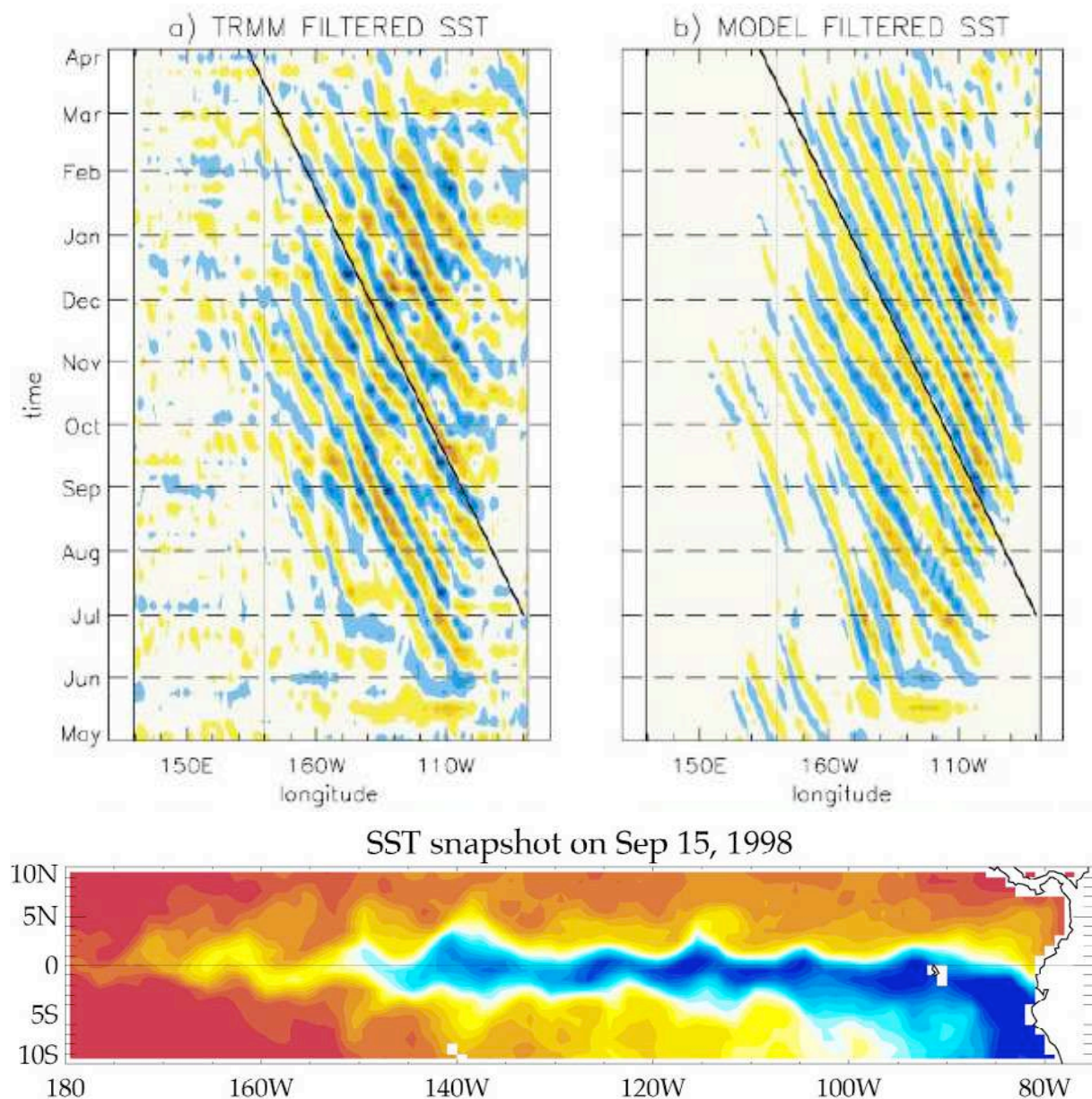


Figure 10. From Vialard et al. (2003). Time–longitude section of 50-day high-pass filtered (a) observed TRMM SST and (b) modeled SST along 2°N for May 1998–March 1999. The thick line corresponds to a propagation speed of 0.5 m s^{-1} . The lower panel shows a SST snapshot with undulations of the SST fronts on poleward edges of the cold tongue, characteristic of TIWs.

TIWs were first spotted as undulations of the SST front to the north of the cold tongue in the Pacific ocean (Fig. 8, Legeckis, 1977). TIWs are characterized by SST variations of 1-2°C, periods of 20-40 days, wavelength of ~1000-2000 km and westward phase propagation of around 0.5 m.s⁻¹ (e.g. Qiao and Weisberg, 1995; Fig; 10). TIWs have strong seasonal (and interannual) amplitude variations: they strength varies with the cold tongue (they are almost suppressed in September-October or during El Niños; e.g. Vialard et al., 2001). I will discuss the possible role of TIWs in the tropical Pacific mean state and ENSO cycle in section 2.2.

Similarly to the MJO (a primarily atmospheric phenomenon with an oceanic signature), the TIWs also have an atmospheric signature (e.g. Xie et al., 1998, Chelton et al. 2001). I will discuss in section 2.2 if the TIW-atmospheric signature feedbacks on TIW themselves (i.e. if *air-sea coupling* is to some extent important for TIWs).

1.4.2. Interannual variability

Fig. 11 gives an overview of the amplitude of interannual variability of the SST and convection over the Indo-Pacific domain. The interannual variability of SST in the eastern and cenral Pacific cold tongue associated with ENSO is the most striking pattern on that plot. In comparison, the SST variability associated with the IOD, along the coast of Java and Sumatra might seem negligible. However, because of the high mean temperature of the Indian Ocean (close to the threshold for deep atmospheric convection over a large fraction of the basin and the year), even modest SST anomalies can generate significant deep convection anomalies, and hence tropospheric wind response.

The pattern of interannual anomalies of OLR confirm this notion that the warm pool is the hotspot of convective variability: the region of strong convective variability is indeed largely encompassed (or along the edges) of the warmest water (Fig. 11 and Fig. 1), as was the case for intraseasonal variability (Fig. 8).

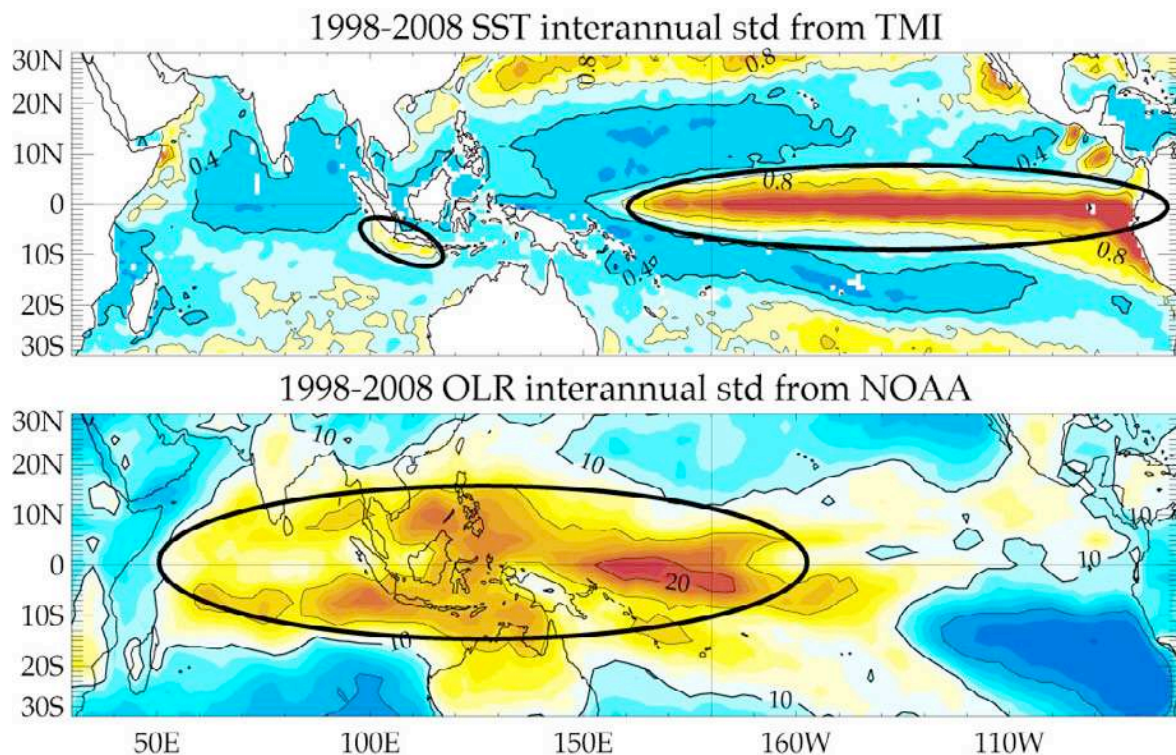


Figure 11. Amplitude of SST (°C, TMI product, Wentz et al. 2000) and OLR (W.m⁻², NOAA interpolated OLR, Liebmann and Smith, 1996) interannual variability. This was estimated as the standard deviation of monthly interannual anomalies these two fields. Regions of strong variability that will be discussed later in the manuscript have been outlined.

There is a tendency of the IOD and ENSO to co-occur (e.g. Schott et al 2009). By regressing interannual anomalies to an index of ENSO, figure 12 gives an overview of the spatial patterns of convection, surface wind and SST anomalies associated to a mature ENSO and IOD. In the next two sections, I will describe briefly the spatial patterns and timescales associated to both phenomenons, and will come back to the details of the processes in sections 2.3 and 3.4.

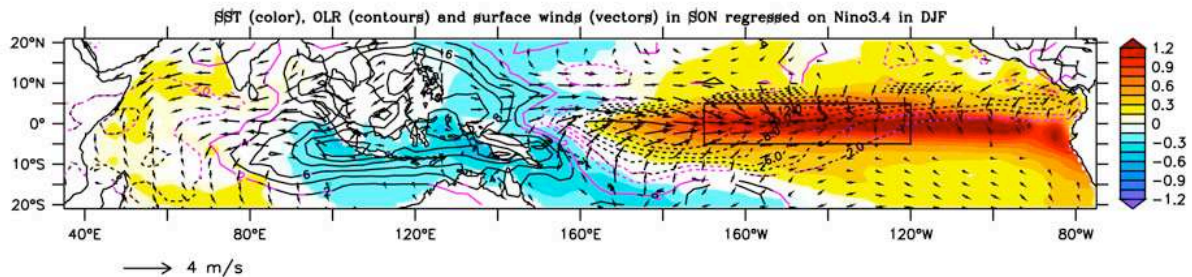


Figure 12. SST (color, °C), OLR (contours, W/m²) and winds (vectors) anomalies in fall (Sep-Nov) during an El Niño year. The fields are regressed on the Niño3.4 (black box, (170°W-120°W; 5°S-5°N) SST anomaly in Dec-Feb. Only values significant at the 90% level are plotted. Since there is a tendency for IODs to co-occur with ENSO, this analysis extracts the typical structure of both ENSO and the IOD.

1.4.2.1. El Niño

Figure 12 shows the trademark features of an El Niño: a weakening of the cold tongue, and an associated warm SST anomaly in the central and western Pacific. The atmospheric response to this change in SST distribution is a shift of convection from the maritime continent to the western and central Pacific, and a southward shift of the ITCZ in the eastern Pacific. The wind response to this anomalous tropospheric heating agrees well with the one predicted by the Gill model (Fig. 2), with predominantly westerly anomalies to the west of the anomalous tropospheric cooling.

Now that I have brushed ENSO's spatial structure, let me review quickly its temporal characteristics. First, ENSO is phase locked to the annual cycle, with the peak of ENSO occurring most generally at the end of the year (November-December). The SST and wind anomalies associated to an ENSO typically start developing in April-May. ENSO then culminates in November-December and has receded by March-April of the following year (e.g. Harrison and Larkin, 1998). The typical duration of ENSO events is hence one year. Spectrums of the average SST anomalies in the "Niño3.4 box" (see Fig. 12 for definition), a current index for El Niño, have a wide spectrum in the 2-7 years range, with most energetic fluctuations around 3-4 years. This is the typical return period of an ENSO.

1.4.2.2. Indian Ocean variability

The Indian Ocean had long been known to exhibit variability associated with ENSO. Increased convection over the central Pacific during an El Niño induces anomalous subsidence over the Indian Ocean (Fig. 2) and thus increased solar forcing that tends to raise the SST quite uniformly over the basin (Klein et al., 1999; Lau and Nath, 2000).

It was suggested quite early that, in addition to this uniform variability associated with ENSO, there was also a co-variability between zonal winds in the central equatorial Indian Ocean and the east-west temperature gradient (Reverdin et al., 1986). This aroused the attention of the scientific community more acutely after the 1997 event in the Indian Ocean and the papers it generated (e.g. Saji et al., 1999; Webster et al., 1999; Murtugudde et al., 2000). It now appears more clearly that the "Indian Ocean Dipole" (IOD) is an independent mode of variability of the Indian Ocean, but that it often (but not always) co-occur with

ENSO (e.g. Yamagata et al., 2004; Schott et al., 2009). Because of this tendency of both phenomena to co-occur, it is difficult to separate their relative influences from observations only, as illustrated by Figures 11 and 12, where large convective anomalies develop in between the Indian and Pacific Oceans.

Figure 12 captures the patterns of the IOD at its peak, in boreal fall. The IOD is associated with a well-defined cold anomaly along the coast of Java and Sumatra, and more variable warming of the western Indian Ocean. The cooling of Java and Sumatra is associated to a local suppression of convection there. As predicted by the Gill model (Fig. 2), this results in anomalous easterlies over the central Indian Ocean.

The Indian Ocean dipole has a shorter life span than El Niño. Its surface signature becomes visible in May-June, peaks in October, and then quickly recedes, largely disappearing by the end of the year for a total duration of about 6 months (e.g. Saji et al, 1999). The IOD has a biennial tendency.

The purpose of this chapter was to introduce the main characters that will come back in the following ones: the MJO and TIWs at intraseasonal timescale, and the IOD and ENSO at interannual timescale. Now we'll get to know these characters a bit more in the next chapters.

2. Pacific Basin

In this chapter, I will first give an overview of the observational system in place in the Pacific Ocean, and which allowed to make huge progress in the understanding of variability in this ocean. I will then proceed to give a more detailed description and selected results, first about TIWs and then about El Niño.

2.1. Introduction

Because of the overwhelming influence of El Niño on the global climate, the tropical Pacific was put early at the heart of research on global climate. The main objective of TOGA (Tropical Ocean-Global Atmosphere, a research international initiative from the World Climate Research Program) was to improve the understanding and predictability of El Niño. In order to achieve the TOGA goals, a strategy of large-scale, long-term monitoring of the upper ocean and the atmosphere has been planned. One of the results of this effort was the development of the TAO (Tropical Atmosphere Ocean) array (e.g. McPhaden et al., 1998). NOAA largely supported this effort (with the PMEL at the frontline), with contributions from Japan and France for the western part of the array.

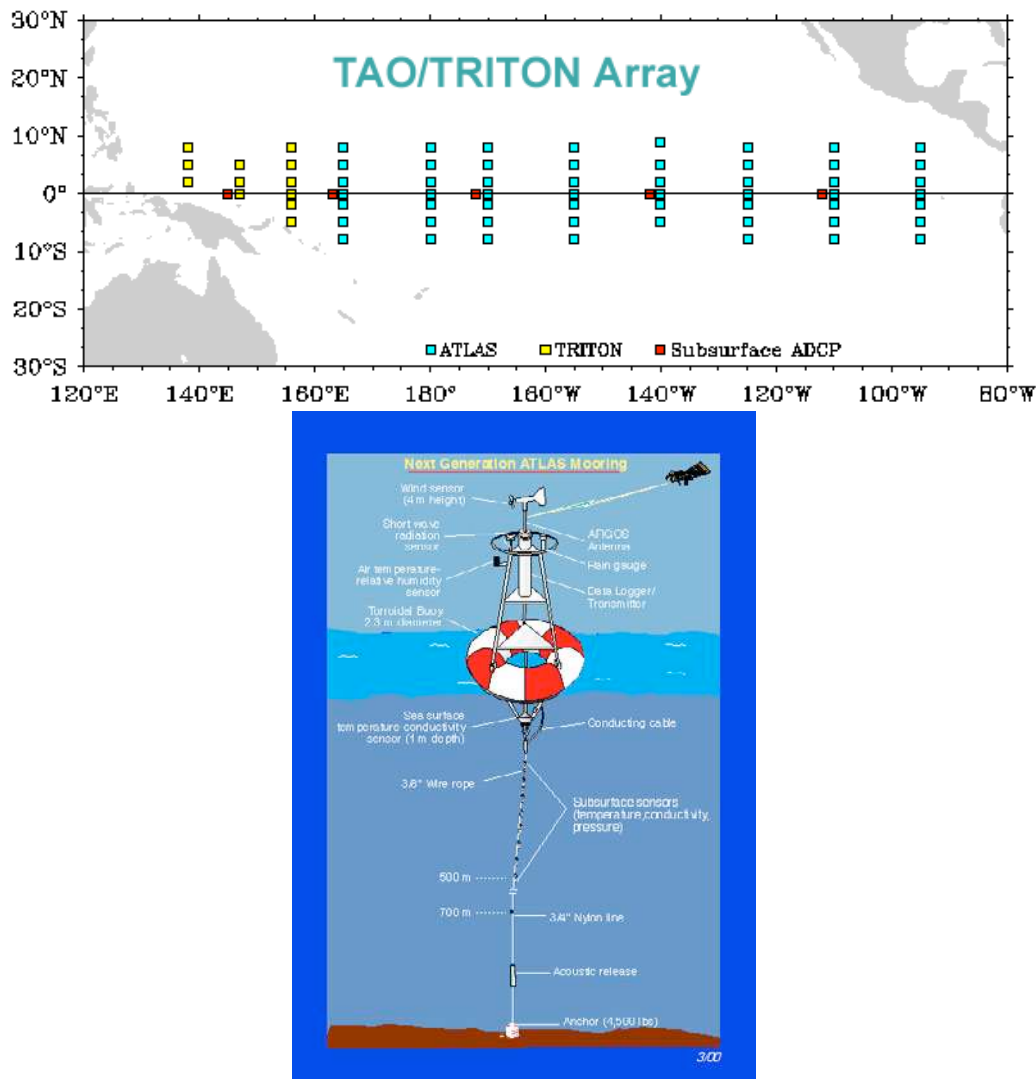


Figure 13. Distribution of moorings from the TAO/TRITON array (above) and sketch of the design principle ATLAS mooring. There are about 70 active moorings in the TAO array.

The TAO/TRITON array is comprised of about 70 moorings. Each of these moorings records subsurface temperature and salinity at selected depths between $\sim 1\text{m}$ and 500m. The surface platform has wind, rainfall, downwelling shortwave radiation, air temperature and humidity measurements. In combination with surface SST, these parameters allow to estimate air-sea exchanges of momentum, heat and freshwater by applying bulk formulae (e.g. Fairall et al. 2003).

The moorings transmit daily averages of most parameters to land through an Argos antenna. Higher resolution data (generally 10-minute averages) is recorded internally and is retrieved upon mooring servicing. Some of the data (e.g. surface winds, SST, subsurface temperature) is transmitted to the GTS (Global Telecommunication System) and is assimilated into meteorological analyses and in oceanic analyses used to initiate seasonal forecasts (section 2.3.2.b). All of the data is available freely and timely through the Internet to the scientific community (<http://www.pmel.noaa.gov/tao/>). With about 600 refereed publications using the TAO data since the beginning of the array in 1986, this array is a living demonstration of how observations are the drivers of science. A similar array is now quickly developing in the Indian Ocean (section 3.1) and will hopefully allow a similar flourish of scientific results in the least observed of the three tropical oceans.

2.2. Tropical Instability Waves

2.2.1. Background information

Spatio-temporal properties of TIWs. As we saw earlier, TIWs appear in space-borne sea surface temperature (hereafter SST) as well as ocean color measurements (Legeckis 1977, Chavez et al., 1999, Chelton et al., 2000, Menkes et al., 2002), as large scale westward-propagating oscillations of the temperature front separating cold and rich waters of the equatorial upwelling from warmer and nutrient-depleted waters to the north. These oscillations have a longitudinal scale of 1000-2000 km (Qiao and Weisberg, 1995) and propagation speed of about $0.3\text{-}0.5\text{ m.s}^{-1}$ (Weidman et al., 1999). They are associated with monthly-timescale variations in sea level (Busalacchi et al., 1994, Perigaud 1990; Weidman et al. 1999), as well as in currents north of the equator. These features are associated with anticyclonic vortices (Flament et al. 1996; Kennan and Flament 2001; Menkes et al. 2002) as first suggested by Hansen and Paul (1984).

Instability mechanism. There is no consensus on the instability mechanisms that give rise to TIWs (Weidman et al. 1999). Some studies suggest that barotropic instability of the shear region between the North Equatorial Countercurrent and South Equatorial Current could be important (Cox 1980), while others stress the importance of the shear between the Equatorial Undercurrent and the South Equatorial current (Luther and Johnson 1990; Qiao and Weisberg 1998; McCreary and Yu 1992). Other processes (such as baroclinic, Kelvin–Helmholtz or frontal instability) may also contribute to TIWs (Luther and Johnson 1990; McCreary and Yu 1992; Masina et al. 1999). More recently, TIWs have been described as the resonance of the first and second meridional mode, first baroclinic mode of Rossby Waves, modified to include interactions with the mean flow (Lyman et al., 2005), but with no clear explanation of how this relates to other instability mechanisms.

Impact of TIWs on heat budget. At seasonal scale, observations by Stevenson and Niiler (1983), Hansen and Paul (1984), Bryden and Brady (1989), Baturin and Niiler (1997), Swenson and Hansen (1999), Wang and McPhaden (1999) have shown that TIWs play a large role in the cold tongue heat budget. Estimates in those studies suggest that the horizontal TIW flow induces large equatorward transport of heat, equivalent or stronger than the effect of the seasonal surface forcing.

Atmospheric signature of TIWs. Several observational studies have shown that TIWs have an atmospheric response (Xie et al., 1998; Liu et al., 2000; Chelton et al., 2000). Wind is accelerated over warm anomalies and decelerated over cold ones, producing centers of convergence and divergence collocated with maximum SST gradient regions (Fig. 14). The convergence (divergence) centers in turn lead to increased (decreased) water vapor content in the lower layers of the atmosphere. These spatial patterns are consistent with the suggestion by Hayes et al. (1989) that the modulation of the wind is linked to the impact of TIW temperature anomalies on the stability of the atmospheric boundary layer (ABL). In situ data analysed by Hashizume et al. (2002) is also consistent with this mechanism. However, Hashizume et al. (2001) and a modeling study by Small et al. (2003) suggest that the zonal pressure gradient driven by the temperature anomalies is also an important factor, as initially suggested by Lindzen and Nigam (1987).

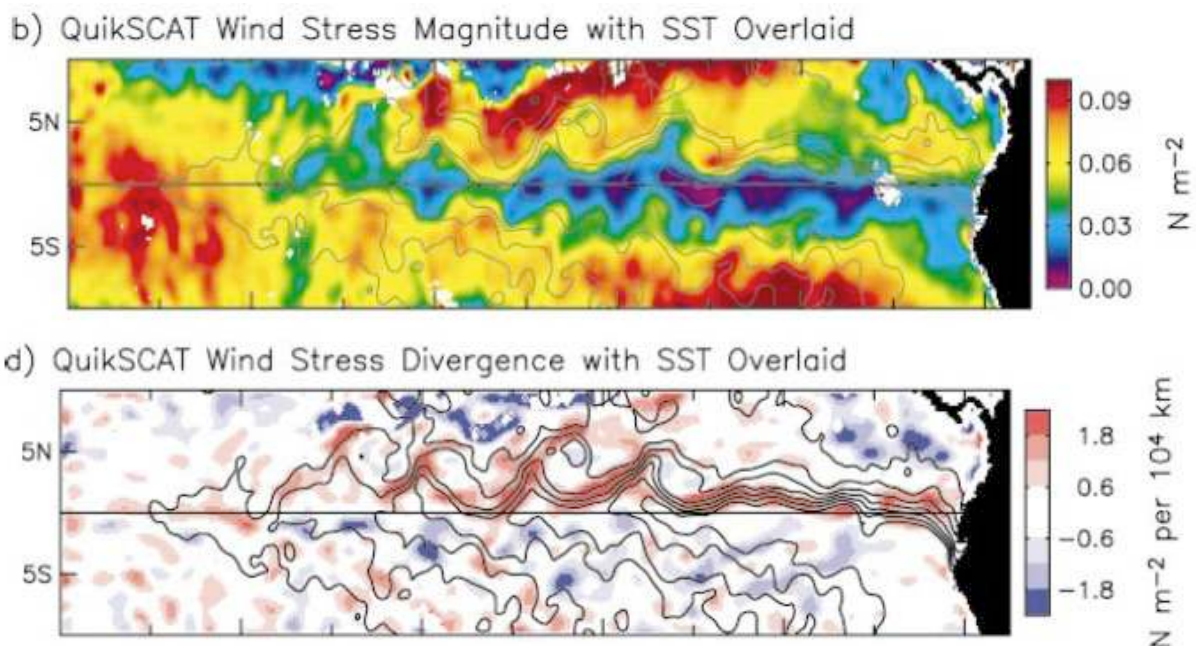


Figure 14. From Chelton et al. (2000). Snapshot of SST (contours) and wind stress magnitude (colors) on top; and of SST (contours) and wind stress divergence on bottom. Decreased vertical mixing in the atmospheric boundary layer causes the easterlies to slow down over cold cusps, causing strong divergence on the leading edge of the TIW.

2.2.2. Selected results

Above, I have presented background information on some aspects of TIWs. In this section, I will present a selection of results pertaining to most of the aspects discussed above. The results in this chapter are highlights from the following publications: Vialard et al. (2001), Vialard et al. (2002), Vialard et al. (2003b), Pezzi et al. (2004), Gorgues et al. (2005), Menkes et al. (2006), Dutrieux et al. (2008).

2.2.2.1. Structure and circulation of TIWs

TIWs are associated with anticyclonic eddies north of the equator, or tropical instability vortices (TIVs). TIVs are about 500 km in diameter, and are responsible for the undulating shape of the equatorial front. They are clearly revealed by surface drifter trajectories (Hansen and Paul 1984; Flament et al. 1996; Kennan and Flament 2000; Menkes et al. 2002; Foltz et al. 2004). Revealing the exact circulation pattern within these vortices is important, because it will explain some of their transport properties, and also their dynamical properties, as we'll see below.

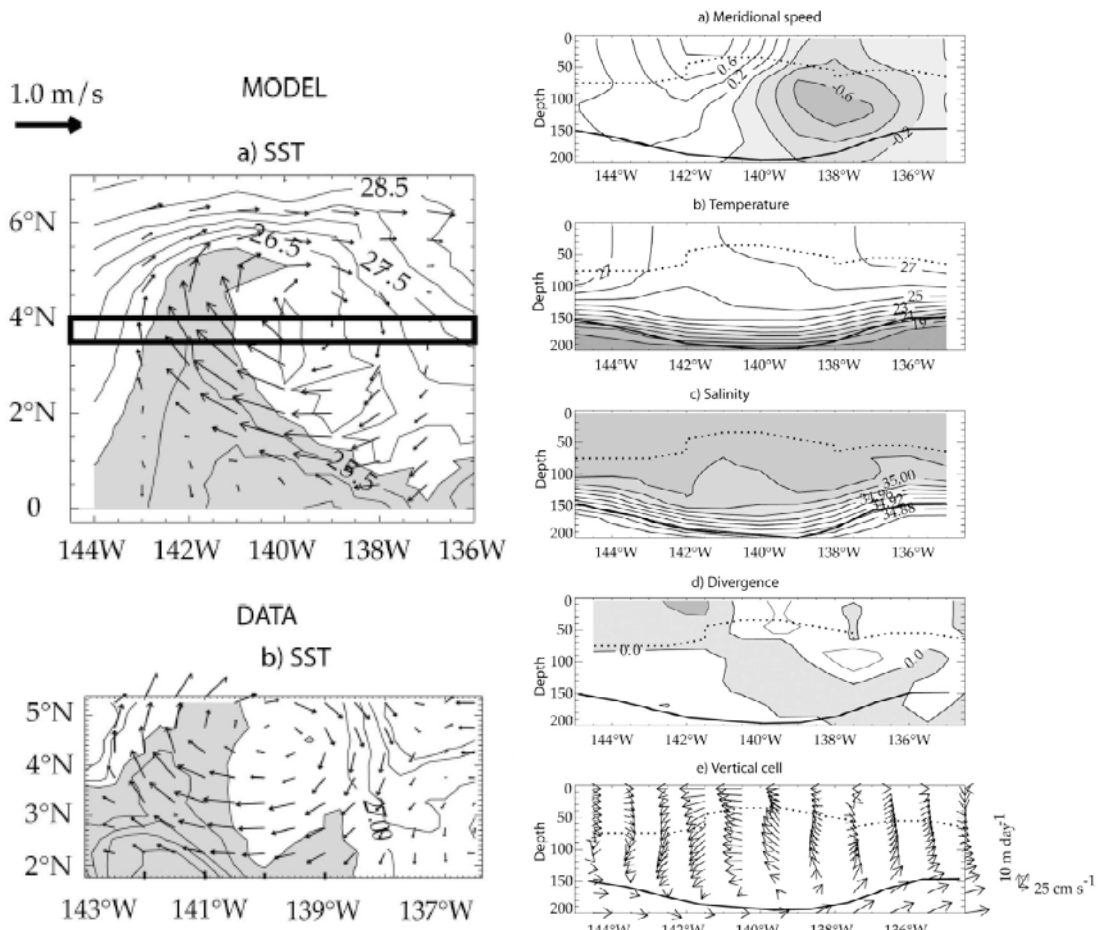


Figure 15. From Menkes et al. (2006). (Left) Horizontal surface structure of SST and currents of a TIV in both model and observations. (Right) Zonal cross section at 4°N (black box indicated on the left) in the model. The results above are quite similar to observations of Kennan and Flament (2000).

Fig. 15 shows the typical circulation pattern within a TIV. There is a clear anticyclonic circulation at the surface, which drives the undulations of the SST front. Note that there is a strong cross-isotherm flow in the southern part of the eddy, which is associated to strong zonal heat advection (next section). The velocity has a tilted structure with maximum northward flow at the surface, while the return southward flow is maximum at ~100m. The anticyclonic vortex is associated with a sea level maximum and a thermocline depression at its centre. There is surface convergence (and downwelling) in the leading edge of the vortex, and divergence (and upwelling) in its trailing edge.

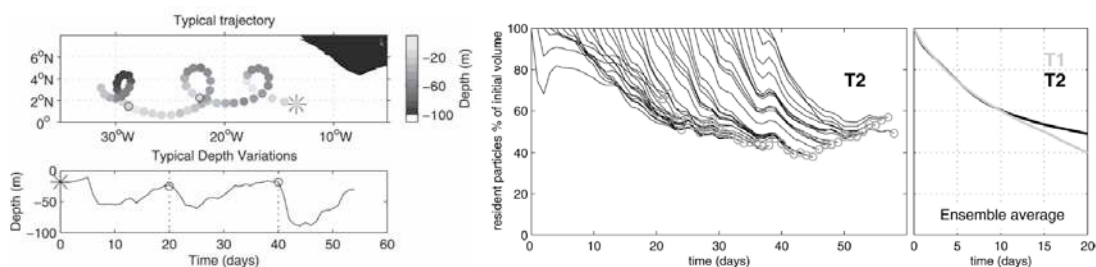


Figure 16. From Dutrieux et al. (2008), here for a numerical experiment of TIVs in the Atlantic ocean. The left panels show the Lagrangian trajectory of a particle inside a TIV and its depth variations. The right panel show how long particles typically reside within the TIV structure. Whereas the TIV remains a coherent dynamical structure throughout its zonal propagation, it constantly exchanges water with its environment.

This picture is consistent with the Lagrangian analysis of Fig. 16. Particles within the vortex describe a cycloidal trajectory, diving in the southwestern part of the vortex, and progressively rising back to the surface as they travel back southward. This typical trajectory of a particle residing inside the vortex should however not hide the fact that the vortex constantly exchanges mass with its environment. Fig 16. shows that after 20 days, the vortex has typically exchanges half of its mass with surrounding waters.

This strong exchange of water with the environment suggests two important consequences. First, to be able to contribute to long term heat transport (next section) throughout the basin, the eddies need be associated with a net particle transport all along their trajectory, as suggested by figure 16. Second, there is some ambiguity about TIWs, which are considered by some largely as a superposition of linear equatorial waves (e.g. Lyman et al. 2005, 2007) and by others as fully non-linear vortices (Flament et al., 1996). In general, a vortex is seen as a body of water in rotation that is more or less isolated from its surroundings. On the contrary, a dispersive linear wave can have a similar current signature, but will not transport mass. TIVs thus appear to be on the fringe of the two cases, because they transport mass zonally over long distances, but still exchange a significant amount of properties with their environment.

2.2.2.2. Heat and salt transport by TIWs

We saw in the previous section that TIWs are associated with strong cross-isotherm currents in the mixed layer. Fig 17. shows that this cross isotherm flow is associated to a significant heating slightly north of the equator (mostly by zonal advection, with some contribution of meridional advection) and a cooling further north (contributed both by zonal advection and meridional advection of the mean SST gradients by meridional current anomalies, Menkes et al. 2006). These terms contribute strongly to the surface layer heat budget at the TIW scale (and a detailed analysis is given in Menkes et al. 2006), but do not average to zero over longer time-scales (last panel of figure 17). This results in a strong horizontal transport of heat and salt, which contributes significantly to the long-term heat budget of the tropical Pacific.

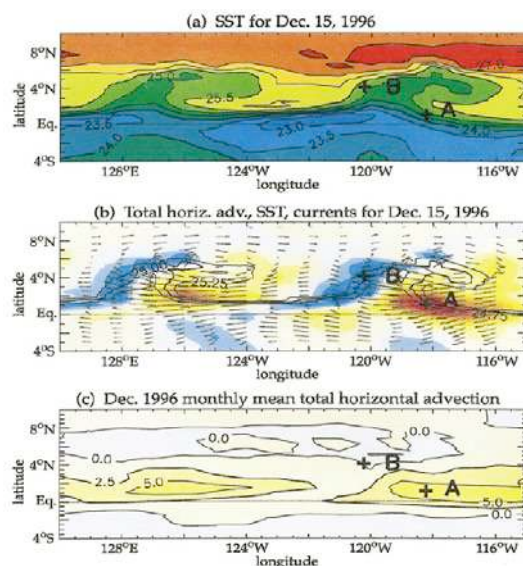


Figure 17. Model results from (Vialard et al. 2001). a) Snapshot of model SST showing TIW cusps; b) Corresponding snapshot of currents (vectors), horizontal advection (colors) and selected isotherms (contours); c) Monthly average of advection terms. The strong zonal advective warming in the trailing edge of the TIW (b) contributes to long-term warming of the cold tongue (c).

At seasonal scale, observational studies have shown that TIWs play a large role in the cold tongue heat budget (e.g. Baturin and Niiler 1997, Swenson and Hansen 1999, Wang and McPhaden 1999). Estimates in those studies suggest that the horizontal TIW flow induces large equatorward transport of heat, equivalent or stronger than the effect of the seasonal surface forcing. In these studies based on observations, however, only the lateral transport of heat by TIWs was quantified, and not the vertical component due to data limitations. However, [Vialard et al. \(2001\)](#) noted that there may be a compensation between the climatological lateral and vertical eddy heat advection associated with TIWs, although they did not explicitly compute vertical eddy heat advection. Thus, the potential compensation between horizontal and vertical TIW-induced mean advection remained to be quantified. If such compensation indeed exists, the TIWs contribution to the long-term budget of the cold tongue might be smaller than what was previously estimated in observational studies that only took into account horizontal heat flux estimates.

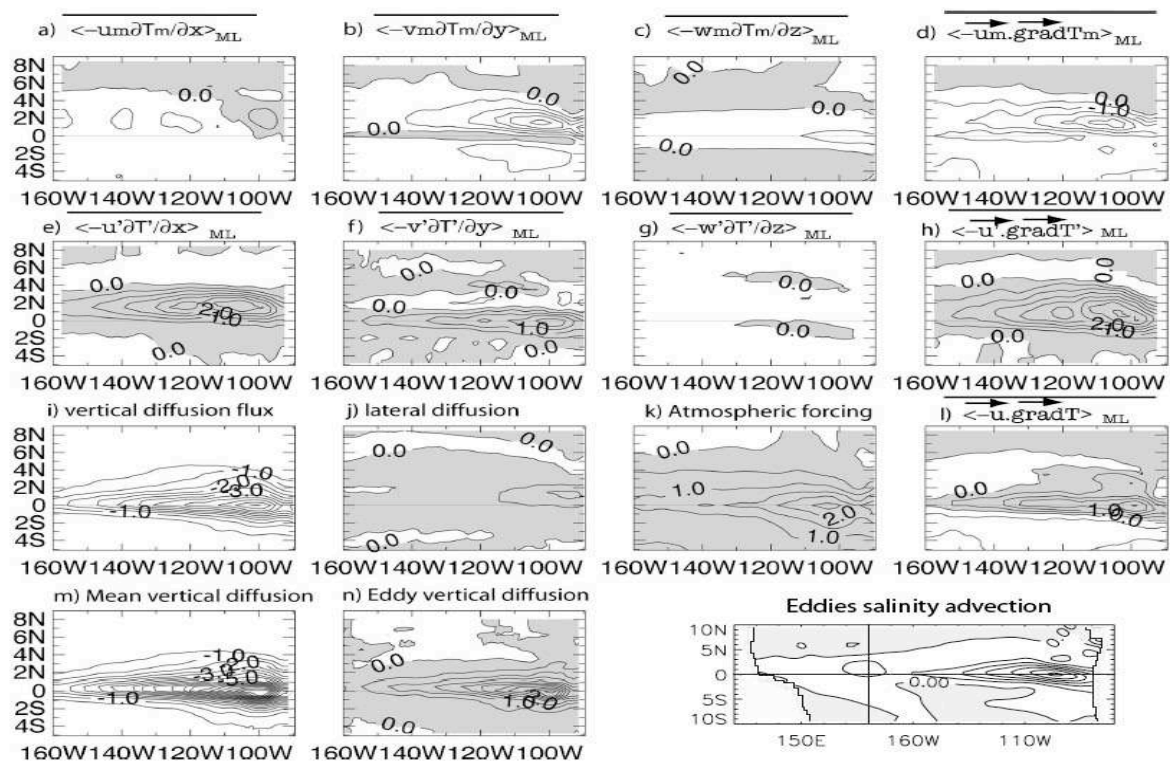


Figure 18. Model results from [Menkes et al \(2006\)](#) and [Vialard et al. \(2002\)](#). Decomposition of the mixed layer heat balance into its various components. The first row shows advection by low-frequency currents. The second row show eddy-terms (i.e. advection by TIWs). The third row shows vertical and lateral diffusion, atmospheric forcing and total advection (eddies + low-frequency). The last row shows the decomposition of the vertical diffusion term into a low-frequency and eddy components. The last panel on the last row shows advection of mixed layer salinity by TIWs. TIWs contribute significantly to long-term warming and freshening of the cold tongue.

A modeling study by [Jochum et al \(2004\)](#) evaluated both meridional and vertical advective heat fluxes associated to TIWs in the Atlantic ocean in the top 20m, and concluded that there was an almost complete compensation between the meridional heat fluxes and vertical heat fluxes. In [Menkes et al. \(2006\)](#), we followed a more physical approach by computing the average mixed layer budget (rather than the top 20m) and decomposing each term in a mean current and TIW contribution (Fig. 18). We also used an advection computation rather than the flux divergence computation. This approach is better suited for

this kind of study, since flux divergence studies do not allow to separate the influence of mass convergence (see [Menkes et al. 2006](#) for details).

In contrast to what has been argued by [Jochum et al. \(2004\)](#), TIW-induced vertical advection (cooling) is negligible in the SST budget (Fig 18g). It however plays a role when considering the heat budget over the upper 200m. Cooling by vertical mixing, however, is structured at the TIW scale and almost compensates for lateral advective heating in the cold cusps. This study lead to a thorough evaluation of all the contributions to the SST balance in the TIW-active region, and confirmed the importance of TIWs in the long term heat budget. Within 160°W-90°W, 2°S-6°N, where TIWs are most active, TIW-induced lateral advection leads to a warming of 0.8°C.month⁻¹ (vertical TIW cooling being negligible), of the same order as the 0.95°C.month⁻¹ effect of atmospheric fluxes, while the mean currents and vertical mixing cool the upper ocean by -0.65°C.month⁻¹ and -1.13°C.month⁻¹ respectively. In the study of [Vialard et al. \(2002\)](#), a similar estimate of contribution of TIWs was made for the salt balance of the tropical Pacific mixed layer (last panel of Fig. 18). The TIWs contribute to transport freshwater from under the ITCZ southward and then westward along the equator. The resulting long-term advection of salt by TIWs is a freshening north of the equator, equivalent in magnitude to the contribution of zonal advection by low frequency currents or vertical mixing.

I will discuss the potential role of heat transport by TIWs in the ENSO cycle in section 2.3.

2.2.2.3. Phase locking of TIWs to the wind

As I mentioned earlier, there is no clear consensus about the exact instability mechanism of TIWs. However, it is quite clear that TIWs are the result of an instability, since they also occur in experiments with constant forcing. If TIWs were developing through amplification of small random perturbations of the background flow, one would expect their phase to be random. However, previous studies suggested this is not the case. [Allen et al. \(1995\)](#) showed that their model correctly predicted observed TIW phase, and suggested that the development of TIWs is phase locked to the background flow fluctuations induced by intraseasonal wind variability. [Benestad et al. \(2001\)](#) showed that TIWs phase in their model was shifted by one week when they shifted the intraseasonal variability of the wind forcing by the same amount.

In [Vialard et al. \(2003\)](#), we took a different approach and investigated the sensitivity of TIWs to initial conditions in an oceanic model, which reproduces many features of observed TIWs. The model was run using realistic forcing for the 1993–99 period and rerun starting from different initial conditions (restarted in July 1993 from the 1993–96 average of the previous run). As expected, TIWs are initially completely uncorrelated in the reference and perturbation experiments. After a few years, however, the TIW phases in the two experiments converge (Fig. 18). In experiments with small initial perturbations, Small differences sometimes grow locally in space and time (i.e., a few TIW cusps can be located differently in the control and perturbed experiments), but never enough to significantly harm the phase agreement over the whole active TIW region. Additional experiments with idealized wind forcing allowed to show that TIWs are phase-locked to the wind forcing and that the phase locking is strongest when the full spectrum of the winds is used rather than, e.g., the seasonal cycle. In the case of constant wind forcing, there is obviously no phase locking, but a limit cycle behaviour.

Those results hence suggest that a numerical model able to reproduce correctly the spatio-temporal characteristics of the TIWs should be able to predict accurately their phase from the information of wind forcing only. To my knowledge, current theories of TIWs do not explain this phase locking to the wind forcing.

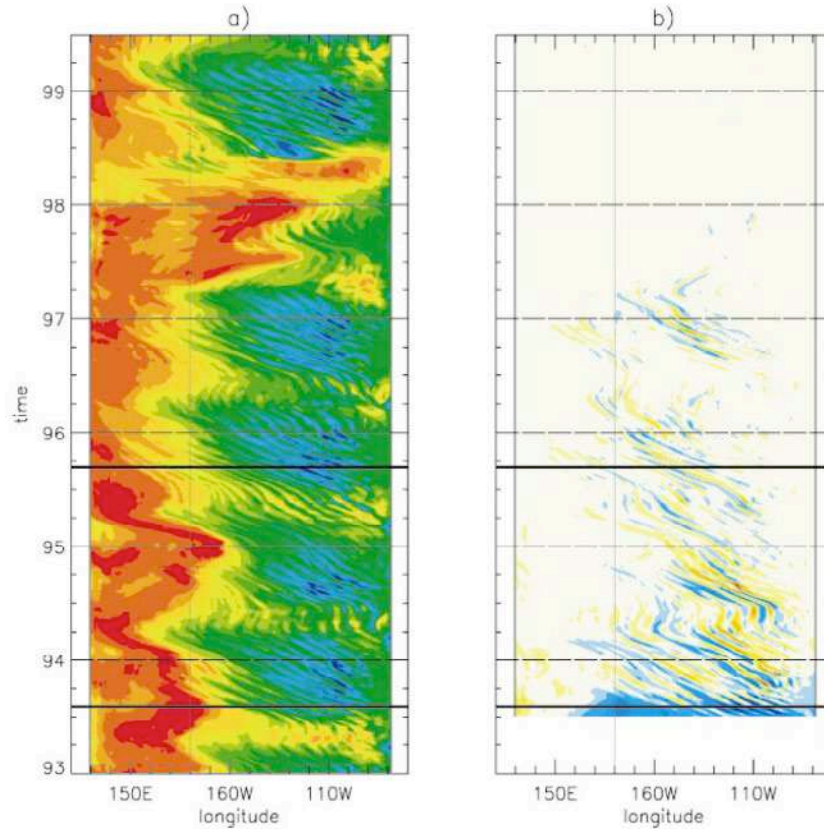


Fig 19. Modelling results from *Vialard et al. (2003)*. Panel a) shows a time-longitude plot of SS at 2°N in a control experiment with realistic winds for the 1993-1999 period. TIWs are clearly visible in this experiment. Panel b) show the difference between panel a) and a sensitivity experiment restarted from the 1993-1996 average of the control run in mid 1993. TIWs come back in pphase after a few year in two experiments with a very different initial state.

2.2.2.4. Air-Sea interactions in TIWs

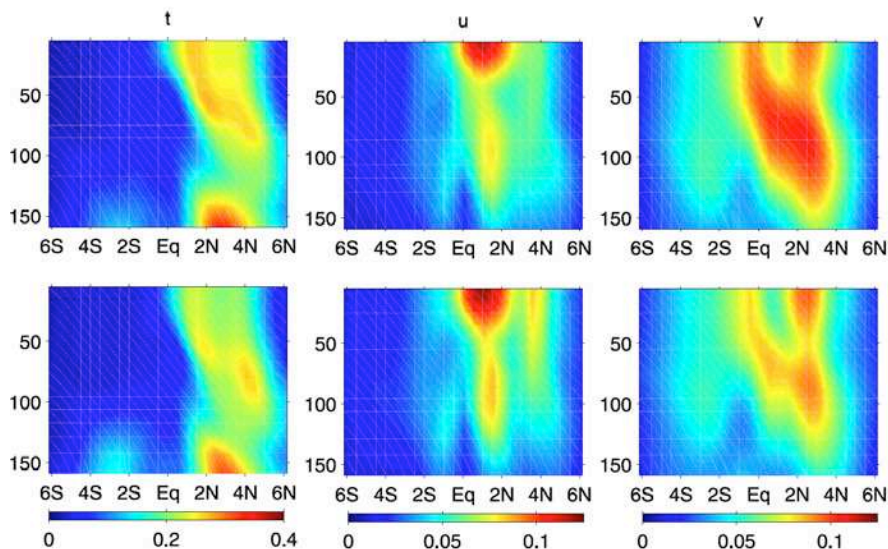


Figure 20. Modelling results from *Pezzi et al. (2004)*. Average standard deviation of temperature, zonal and meridional current between 90°W and 150°W for control experiment with no coupling (first row) and experiment with simple air-sea coupling at TIW-scale (second row). Active air-sea coupling tends to diminish the amplitude of TIWs.

We saw earlier that TIWs have an atmospheric response in wind stress, due in large part to the modulation of vertical mixing in the atmospheric boundary layer by the TIWs cold and warm patches. One interesting question is: does this modulation feedback on TIW properties themselves. To that end, we included a very simple parameterisation of coupling in the ocean model already used to study TIWs in Vialard et al. (2001), Vialard et al. (2002), Vialard et al. (2003b), Menkes et al. (2006). Although very simple, this parametrisation reproduced qualitatively well the observed coupling between wind stress and SST, with a reasonable amplitude. Active coupling results in a negative feedback on TIWs, slightly reducing their temperature and meridional current variability, both at the surface and sub-surface (Fig. 20). This reduced activity modulates the meridional heat and momentum transport, resulting in modest changes to the mean state, with a cooler cold tongue and stronger equatorial currents.

A recent excellent study by Small et al. (2009) pointed out that there are in fact two sources of modulation of wind stress by TIWs: 1) ocean surface currents altering the relative motion between air and sea and hence the stress fields and 2) SST gradients forcing changes in stability and near-surface winds. They could evaluate both effects in their study combining coupled modeling and observations. They corroborated our result that the stability effect only leads to a modest reduction in TIW activity. On the other hand, the different spatial pattern of wind curl associated with the effect of currents drives a much more significant reduction in TIW activity.

2.2.2.5. Biogeochemical impact of TIWs

TIWs also modulate the distribution of biogeochemical parameters. Satellite pictures show clear meridional oscillations of the front separating equatorial nutrient-rich water and oligotrophic water from the north (Chavez et al. 1999). TIW-induced upwelling has been suggested to have a net fertilization effect on the climatology of the equatorial region (Yoder et al. 1994; Strutton et al. 2001; Menkes et al. 2002).

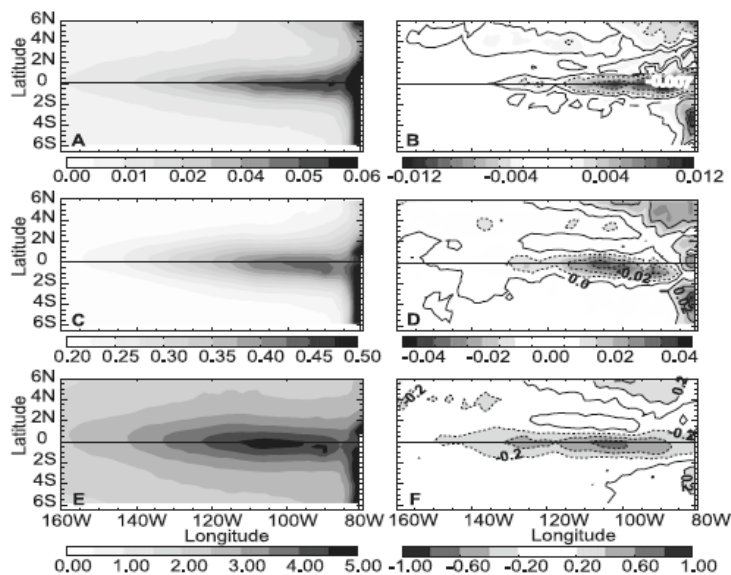


Figure 21. Modelling results from Gorgues et al. (2005). The left column shows the eastern Pacific long-term average values for iron (in nM) (A), chlorophyll (mg m^{-3}) (C) and new production ($\text{mmolN m}^{-2} \text{day}^{-1}$) in a biogeochemical model simulation with realistic forcing. The right column shows difference to the left column in an offline experiment where TIWs have been filtered out. Contrary to the previous conception, TIWs tend to diminish the iron concentration in the cold tongue.

In Gorgues et al. (2005), we used a biogeochemical model to show that, contrary to this suggestion, TIWs induce a decrease of iron concentration by 10% at the equator and by about 3% over the Wyrтки box [90°W–180, 5°N–5°S] (Fig. 21). Chlorophyll decreases by 10% at the equator and 1% over the Wyrтки box. This leads to a decrease of new production up to 10% at the equator (4% over the Wyrтки box). TIW-induced horizontal advection exports iron-rich equatorial water to the north, but also brings iron-depleted water to the equator leading to a net decrease in iron. Additional iron decrease is caused by TIW-induced iron vertical diffusion. These two mechanisms are partly counter balanced by a decrease of iron biological uptake, driven by lower phytoplankton concentrations, and to a lesser extent by TIW-induced iron vertical advection.

2.3 El Niño

2.3.1. Background information

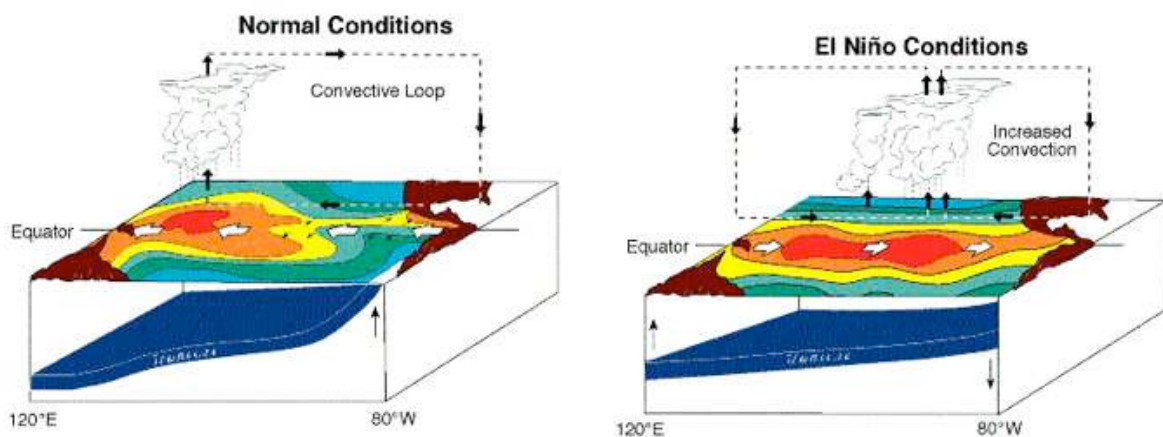


Figure 22. Schematical view of the tropical Pacific ocean during a normal year (left) and during an El Niño (right). The transition from a normal to an El Niño year occurs because of a positive interaction loop named the Bjerknes feedback.

At the simplest level, El Niño develops as the result of the Bjerknes feedback (Bjerknes, 1966), a positive ocean-atmosphere interaction that links the strength of easterlies to surface temperature in the Pacific cold tongue. A warm anomaly in the central Pacific induces a westward displacement of the atmospheric deep convection, and westerly wind anomalies in the central and western Pacific (Fig. 2). The westerly wind anomaly drives an ocean response that reinforces the initial Sea Surface Temperature (SST) anomaly: the downwelling Kelvin wave that is excited has a current contribution that pushes the warm pool to the east and depresses the thermocline in the west. This positive feedback loop eventually leads to anomalous conditions such as those displayed on Figure 22, typically culminating in boreal winter.

This simple instability mechanism is at the heart of all ENSO theories. But it is however incomplete, primarily because it does not describe the return to normal conditions after an El Niño. There are several mechanisms to explain this return to normal condition, and they all involve the ocean as the “memory” to the coupled ocean-atmosphere system. I.e. while the tropospheric wind response is in quasi equilibrium with SST anomalies, the ocean response to these wind perturbations is much slower, and deterministic through, e.g., equatorial wave dynamics. This is what induces some predictability in ENSO, and what allows the coupled-system to revert to its normal state. Four types of negative feedbacks involving this slow response of the ocean have been proposed, and most of them seem to be valid at times (i.e. there is more than one process that can terminate ENSO, and several of them sometimes act together). These processes are:

- the “*delayed oscillator*” (Suarez and Schopf 1988, Battisti and Hirst 1989) was the first to be proposed. Westerly anomalies during the rise of El Niño force upwelling Rossby waves, which reflect at the western boundary and come back after a few months as upwelling Kelvin waves. In the original version of the delayed oscillator, thermocline anomalies associated to these waves tend to cool the SST in the central Pacific, eventually terminating the El Niño. The advective-reflective oscillator was proposed by Picaut et al. (1997). In essence, the idea is not so different than the one of the delayed oscillator (reflected waves induce the termination of El Niño), but this model is more physical in that it underlines the role of zonal advection for modifying SST in the central Pacific. Zonal advection is indeed one of the primary drivers of SST anomalies in the central Pacific during El Niños (see, e.g., the review of Picaut et al. 2001).
- The equatorial Pacific Warm Water Volume (WWV) is an essential parameter in the ENSO cycle (e.g. Meinen and McPhaden, 2000). The “*recharge oscillator*” model of ENSO (Jin, 1997) provides a simple physical explanation: the WWV controls temperature of water upwelled in the eastern Pacific; a high WWV favors a warm anomaly, leading to an El Niño via the Bjerknes feedback. The zonal wind anomalies during an El Niño then induce a zonal pressure gradient that tends to chase warm water away from the equatorial strip, inducing negative WWV anomalies after the ENSO peak and a transition to La Niña.
- The “*western Pacific oscillator*” was proposed by Weisberg and Wang (1997). Easterly wind anomalies tend to develop in the far western Pacific at the height of ENSO (e.g. Wang et al. 1999). These equatorial easterly wind anomalies cause upwelling and cooling (e.g. Vialard et al. 2001) that proceed eastward as a forced ocean response providing a negative feedback to terminate ENSO. Boulanger and Menkes (2001) and Boulanger et al. (2003) demonstrated that, for the 1997–98 El Niño, about two-thirds of the Kelvin wave amplitude is actually forced by easterly wind in the western Pacific and the other one-third is due to wave reflection at the western boundary.

The Unified Oscillator for ENSO

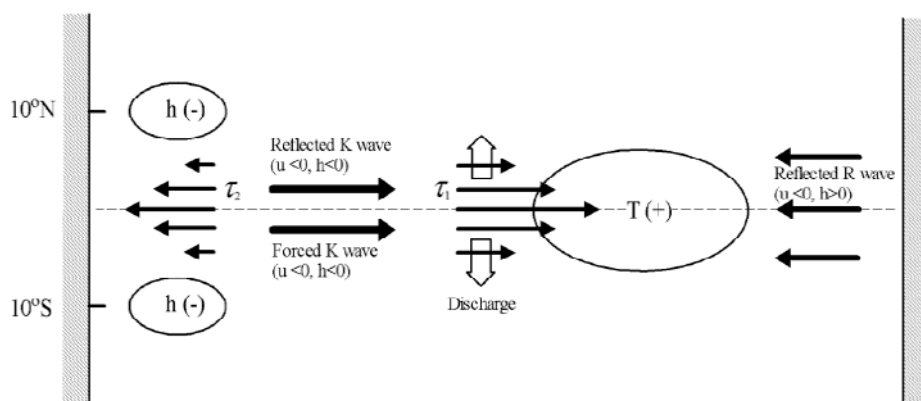


Figure 23. From Wang and Picaut (2004). A summary of the important elements in the main paradigms for negative feedbacks that terminate an ENSO.

While the ocean provides some predictability to ENSO by inducing some long timescales, the atmosphere has a tendency to reduce this predictability because of stochastic forcing. A lot of studies have illustrated the potential role of intraseasonal wind anomalies in the western Pacific on ENSO development through the generation of Kelvin waves (e.g. Kessler and McPhaden 1995; McPhaden 1999; Vialard et al. 2001; McPhaden et al. 2006; Lengaigne et al. 2004). These anomalies include westerly wind bursts (WWBs) and the

Madden Julian Oscillation. WWBs are somewhat related to the MJO (they occur more frequently within the background westerly flow associated with the active phase of the MJO, Seiki and Takayabu, 2007), but are synoptic features, while the MJO is planetary scale. In both case, the basic mechanism is the same: the westerly winds force downwelling Kelvin wave, which tend to push the warm pool eastward and depress the thermocline in the western Pacific. In the case of the MJO, however, it is not obvious how a weak, zero-average signal (the MJO also has suppressed phases, associated with *easterly* wind anomalies) can induce a low frequency response of the coupled system. It has been suggested that the westerly MJO wind anomalies are more efficient than the easterly, because it pushes the warm pool eastward and extends the fetch of the region over which the MJO is active (Kessler and McPhaden 1995; Hendon et al. 1998). It has also been suggested that resonance at lowest frequencies makes the low-frequency tail (periods longer than ~60 days) of the MJO more efficient in generating coupled model response than the higher frequency part (Hendon et al. 1998; Zavala-Garay et al. 2008).

2.3.2. Selected results

The results in this chapter are highlights from the following publications: Vialard et al. (2001), Radenac et al. (2001), Picaut et al. (2001), Vialard et al. (2002), Zavala-Garay et al. (2008) for the processes of El Niño; and Troccoli et al. (2002), Tang et al. (2003), Weaver et al. (2003), Moore et al. (2003), Vialard et al. (2003a), Vossepoel et al. (2004), Tang et al. (2004), Vialard et al. (2005), Ricci et al. (2005), Moore et al. (2006) for the prediction and predictability parts.

2.3.2.1. Processes of El Niño

The 1997-98 El Niño was the strongest and best-observed of the 20th century (e.g. McPhaden, 1999). Modeling studies of the 1997-98 El Niño by Vialard et al. (2001), Radenac et al. (2001), Vialard et al. (2002) illustrate many important processes in the rise and fall of an El Niño.

Role of westerly wind bursts

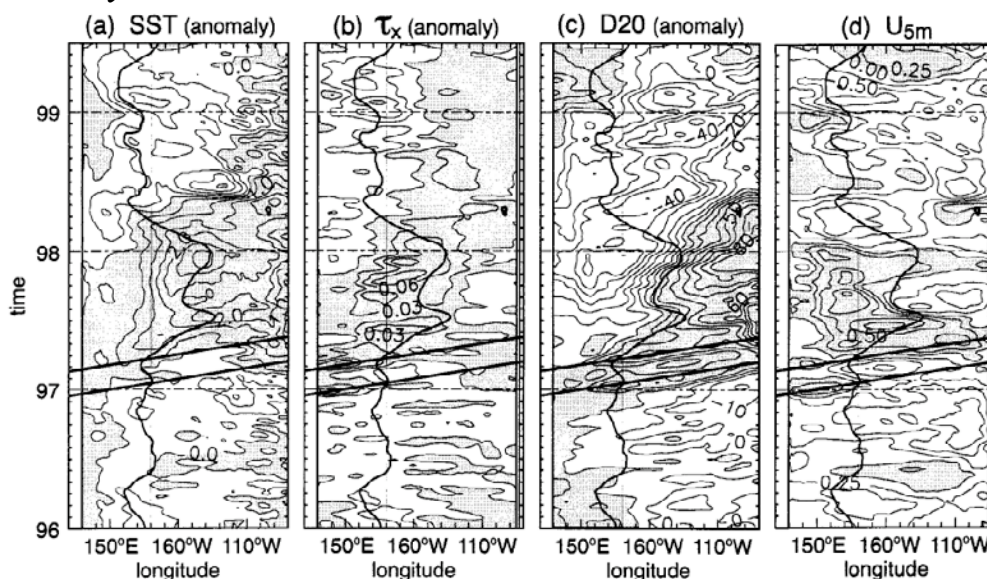


Figure 24. Modelling results from Vialard et al. (2001). Longitude-time section of 2°N-2°S averaged a) SST, b) Zonal wind stress, c) depth of the 20°C isotherm interannual anomalies and d) zonal surface current, during the 1997-98 El Niño. The thick contour in all 3 plots is the model's 28°C isotherm. The two thick lines indicate the downwelling Kelvin waves associated with the December 1997 and March 1998 WWBs.

Fig. 24 shows ocean model results for the 1997-98 El Niño, using realistic forcing. The model displays two very clear downwelling Kelvin waves (Fig. 24c) associated with the westerly wind bursts of December 1997 and March 1998 (Fig. 24b). These Kelvin waves seem to initiate the warm pool eastward displacement in the central Pacific, and weakening of the cold tongue in the eastern Pacific (Fig. 24a). An analysis of surface layer heat budget (Fig. 25, [Vialard and Delecluse, 1998a](#) for the description of the method) allows to understand better the various processes of the SST change associated with this Kelvin wave.

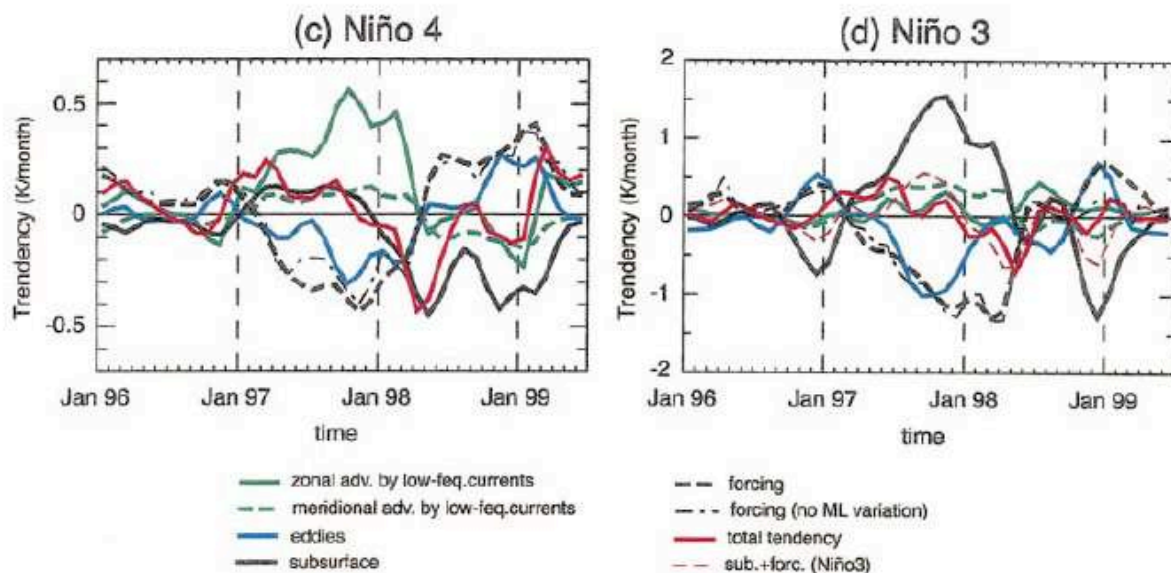


Figure 25. Modelling results from [Vialard et al. \(2001\)](#). Interannual anomalies of the surface layer heat budget during the 1997-98 El Niño averaged in the Niño 4 (5°N - 5°S , 50°W - 160°E ; left) and Niño 3 (5°N - 5°S , 90°W - 150°W ; right) boxes. Zonal advection dominates the SST changes in the central Pacific, while vertical processes are very important in the cold tongue. TIWs suppression provide a negative feedback to El Niño growth.

In the central Pacific (Niño4 box), the main process responsible for SST rise (initially, but also until the end of 1998) is zonal advection: it is the zonal current anomaly associated with the downwelling Kelvin wave that initially pushed the warm pool eastward. In the eastern Pacific, the main contribution is from vertical processes (vertical advection and mixing): the deepening of the thermocline results in diminished cooling.

Role of salinity and zonal advection

As we have seen above, zonal advection plays a fundamental role in the central Pacific, while vertical processes tend to be more important in the eastern part of the basin. During my PhD, I had shown that the peculiar haline structure of the warm contributes to the strong role of zonal advection in the central Pacific.

The eastern edge of the western Pacific warm pool corresponds to the separation between the warm, rainfall-induced low-salinity waters of the warm pool and the cold, high-salinity upwelled waters of the cold tongue in the central-eastern equatorial Pacific. Although not well defined in sea surface temperature (SST), this eastern edge is characterized by a sharp salinity front (Fig 26., [Vialard and Delecluse, 1998ab](#)). This front is the result of the zonal convergence of the western and central Pacific water masses into the eastern edge of the warm pool ([Vialard and Delecluse, 1998b](#)). This occurs through the frequent encounter of the eastward jets in the warm pool and the westward South Equatorial Current in the cold tongue. These wind-driven zonal currents are advecting the warm pool back and forth over thousands of kilometers, in synchrony with the ENSO cycle. The strong haline stratification in the fresh

pool contributes to trap atmospheric momentum in the surface layer and to increase the warm pool zonal movements (Vialard and Delecluse, 1998a).

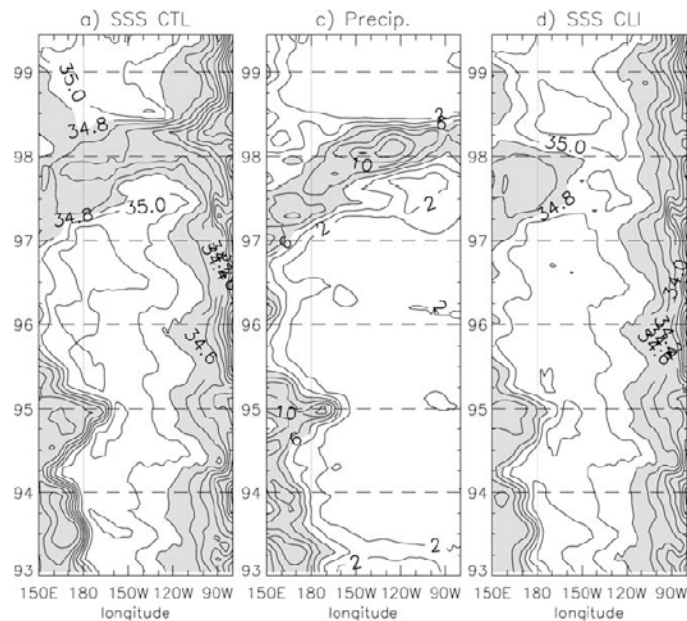


Figure 26. Modelling results from Vialard et al. (2002). Time-longitude section of 2°N-2°S a) SSS, and b) precipitation in a control experiment using realistic forcing. Panel c) shows a sensitivity experiment with climatological precipitation. The front movements are due to zonal advection and not to precipitation anomalies. However, precipitation makes a strong contribution to the freshening in the eastern Pacific.

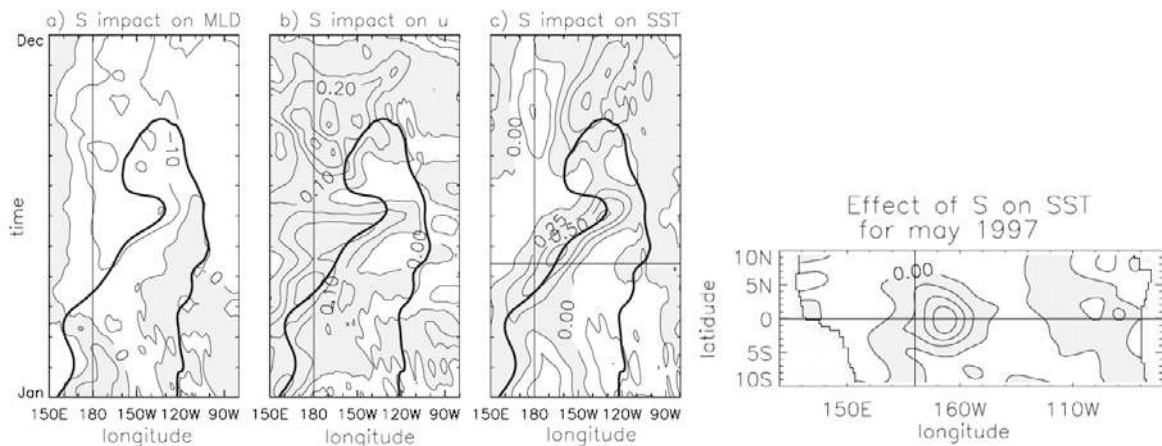


Figure 27. Modelling results from Vialard et al. (2002). Longitude-time sections of estimated salinity effects during 1998 on (a) mixed layer depth (contour every 10 m), (b) surface zonal current (contour every 0.1 m s^{-1}) and (c) SST (contour every 0.25°C). Positive values (shaded) indicate that salinity effects favour warmer water, deeper mixed layer, or surface currents more to the east. The thick line indicates the position of the 34.8 psu isohaline. The map shows the salinity effect on SST in May 1997 (contour every 0.25°C , horizontal line in panel c). Salinity effects tend to favour eastward migration of the front and can induce monthly anomalies of $\sim 0.75^\circ\text{C}$ over $\sim 1000\text{-}2000 \text{ km}$.

The numerical experiments I had performed during my PhD suffered from a strong salinity bias, which might have resulted in an overestimate of the salinity effects. They also did not cover the strong, well observed 1997-98 El Niño. I thus re-evaluated my PhD results with a new modeling experiments using better wind forcing, and a flux correction approach

which resulted in a spectacular agreement between the model SSS and TAO observations (Vialard et al. 2002).

Since deep atmospheric convection moves zonally along with the warm and fresh pool (Fig. 26), there was always a doubt about the relative contribution of rainfall and zonal advection in producing the fresh pool zonal displacements. In an experiment with climatological freshwater forcing (Fig. 26d), the front is slightly eroded, but still displays zonal displacements consistent with the control experiment and observations (Vialard et al. 2002). Zonal advection is hence the main mechanisms for the salinity (and temperature) front zonal displacements in the central Pacific. On the other hand, east of 150°W, the salinity is strongly degraded when using climatological precipitation. Interannual variability of rainfall is hence important for the surface salinity balance in the eastern Pacific.

A sensitivity experiment was then performed to evaluate the effect of salinity during the 1997-98 El Niño (Fig. 27). Neglecting salinity stratification results in a deeper mixed layer in the warm / fresh pool (Fig. 27a). The westward wind anomalies of the WWBs and El Niño are thus distributed over a thicker layer and result in less intense eastward currents (Fig. 27b). The eastward advection of the warm pool is thus less efficient, and the warm pool eastward extension is diminished by about 2000 km during most of the El Niño. The SST anomalies might appear rather weak (around 0.5 to 0.75°C, Fig 27), but they are located in a region where the mean SST is close to the convective threshold, and where small SST changes can induce a significant response (e.g. Palmer and Mansfield, 1984).

Role of western Pacific winds

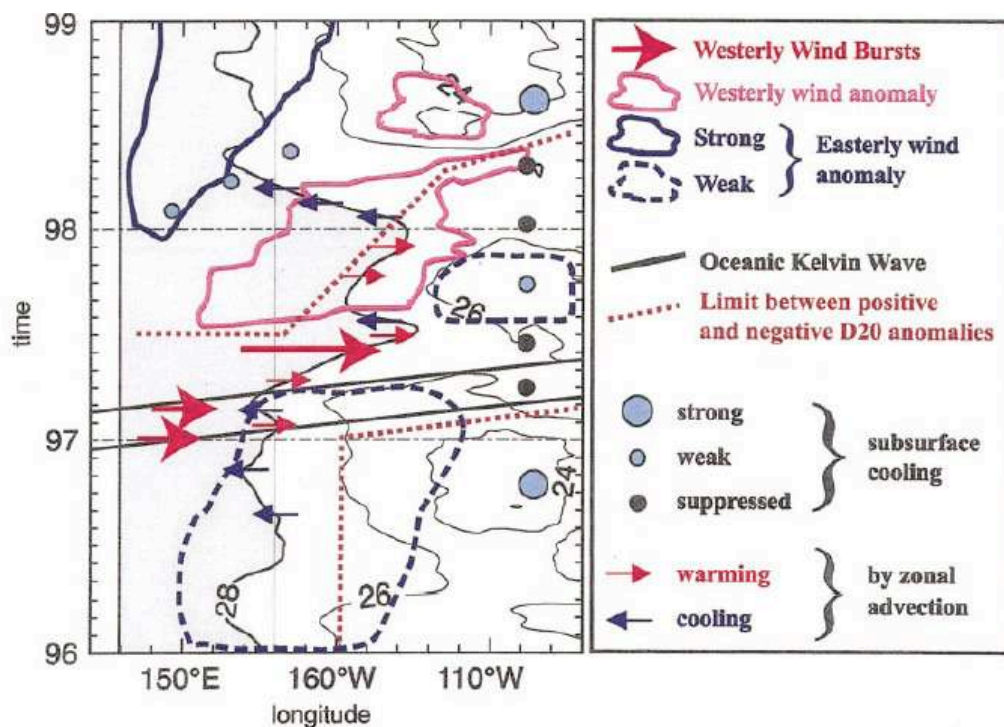


Figure 28. Figure from Vialard et al. (2001). Sketch summarizing the main processes at work during the rise and fall of the 1997-1998 El Niño.

While El Niño was reaching its mature phase, large-scale easterly wind anomalies developed and strengthened in the far western Pacific ocean (Fig. 24) and spread eastward, from the end of 1997 onward. These easterly anomalies, combined to the delayed oscillator mechanism, contributed to the end of the El Niño. In the far-western Pacific, because of the shallower than normal thermocline (Fig. 24), these easterlies cooled the SST by vertical

processes (Figs. 25, 28). In the central Pacific, easterlies pushed the warm pool back to the west through zonal advection (Figs 24, 25, 28). In the east, they led to a shallower thermocline, which ultimately allowed subsurface cooling to resume and to quickly cool the surface layer (Figs 24, 25, 28).

Role of TIWs

Tropical instability waves feed on the current horizontal shear between the SEC and EUC and SEC and NECC and/or density contrast between the cold tongue and waters to the north of it. When these current shear and density gradients become weaker (e.g. in May during the seasonal cycle or during El Niño events), the TIW activity in the eastern and central Pacific diminishes drastically (Fig. 19). Since TIWs are a source of heat (and freshwater) to the cold tongue (section 2.2.2.2, Fig. 17), the suppression of this heat source represents (in anomaly) a negative feedback to the development of El Niño (blue curve in Fig. 25). This negative feedback is almost as large as the one from surface heat fluxes (the flux feedback arises because of increased cloudiness over warm waters, and larger heat losses due to evaporative and longwave cooling). The anomalous contribution of TIWs heat transport is one of the three dominant terms in the eastern Pacific interannual heat balance (along with atmospheric forcing and subsurface processes). On the basis of this and other related studies, there has been a suggestion that TIWs could play some role in explaining the asymmetries of the ENSO cycle. El Niño events indeed tend to have a larger amplitude than La Niña events. This was suggested to be due to the TIW feedback (e.g. An 2008). The total suppression of TIWs (as during the 1997-98 El Niño) indeed provides an upper bound for the TIW-heat transport negative feedback, while TIWs activity has no such obvious upward bound during a La Niña.

2.3.2.2. Predictability and prediction

As was mentioned above, it is the ocean that provides the “memory” of the coupled system for ENSO. In particular, the detailed distribution of the mass field in the equatorial Pacific is important for the evolution of the ENSO phase (e.g. is the WWV volume large or depleted within the discharge oscillator paradigm; is there an upwelling equatorial Kelvin wave on its way to the eastern Pacific, etc...). It thus seems advisable to initialize coupled forecasts of ENSO with an oceanic state which is as accurate as possible. Furthermore, the ENSO variability is such an important piece of the climate variability, with global teleconnections that reliable ENSO forecasts seem to be the pre-requisite of any seasonal forecasting system (Palmer and Anderson, 1994).

I spent 3 years the seasonal forecasting group at ECMWF from 1999 to 2001. I was in charge of the ocean data assimilation system there. That’s how I got involved in ocean data assimilation and seasonal forecasts. The present document is mostly concerned with mechanisms, so I won’t dive into the technicalities of the data assimilation and predictability studies. I will however give a brief account of the most significant advances I contributed to in this field.

Estimating the state of the Pacific Ocean

As underlined above, the estimate of the oceanic state needs to be as accurate as possible to initialize seasonal forecasts with a coupled general circulation model. The step by which available oceanic observations (in situ profiles, sea level, SST, etc..) are combined with the estimated state from the model is called data assimilation. Most of the methods used in ocean data assimilation are issued from Numerical weather forecast. There are, however, some specificities to the ocean data assimilation problem, which require some care.

One of these problems is that there are much more observations of temperature profiles than salinity profiles. In the real ocean a lot of the changes at the thermocline depth are due to vertical displacements (due to Ekman pumping, remote forcing, a passing eddy...) that affect both the temperature and salinity profiles. Assimilating temperature data only can generate spurious mixing in some region where salinity tends to destabilize the profile. A practical solution to that is to also correct the temperature profile below the mixed layer by assuming that T-S properties are conserved (Troccoli et al. 2002; Segshneider et al. 2001). This technique was also adapted and applied with a variational data assimilation approach, and resulted in increased consistency of the oceanic analysis (Ricci et al. 2005), and reduced largely the spurious features associated with univariate assimilation of temperature profiles.

The “classical” approach to data assimilation is sequential: the model is run forward to obtain a new estimate of the ocean state. This state is combined with available observations using the so-called “BLUE” (best linear unbiased estimator) approach, either using a statistical approach (optimal interpolation) or variational approach (3D-Var). In this estimation step, it is essential to prescribe the statistical properties of the resulting analysis as well as possible. These statistical properties should include physical properties, which are desirable for the solution, such as geostrophy, or, as mentioned above, conservation of T-S properties below outside mixing regions. Another complementary way to obtain solutions with desirable physical properties is to use the model himself as a constraint in the assimilation step. This is done by minimizing a cost function measuring the distance between the model trajectory and observations, by controlling some model variables (most often the initial conditions). I contributed to the development and physical evaluation of such a four-dimensional variational method (4D-Var) approach (Weaver et al. 2003, Vialard et al. 2003b). The 4D-Var indeed improved some aspects of the analysed solution over the 3D-Var. The better performance of 4D-Var is attributed to multivariate aspects of the analysis coming from the use of the linearized ocean dynamics as a constraint. In addition to these experiments, where the oceanic initial state was used as a control variable, we also experimented with controlling the wind forcing (Vossepoel et al. 2004). This is arguably a better approach for ocean large-scale circulation, which is deterministically forced by the atmosphere. However, in practice, because of model error, controlling initial conditions seems to remain a more practical approach.

A practical approach to El Niño ensemble forecasting

Once an oceanic initial state is available, another problem of seasonal forecast is to estimate correctly the uncertainties in the forecast. Seasonal forecasts are subject to various types of errors: amplification of errors in oceanic initial conditions, errors due to the unpredictable nature of the synoptic atmospheric variability, and coupled model error. Ensemble forecasting is usually used in an attempt to sample some or all of these various sources of error. How to build an ensemble forecasting system in the seasonal range remains a largely unexplored area. I tested and compared various ensemble generation methodologies for the European Centre for Medium-Range Weather Forecasts (ECMWF) seasonal forecasting system (Vialard et al. 2005). A series of experiments using wind perturbations (applied when generating the oceanic initial conditions), sea surface temperature (SST) perturbations to those initial conditions, and random perturbation to the atmosphere during the forecast, individually and collectively, was compared with the more usual “lagged-average” approach (e.g. starting one forecast every day, and then using one month worth of forecast as an ensemble). SST perturbations are important during the first 2 months of the forecast to ensure a spread at least equal to the uncertainty level on the SST measure. From month 3 onward, all methods give a similar spread. This spread is significantly smaller than the rms error of the forecasts. There is also no clear link between the spread of the ensemble and the

ensemble mean forecast error. These two facts suggested that factors not presently sampled in the ensemble, such as model error, act to limit the forecast skill. This study hence suggested that methods that allow sampling of model error, such as multimodel ensembles, should be beneficial to seasonal forecasting.

Generalized stability analysis of the tropical Pacific Ocean-atmosphere system

In addition to the practical approach above to estimating predictability of the coupled system, some objective methods exist to estimate error growth in the coupled system. These methods are derived from the so-called “generalized stability analysis method” (Farrel and Ioannou, 1996ab). These methods allow computing explicitly the fastest growing perturbations over a finite time. In systems governed by geophysical fluid dynamic equations, there are indeed perturbations that can grow faster than most unstable mode of the linear system over a finite time because of a property called “non normality”. One can even have transient growth in an asymptotically stable system. This method thus provides the most general way to qualify the patterns of fastest growing perturbations in a model, and is used routinely for the ensemble long weather forecasts at ECMWF (e.g. Molteni et al., 1996). This method requires an “adjoint” model, similar to the one used in 4D-Var data assimilation (Weaver et al. 2003, Vialard et al. 2003b).

Generalised stability analysis had previously only been applied in simple coupled models (e.g. Moore and Kleeman, 1996). In Moore et al. (2003, 2006) we used a full Ocean General Circulation Model coupled to several simplified representations of the atmosphere (the so-called “hybrid” approach) to perform a generalized stability analysis. We found that the structure of the optimal perturbations was more controlled by atmospheric dynamics than by oceanic ones.

I also contributed to a similar work, investigating optimal perturbations of the meridional heat transport in the Atlantic ocean in a planetary geostrophic model and in a general circulation model (Sévellec et al., 2008, 2009).

3. Indian Basin

In the sixties and seventies, the Indian Ocean received a lot of attention from physical oceanographers. The strong and striking annual cycle of the winds associated with the Indian monsoon indeed made it an ideal ocean to test the concepts of the equatorial linear wave theory. And the linear equatorial wave theory indeed had brilliant successes in explaining many features of, e.g., the Wyrtki jet (Wyrtki, 1973) or the Somali current reversal (Lighthill, 1969). But, with the rise of the TOGA decade, the Indian Ocean suffered from the shade from the powerful El Niño in the neighbouring Pacific. While the Pacific, and then the Atlantic, witnessed the development of a basin-scale observing system (with the basin-scale TAO and PIRATA mooring arrays as central pieces), the Indian Ocean became the least observed of the three tropical oceans.

While this was partially due to logistical problems and vandalism in the Indian Ocean, this was also linked to the fact that climate scientists largely perceived the Indian Ocean as passive, contrary to the Pacific (and Atlantic Oceans), which clearly had identified modes of variability. In fact, early studies had already pointed to the existence of an independent mode of variability in the Indian Ocean (e.g. Reverdin et al. 1986, Hastenrath et al 1993), but it was not until the strong 1997 IOD (Webster et al. 1999, Saji et al. 1999, Murtugudde et al. 2000) that the Indian Ocean received the attention it deserves. One consequence of this was the design of an observing system by the CLIVAR Indian Ocean Panel, which eventually led to the RAMA mooring array. Another consequence was the increased number of process studies in the Indian Ocean, including the Cirene cruise, for which I was chief scientist.

3.1. Background

3.1.1. Interannual variability of the Indian Ocean

We saw briefly in section 1.4 that the Indian Ocean has two main interannual signals: one which is related to El Niño, and one related to the Indian Ocean dipole.

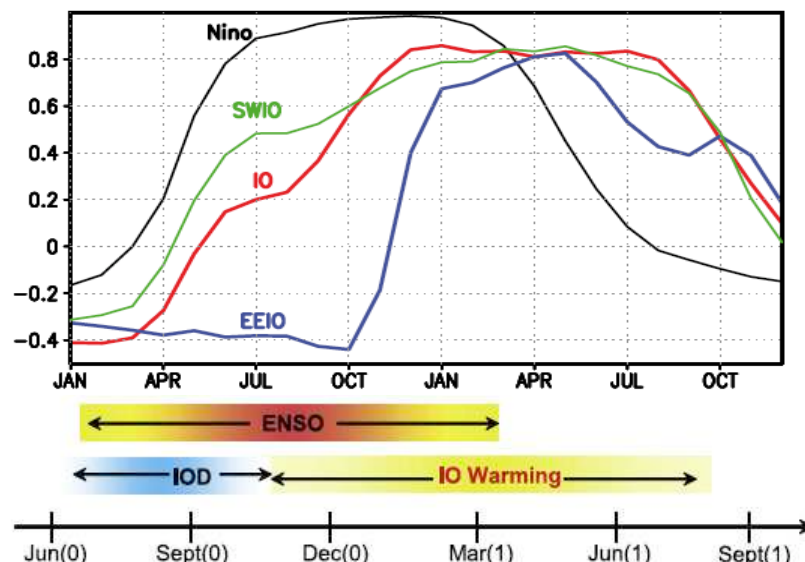


Figure 29. From Schott et al. (2009) (Top) November (year 0)–January (year 1) Niño3 SST correlation with SST averaged in the eastern equatorial Pacific (160–120°W, 5°S–5°N; black), the tropical IO (40–100°E, 20°S–20°N; red), the southwest IO (50–70°E, 15–5°S; green), and the eastern equatorial IO (90–110°E, 10°S–equator; blue). (Bottom) Seasonality of major interannual IO climate modes. The warming in the the Indian Ocean persist after the end of an El Niño (“capacitor effect” of the Indian Ocean) and the IOD tend to co-occur with El Niño.

During an ENSO, the shift in convection in the Pacific Ocean is associated with anomalous subsidence over the Indian Ocean. This leads to increased downward surface shortwave flux that raises uniformly the SST of the Indian Ocean (e.g Klein et al. 1999, Lau and Nath, 2000). The warming starts roughly in July before the peak of ENSO, and persists until the following summer, while SST anomalies in the Pacific Ocean have themselves disappeared (Fig. 29). This long lasting effect of the ENSO influence on the Indian Ocean has been referred to as the “capacitor” effect of the Indian Ocean (e.g. Xie et al. 2009). The tropical Indian Ocean warms in response to El Niño, and this warming continues to affect precipitation in the Indian Ocean and surrounding regions after the end of El Niño.

The IOD has a tendency to co-occur with ENSO. However, 11 out of 19 IOD episodes between 1958 and 1997 happened independently of ENSO (e.g. Saji and Yamagata 2003). Similarly, many coupled general circulation models still display IOD-type variability over the Indian Ocean when the Pacific Ocean is constrained to climatological conditions (e.g. Fischer et al. 2005, Behera et al. 2006). Both observations and models hence tend to support the idea that the IOD is an intrinsic mode of variability of the Indian Ocean, but that El Niño can trigger it.

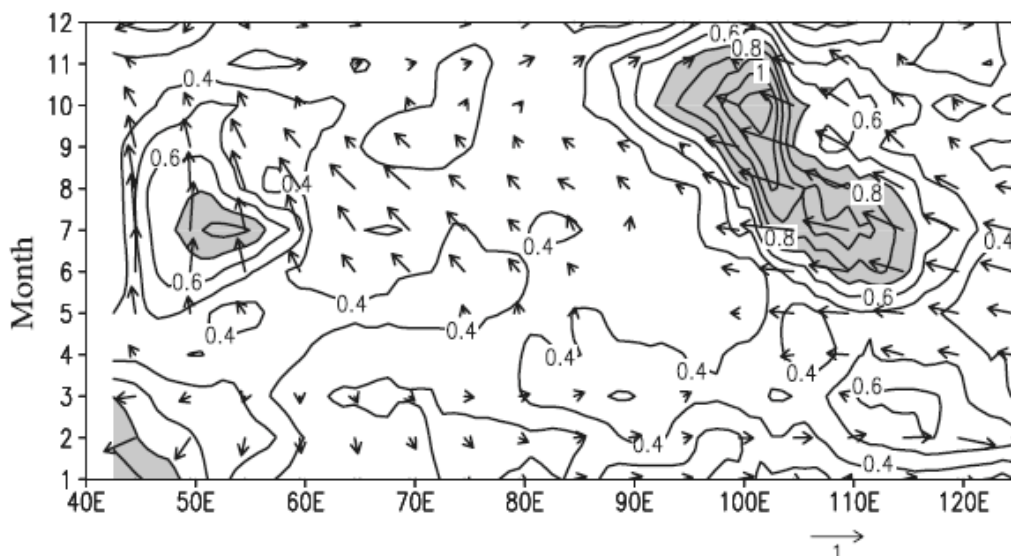


Figure 30. From Xie et al. (2002). Distance-time section of climatological wind stress vectors (N/m^2) and root-mean-square interannual variance of SST (contours; shade $> 0.7^\circ C$) along the equator and the Indonesia coast (east of $97^\circ E$). Along Indonesia, the alongshore (across-shore) wind component is given by the horizontal (vertical) component of the vector. Increased interannual SST variability occurs when the wind favour coastal upwelling along Indonesia, and make the Bjerknes feedback possible.

Southeasterly wind and elevated thermocline are present from April to October near the coast of Sumatra (Fig. 30). This creates a window over which wind perturbations can easily induce SST anomalies and activate the Bjerknes feedback. After that, the Australian monsoon induces westward wind components that deepen the thermocline and close the window for the Bjerknes feedback to act.

During an El Niño, suppressed convection over the maritime continent is associated with easterly wind anomalies over the eastern Indian Ocean, as expected from the Gill model. This induces increased upwelling along the Sumatra coast, which reinforces the suppression of convection and the wind anomalies, thus triggering the Bjerknes feedback. This explains the tendency of the IOD to co-occur with ENSO, but it can also occur when wind or SST perturbations develop in the eastern equatorial Indian Ocean, independently of El Niño.

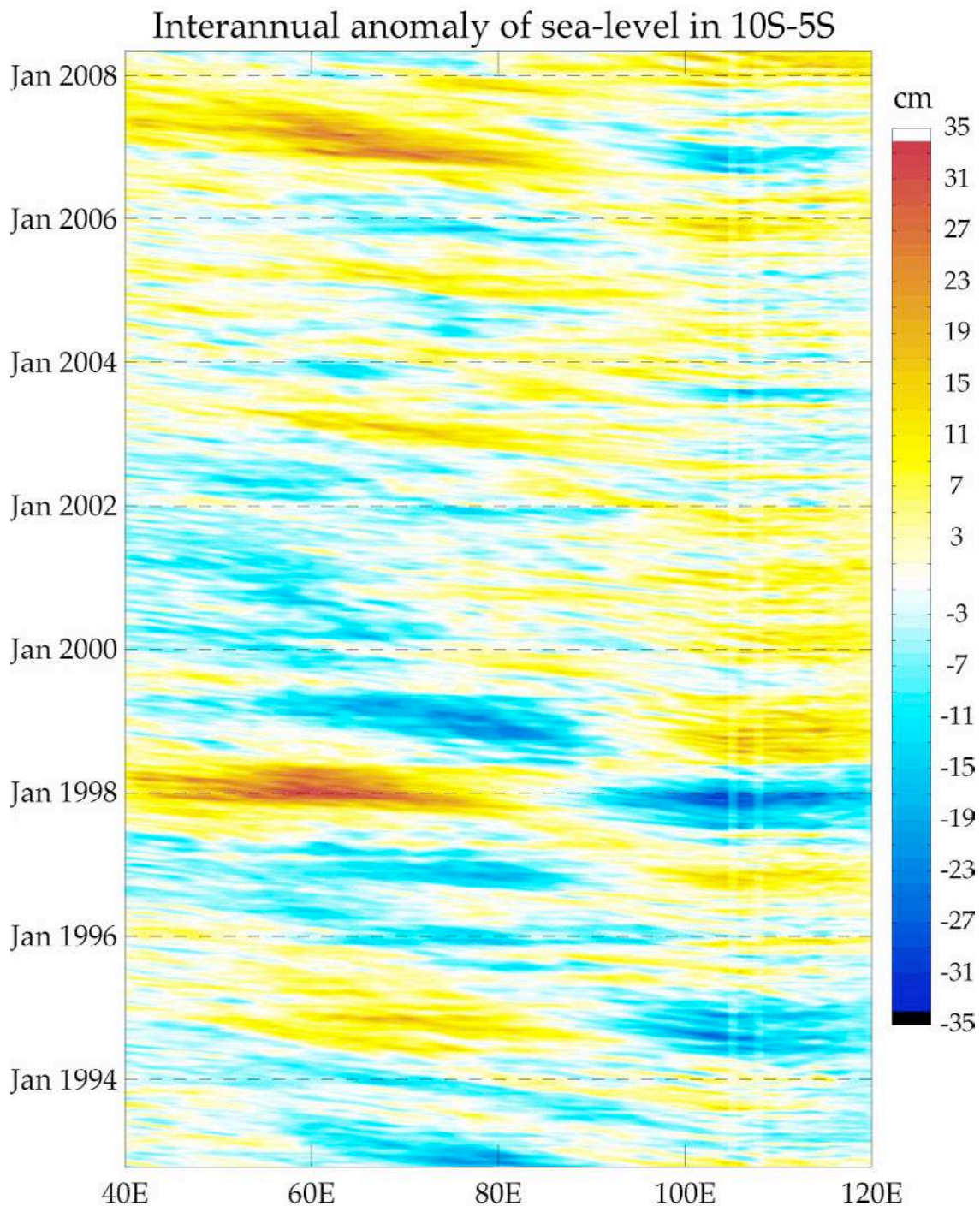


Figure 31. Sea level interannual anomaly in the Indian Ocean averaged between 10°S and 5°S. Strong interannual anomalies develop in this band in response to both the IOD and ENSO.

Marked sea level variability in the 5°S-15°S band of the ocean has been noted long ago (e.g. Perigaud and Delecluse 1993, Masumoto and Meyers 1998), with clear westward phase propagation associated with planetary waves (Fig. 31). Such variability occurs both during an IOD or “pure” El Niño year, although at different latitudes. Because of local coupling in the Indian ocean the surface wind anomalies are more equatorial during an IOD year than a “pure” El Niño year, when they are shifted 5 to 10° southward (Fig. 32). As a result, Ekman convergence occurs mostly between 3 and 10°S during IODs, while it is largest between 8 and 15°S during El Niños (Fig. 32).

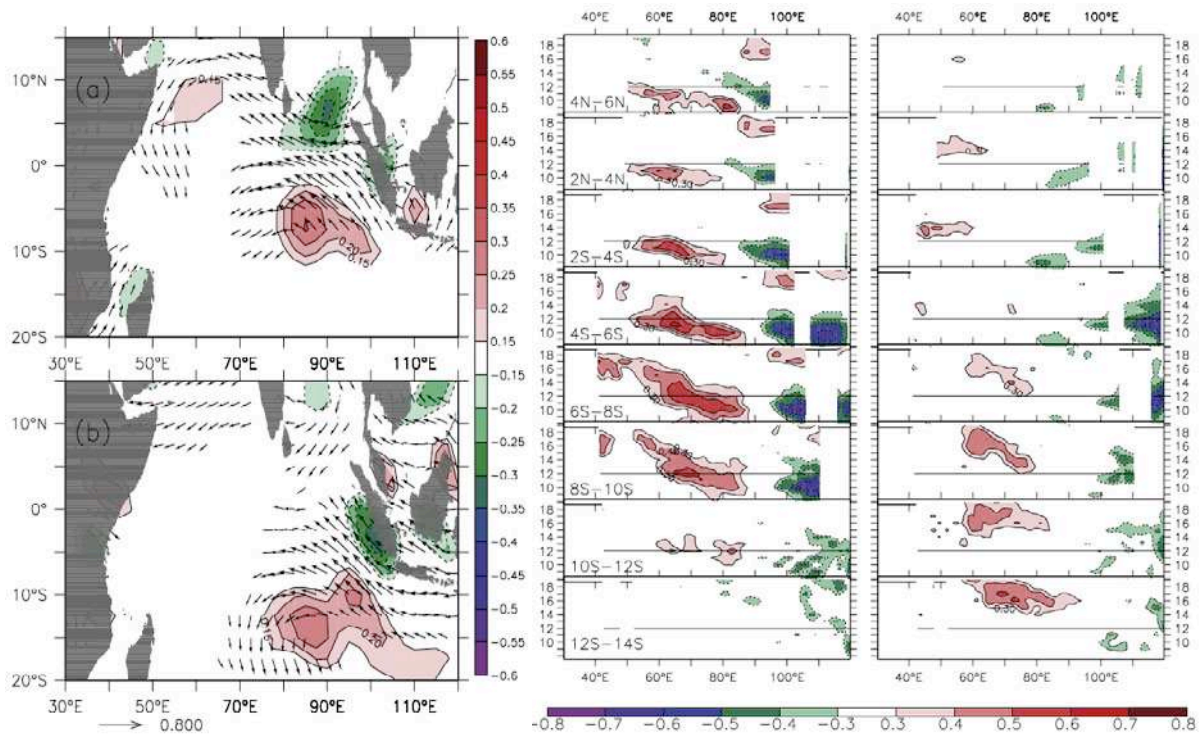


Figure 32. From Yu et al. (2005). (Left) (a) Partial correlation of 1000 hPa winds (vectors) and wind curl (colors) with Indian Ocean Dipole (IOD) index. (b) As Figure 15a but for Niño-3 index. (Right) Lead/lag partial correlation for sea surface height anomalies for (left) September, October, and November (SON)-IOD and (right) October, November, and December (OND)-Niño-3, determined from output fields of the SODA assimilation model for latitude belts as function of calendar month and longitude. Only correlations significant at 99% level are shown. The sea level response to El Niño is weaker and shifted southward compared to the IOD response.

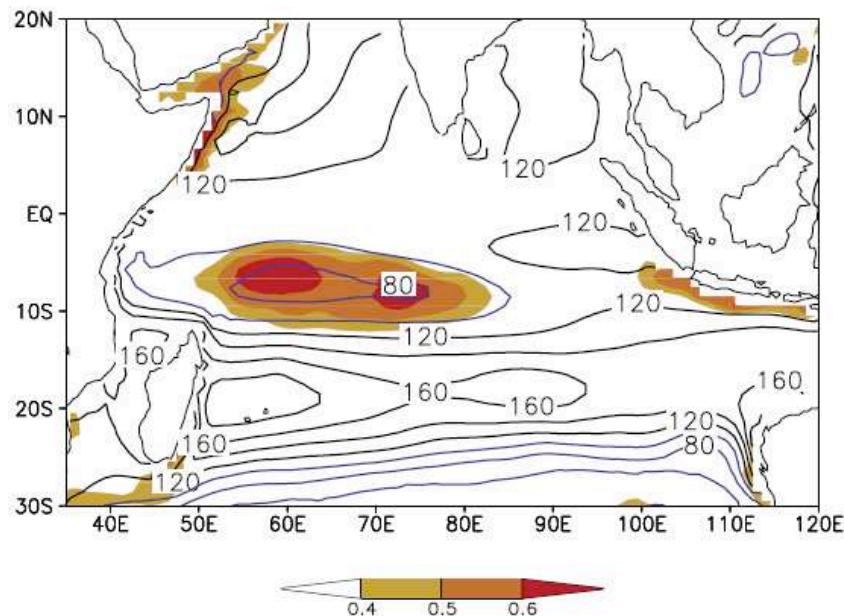


Figure 33. From Xie et al. (2002). Annual mean depth of the 20°C isotherm (contours in m) and correlation of its interannual anomalies with local SST (colour shades). The influence of thermocline depth on the SST interannual anomalies is largest in the thermocline ridge.

In both cases, however, the sea level anomalies persist after the end of the equatorial zonal dipole of SST or the SST anomalies in the Pacific Ocean. Since this region coincides with the thermocline ridge of the Indian Ocean (SCTR), perturbations of the thermocline

depth can easily modulate the connection between the cold subsurface and mixed layer, and hence generate SST anomalies, as demonstrated by the strong correlation between SSTA and 20°C depth anomalies in the southwestern Indian Ocean (Fig. 33). As a result, a SST anomaly persist in this region well after surface heat flux changes associated with ENSO of the equatorial SST dipole of the IOD have dissipated. The SST or heat content anomalies in this region have clear climatic impacts on tropical cyclones-days near La Réunion and Madagascar (Xie et al. 2002), rainfall over the western Ghats during the following monsoon (Vecchi and Harison 2004, Izumo et al. 2008), onset date of the southwest monsoon (Annamalai et al 2005b) or even circulation in the northern hemisphere (Annamalai et al 2007).

3.1.2. MJO and its oceanic signature

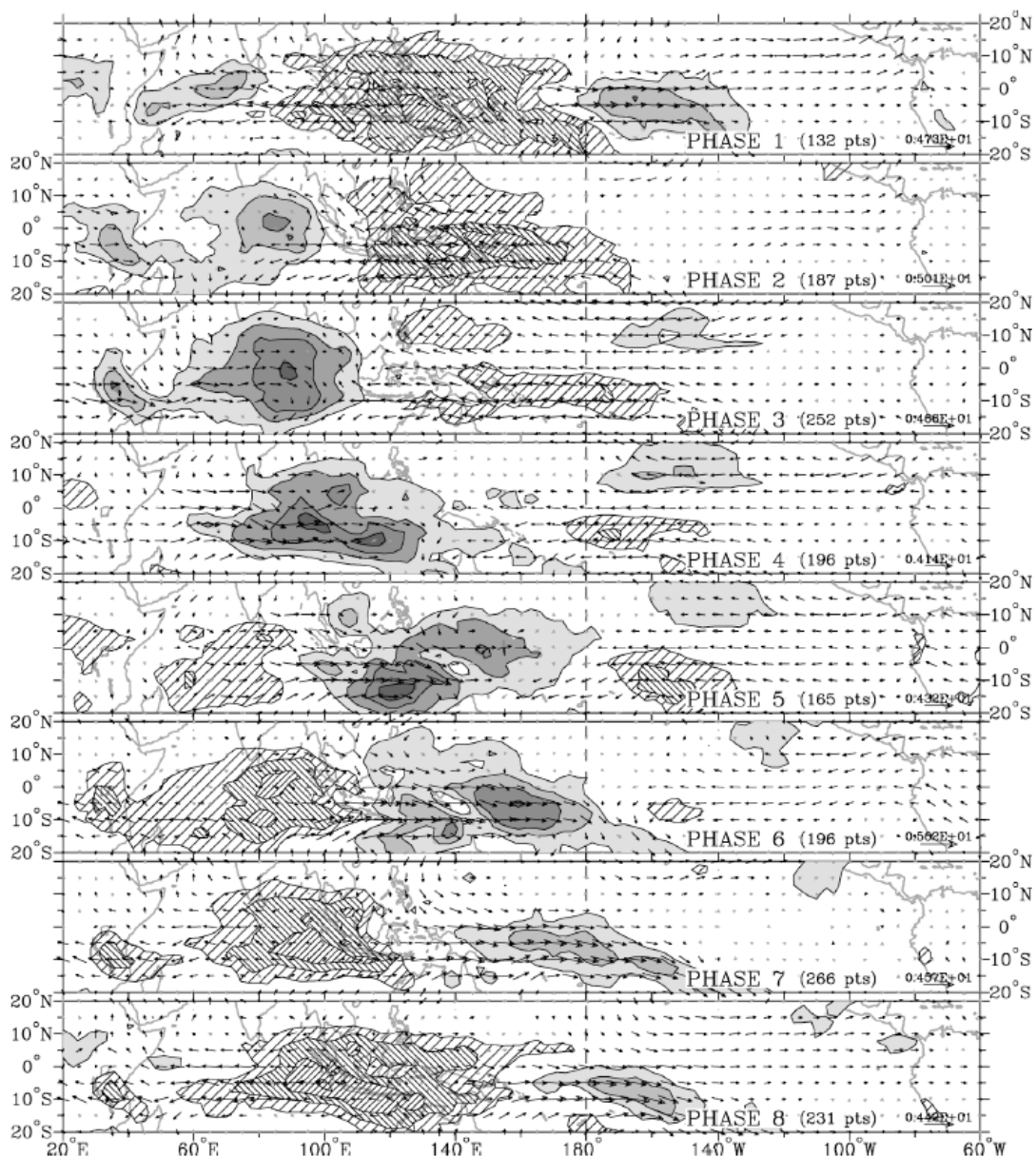


Figure 34. From Wheeler and Hendon (2004). Composite analysis of the MJO in boreal winter (DJF). Shading levels denote OLR anomalies less than -7.5 , -15 , -22.5 and -30 $W m^{-2}$, respectively, and hatching levels denote OLR anomalies greater than 7.5 , 15 , and 22.5 $W m^{-2}$, respectively. Black arrows indicate wind anomalies that are statistically significant at the 99% level.

The Madden-Julian oscillation is the leading mode of atmospheric variability at intraseasonal timescale. The MJO is a large-scale organised perturbation of the atmospheric deep convection, with energetic fluctuations of tropospheric winds at periods of 30-90 days (e.g. Zhang, 2005). The MJO originates from the Indian Ocean and propagates eastward at $\sim 5 \text{ m s}^{-1}$ into the western Pacific (Figs. 34-35). Because of the strong coupling with deep atmospheric convection, the MJO surface signature becomes much weaker beyond the eastern edge of the Pacific warm pool (Figure 8). The MJO has a strong seasonality (Zhang and Dong, 2004): it shifts in latitude with the ITCZ, being most active at about 5 to 15°S in boreal winter (December to March), and shifting north of the equator in summer (Figs. 34-35). The MJO however has a significant signature in the equatorial band all year long.

The Indian monsoon is strongly modulated at the intraseasonal timescale, with active-break cycles of about 30-60 days (e.g. Goswami, 2005). The MJO is tightly associated with active/break phases of the Indian summer monsoon, when northward propagation of convective anomalies is also evident over the Indian subcontinent, Bay of Bengal, Southeast Asia and South China Sea (e.g. Lawrence and Webster 2002). In addition to modulating rainfall over India during summer, the MJO also strongly modulates rainfall over Australia during boreal winter (e.g. Wheeler and Hendon 2004). As was mentioned earlier in section 2.3, another strong potential climate impact of the MJO is its potential role in triggering El Niño after having propagated to the western Pacific Ocean (e.g. McPhaden et al. 2006). Locally in the Indian Ocean, there is also evidence of a potential impact of the MJO on terminating IOD events (e.g. Rao and Yamagata 2004, Rao et al. 2007).

A theory of the MJO should be able to explain the following features: 1) spatial scale: planetary-scale circulation; 2) timescale: 30-80 day timescale; 3) propagation parties: $\sim 5 \text{ m s}^{-1}$ eastward propagation; 4) coupling between dynamics and convection; 5) the observed structure of the MJO (westward winds and surface divergence west of and eastward wind and convergence east of the convective centre, Hendon and Salby 1994 Rui and Wang 1990) and 6) the seasonal change in the MJO patterns (e.g. difference between boreal winter and summer MJO). There is at present no theory able to explain all of these aspects. The fact that many of the existing AGCMs misrepresent many aspects of the MJO variability (e.g. Slingo et al. 1996, Lin et al. 2006) is an additional complicating factor to derive a proper MJO theory. There have been many suggestions of potential mechanisms that can play a crucial role in the MJO: cloud-radiation feedback (e.g. Hu and Randall 1994), water vapour feedback (e.g. Bladé and Hartmann 1993), wind-evaporation feedback (e.g. Emmanuel 1987, Neelin et al. 1987) or Convective Instability of the Second Kind coupled to wave dynamics (wave-CISK, e.g. Lau and Peng 1987). Some of these processes seem to be important in the MJO (e.g. the recharge time of water vapour) but some others clearly don't match the observed structure of the MJO (e.g. the wind-evaporation feedback). The most satisfactory simplified model of the MJO is provided by the frictional convergence feedback (Wang 1988, Wang and Rui 1990). In this model, the coupling of the convective heating to the dynamics induces a coupling between the Kelvin and Rossby wave modes (a response that would look a little bit like the Gill model in Fig. 2, but propagating eastward). It is the convergence induced by surface friction to the east of the convective center that provides the moisture convergence and uplift that maintains the wave. This model possesses a lot of desirable features: it explains the spatial and temporal scale selection of the MJO, has a slow ($< 10 \text{ m s}^{-1}$) eastward propagation, and a phase relation between convection and moisture convergence, which is consistent with observations. This model is however largely based on equatorial wave dynamics and does not provide a satisfactory explanation of the seasonal cycle of the MJO.

I will now discuss the oceanic signature of the MJO in more detail. The MJO modulates the convection, and hence surface wind and heat fluxes. During active phases, the increased cloudiness results in decreased surface downward shortwave flux, while increased surface

winds induce both increased evaporative cooling and mixing in the upper ocean. During suppressed convection, the opposite pattern occurs (increased solar heat flux, and reduced evaporation and mixing). In addition to that, the low wind speeds associated with suppressed convection allow the development of strong diurnal warming (e.g. Duvel et al. 2004). The strong near-surface stratification associated to diurnal warm layers during the suppressed phase induces an additional surface warming which contributes to about 30% of the total intraseasonal SST signal in the western Pacific (e.g. Bernie et al. 2005).

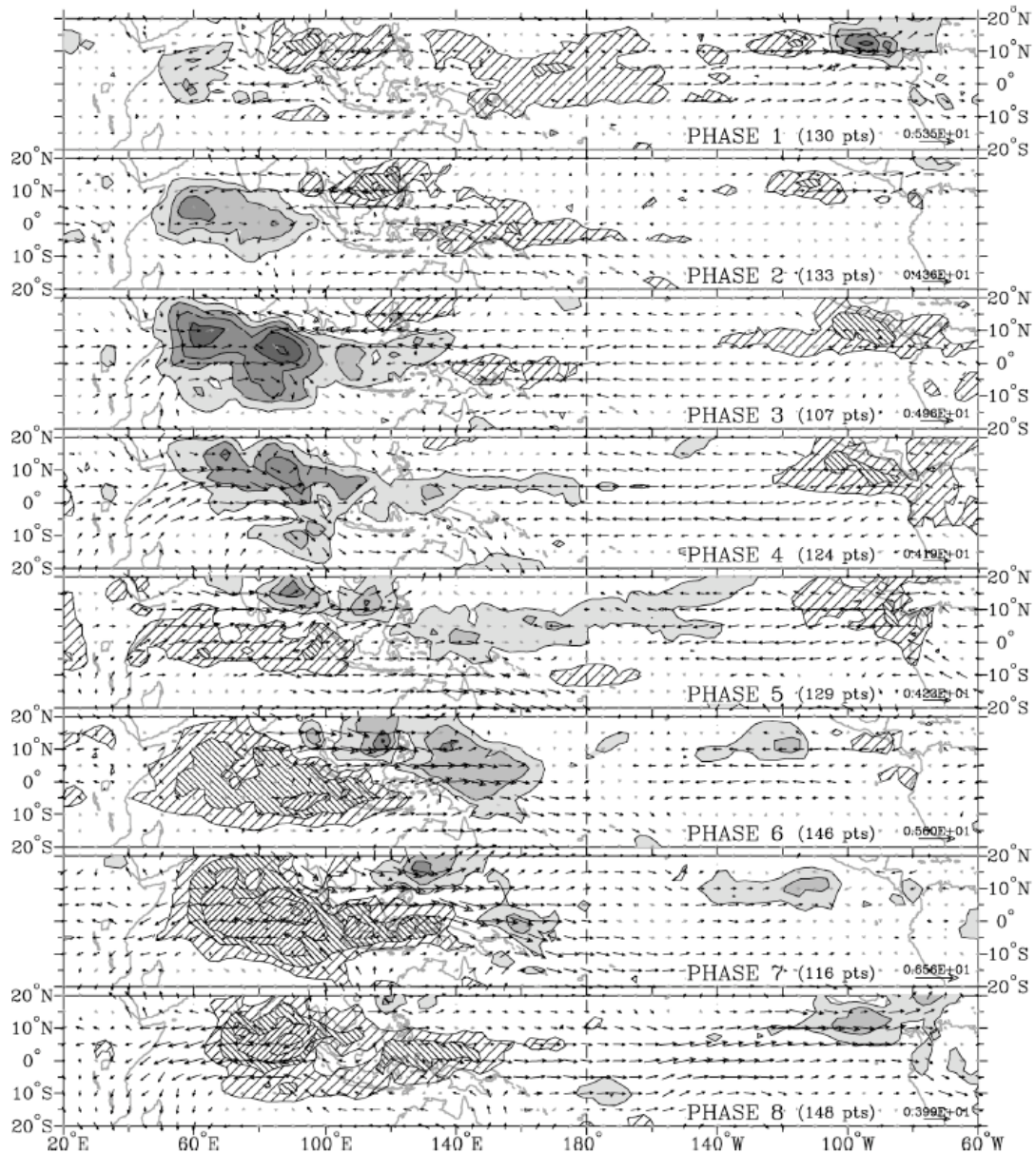


Figure 35. From Wheeler and Hendon (2004). Composite analysis of the MJO during the monsoon onset (MJ).

Up to a recent date, most of the studies of the oceanic SST signature of the MJO were using SST products relying heavily on satellite measurements in the infrared window. This type of measurements suffer from the screening effect of clouds and underestimate strongly the SST signals under convective clouds (e.g. Sengupta and Ravichandran 2001, Duvel and Vialard 2007). As a result, previous studies underestimated strongly the SST signature of the MJO (e.g., Jones et al. 1998; Shinoda et al. 1998; Woolnough et al. 2000). Recent studies using in situ data or TMI SST (which is based on microwave estimates which “see” through

clouds) revealed large SST variations in response to the convection. In summer, there are SST variations of about 2°C peak-to-through amplitude propagating northward in phase quadrature with the convective perturbation in the Bay of Bengal (Sengupta and Ravichandran 2001, Vecchi and Harrison 2002) and South China Sea (Duvet and Vialard 2007). In winter, the study of Duvet and Vialard (2007) showed that the SST signature of the MJO in the western Pacific was quite small in comparison with the SST response in the Indian Ocean (Fig. 36). In the Indian Ocean, there are two regions of strong SST signature of the MJO. The first one is in the North-Western Australian Basin, and has up to now not been studied extensively (I'll come back to this in section 4). The second one is in the SCTR, and has been discussed in a few studies (Harrison and Vecchi 2001, Duvet et al 2004, Saji et al 2006, Duvet and Vialard 2007, Vinayachandran and Saji 2008). All of these studies agree on the fact that the SCTR exhibits maximum response to the MJO because of the shallow thermocline, which maintains a shallow, reactive mixed layer, but disagree on the detailed processes of the oceanic response (section 3.2.3.2).

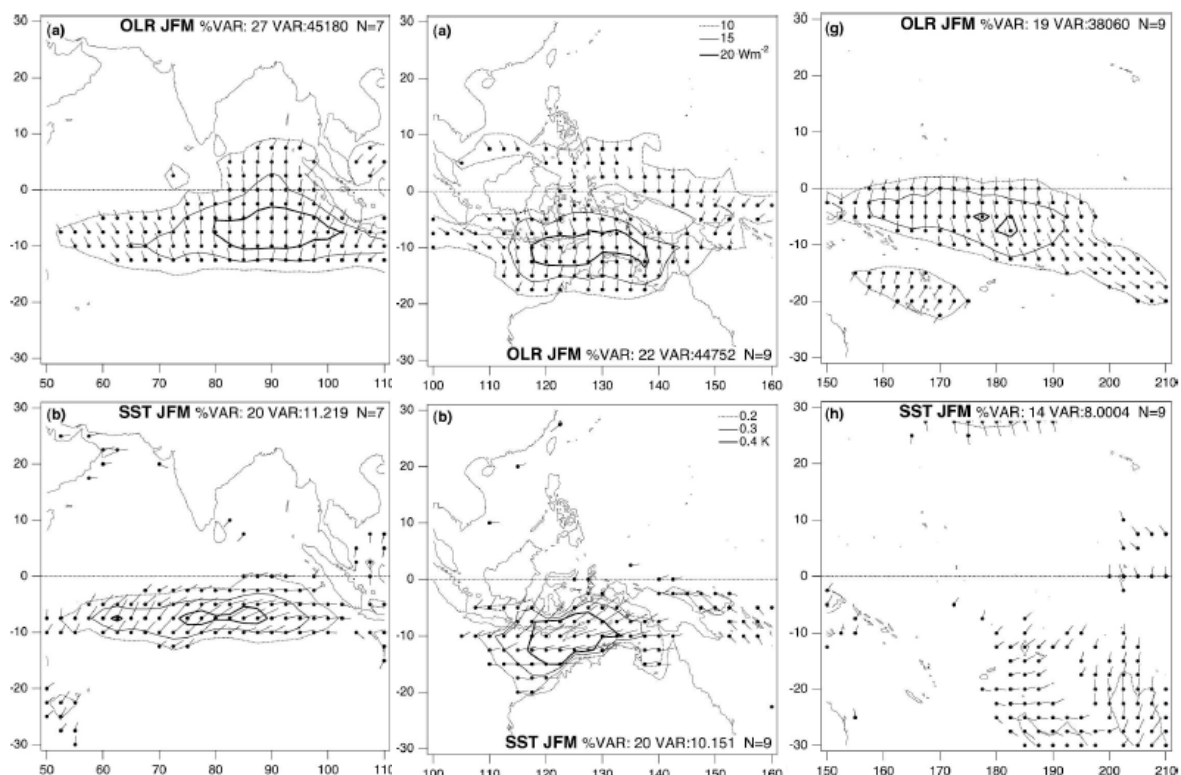


Figure 36. From Duvet and Vialard (2007). Amplitude of large-scale intraseasonal OLR variability (top) and of the SST variability (bottom) associated to it. The analysis has been made over the Indian Ocean (left), Maritime continent (middle) and western Pacific (right) regions. The SST signature of the MJO is large over the SCTR and North Western Australian Basin, but weak over the western Pacific.

Because of the relatively strong SST signature of the MJO in most of the Indian Ocean (the generation region of the MJO), the question of the potential role of air-sea coupling in MJO properties arise. The distribution of intraseasonal variability of convection show a sharp decrease over activity over land (Fig. 8) which already indicates that MJO develops preferably over the sea². Most studies that have addressed this topic used a modelling

² There are several hypotheses to explain this, which are not necessarily related to air-sea coupling (e.g. competition between intraseasonal and diurnal cycle, Zhang 2005) but one possible explanation is that the fast response time of continental surfaces compared to the oceanic mixed layer negatively feedbacks on intraseasonal perturbations (e.g. Bellon et al 2008).

framework and generally found that active coupling did moderately improve the structure of the simulated MJO (e.g. Waliser et al. 1999, Inness et al. 2003a, Maloney and Sobel 2004) or even hindcasts of the MJO (Woolnough et al. 2007). In this last study, it was even shown that considering the modulation of the diurnal cycle of the SST by the MJO further improved the hindcast. Most of the modelling study thus point toward a moderate, but non-negligible impact, of coupling on the MJO properties. None of these modelling studies, however, do reproduce the strong SST signals observed in the SCTR region.

3.1.3. The RAMA array

The Research Moored Array for African-Asian-Australian Monsoon Analysis and Prediction (RAMA) is a new observational network designed to address outstanding scientific questions related to Indian Ocean variability and the monsoons. RAMA is a multi-nationally supported element of the Indian Ocean Observing System (IndOOS), a combination of complementary satellite and in situ measurement platforms for climate research and forecasting (CLIVAR/GOOS IOP et al. 2006). The array was designed in order to answer the main ongoing scientific questions about the response of the Indian ocean to monsoons, its intraseasonal to decadal variability, and its climatic influence. A detailed description of the RAMA array, with some examples of scientific use of its data will be found in (McPhaden et al. 2009). Thanks to major contributions from India, Indonesia and China, the RAMA array has quickly developed in 2007-2008 (Fig. 37). The target date for the completion of the array is 2011. Two major challenges for RAMA are to secure sufficient ship time to service the array and to mitigate the effect of vandalism on the moorings.

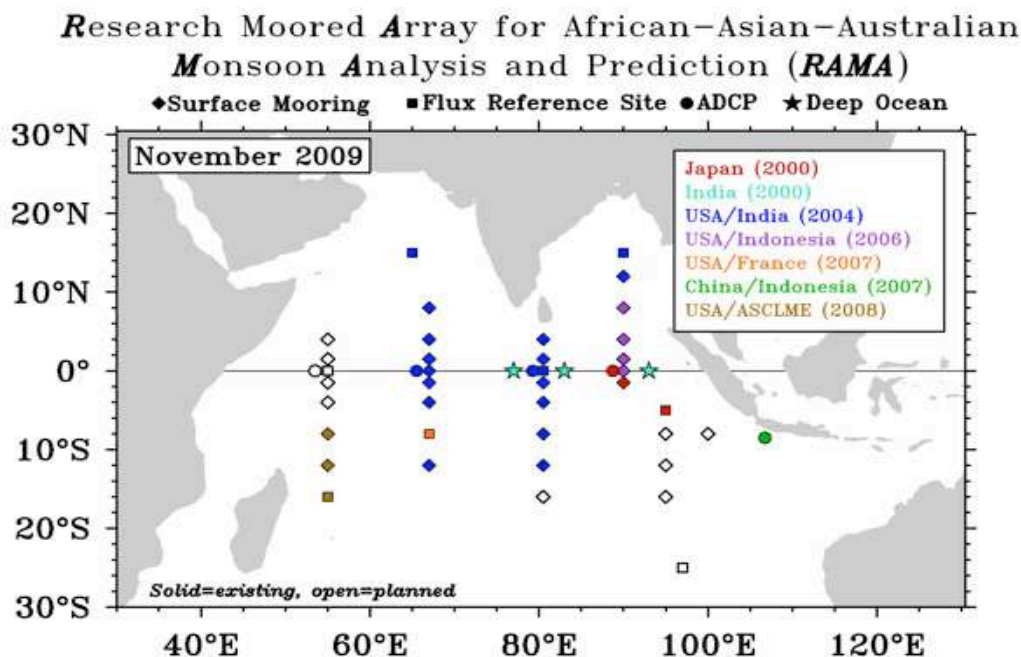


Figure 37. From McPhaden et al. (2009). Status of the RAMA array in November 2009. Open symbols indicate a site yet to occupy. Filled symbols indicate occupied sites, with the colour indicating the nation that deployed the mooring there, in collaboration with PMEL. Losanges indicate regular moorings, boxes indicate flux references sites, circles indicate subsurface ADCPs and stars indicate deep current meter moorings.

There was also a French contribution to the array through the Cirene cruise (next section) in January-February 2007, and the August 2008 Marion Dufresne transit valorisation, during which the mooring at 8°S, 67°E was deployed and serviced.

3.1.4. The Cirene cruise

The Vasco (Duvel et al. 2009) and Cirene (Vialard et al. 2009a) programs are complementary programs whose main goal is to study the ocean signature of the MJO in the SCTR region. More generally, the Cirene cruise aimed at documenting the processes of air-sea interactions at various timescales (synoptic, intraseasonal, interannual) in the SCTR region. The Vasco component relied on deployment of atmospheric balloons from Seychelles, while Cirene allowed collecting oceanic, air-sea interface and atmospheric measurements downstream, close to 8°S, 67°E (see Fig. 38 for the location and route of the of the cruise). Cirene was comprised of two legs in January and February 2007. For most complete description of the cruise, the reader will refer to Vialard et al. (2009a), provided in the Annex of this document. I will describe briefly here the main measurements collected during the cruise.

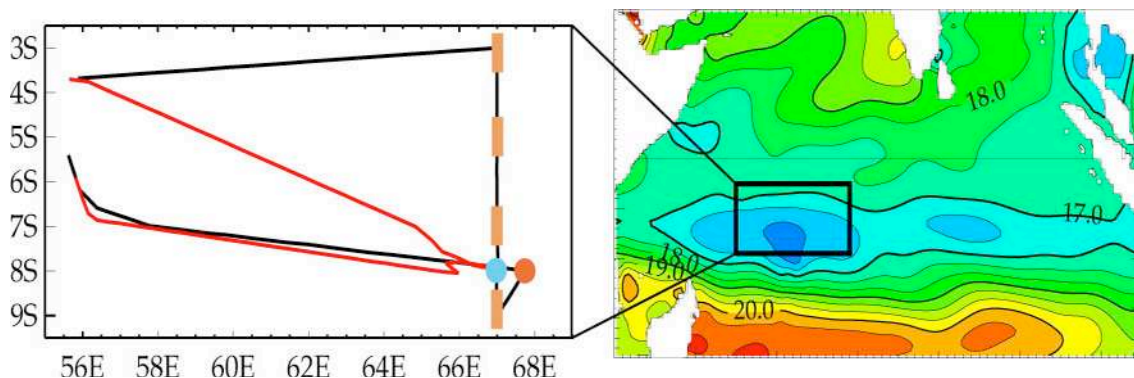


Figure 38. Adapted from Vialard et al. (2009a). (left) Blowup of the region framed on the plot of climatological January-February 0-300m average temperature (right), summarizing the Cirene cruise. The trajectory of R/V Suroît is shown in black (first leg) and red (second leg). The orange rectangles indicate the locations where groups of 3 Argo profilers were deployed. The blue circle indicates the location of the ATLAS and ADCP moorings. The orange circle indicates the location of the long CTD station (12 days during each leg).

As a contribution to the IndoOOS long-term observing system, we deployed 12 Argo-type profilers (see Gould et al. 2004 for a description of the Argo program) and one RAMA mooring at 8°S, 67°E (with extra sensors and a subsurface ADCP during the duration of the cruise). Air-sea interactions are at the heart of the Vasco-Cirene program. We thus collected both atmospheric and oceanic observations during the cruise, with an emphasis on the upper ocean, atmospheric boundary layer, and air-sea interface. Surface temperature and salinity and currents down to 300 m were continuously recorded, and temperature profiles down to 800 m were collected every 50 km along the ship track (Fig. 38). Air-sea fluxes were monitored using a dedicated flux platform installed on a mast 17 m above sea surface on the bow of the ship (Dupuis et al. 2003). An instrumental suite providing measurements of the sea surface and marine boundary layer complemented the air-sea flux estimates from the mast (Minnett et al. 2001). Detailed measurements of the upper-ocean and atmospheric evolution were collected during two long stations (from 14 January to 26 January 2007 and from 4 February to 15 February 2007) at 8°S, 67°30' E. In addition to the continuous measurements described above, we launched four radiosondes per day (at 0000, 0600, 1200, and 1800 UTC) and collected atmospheric temperature, pressure, humidity, and wind measurements up to 300 hPa for most profiles. Upper-oceanic profiles (0–500 m), including temperature, salinity, and pressure, were performed every 20 min. One profile down to 1000 m, with additional current measurements and water sample collection, was performed every 6 h. The air-sea interaction profiler (ASIP, an autonomous high resolution profiler with emphasis on capturing near-surface processes, Ward et al.) was deployed on several occasions during the long stations.

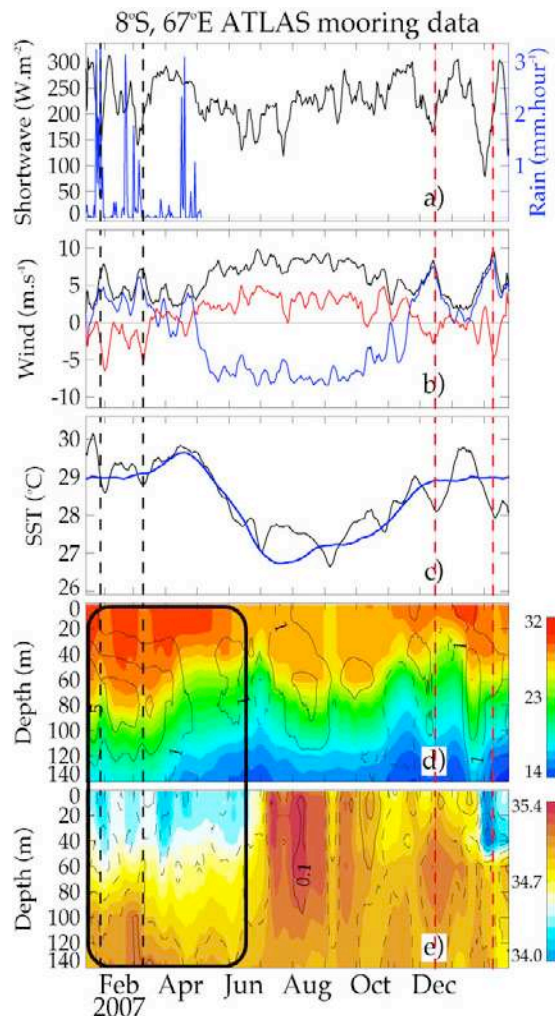


Figure 39. Adapted from [Vialard et al. \(2009a\)](#). Time series of daily parameters transmitted by the ATLAS mooring at 8°S, 67°E since its deployment during Cirene. The panels, from top to bottom, show: a) downward surface shortwave radiation ($W m^{-2}$) and rainfall ($mm hr^{-1}$); b) wind speed (black), zonal wind (blue) and meridional wind (red) ($m s^{-1}$); c) SST (black) and SST climatology (blue) ($^{\circ}C$); d) subsurface temperature (color) and anomalies (contours) ($^{\circ}C$); subsurface salinity (color) and anomalies (contours) (psu). The black dashed lines indicate anomalies associated with two tropical cyclones going past the window in their early stages. The black frame highlights the subsurface anomalies associated with the consequences of the 2006 Indian Ocean Dipole. The red dashed lines indicate two MJO events in late 2007 and early 2008 discussed in [Vialard et al. \(2008\)](#).

We will come back in the following sections on the various results harvested during the Cirene cruise but will already illustrate now how the measurements collected illustrate the three timescales of interest (synoptic, intraseasonal, interannual). Fig. 39 shows variable measured by the ATLAS mooring at 8°S, 67° E during its first year of deployment. The first few months display large subsurface temperature and salinity anomalies which are the result of the 2006 IOD (section 3.3.1). There are also short-lived episodes of high rainfall, winds and SST decrease in January and March 2007, corresponding to tropical cyclones in their early stage of development (section 4.1.1). Finally, there are longer and stronger episodes of rainfall, cloudiness, strong winds and cool SST events in late 2007 and early 2008, corresponding to the oceanic signature of two MJO events ([Vialard et al. 2008](#), section 3.2.3.2).

3.2. Results: MJO oceanic signature

In this section, I will summarize my main results about the oceanic signature of the MJO, obtained either through a modeling approach or observations analysis (either from the Cirene cruise or satellite datasets). I will first discuss the dynamical response of Indian Ocean to intraseasonal variability (section 3.2.1), and then describe its thermodynamical response (section 3.2.2). The papers relevant to section 3.2 are [Duvel et al. \(2004\)](#), [Duvel and Vialard \(2007\)](#), [Sengupta et al. \(2007\)](#), [Vialard et al. \(2008\)](#), [Vialard et al. \(2009ab\)](#), [McCreary et al. \(2009\)](#), [Izumo et al. \(2009\)](#) and [Resplandy et al. \(2009\)](#).

3.2.1. Dynamical response

Although its maximum intensity varies annually in latitude, the MJO has always a significant signature in the equatorial waveguide. Wind stress can directly accelerate zonal currents near the equator. The equatorial signature of the MJO thus induces an energetic response in terms of equatorial waves and currents (section 3.2.1.1) that can then propagate into the Northern Indian Ocean coastal waveguide (section 3.2.1.2).

3.2.1.1. Equatorial waveguide

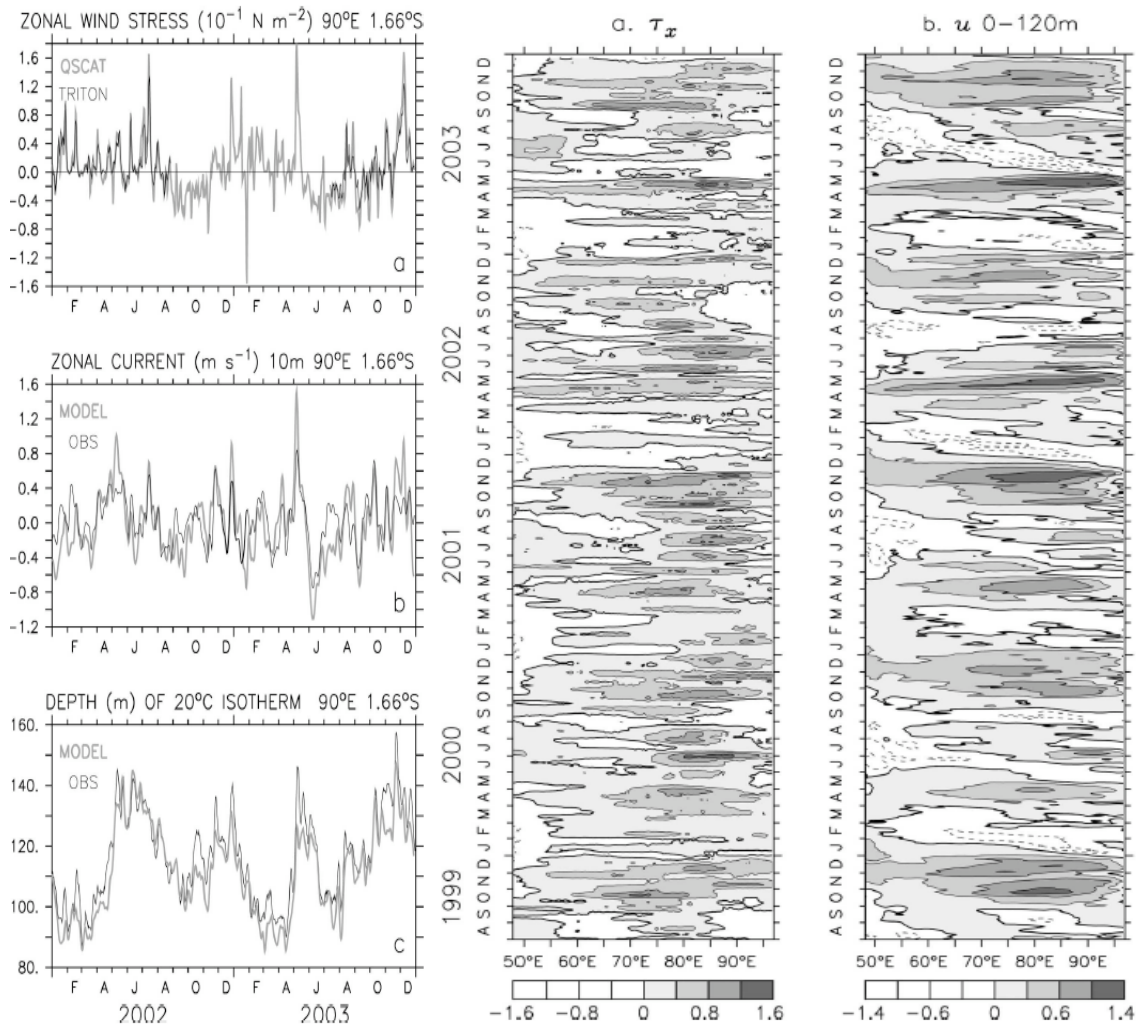


Figure 40. From [Sengupta et al. \(2007\)](#). (Left) Evolution of the (a) zonal wind stress, (b) zonal current, and (c) depth of 20°C isotherm at 1.6°S , 90°E from TRITON data and the QuikSCAT simulation for 2002–03. (Right) Time–longitude plot of 1°S – 1°N averaged (a) 10-day running mean QuikSCAT zonal wind stress (10^{-1} N m^{-2}), (b) 0–120-m zonal current (m s^{-1}). The zonal wind stress and currents along the equator are strongly modulated at intraseasonal timescale.

Satellite and in situ observations show large intraseasonal (10–60 day) variability of surface winds (Fig. 40) and upper-ocean current (e.g. Masumoto et al. 2005) in the equatorial Indian Ocean, particularly in the east. An ocean model forced by the Quick Scatterometer (QuikSCAT) wind stress is used to study the dynamics of the intraseasonal zonal current (Sengupta et al 2007). The model has realistic upper-ocean currents and thermocline depth variabilities on intraseasonal to interannual scales (Fig. 40). At the equator, moderate westerly winds are punctuated by strong 10–40-day westerly wind bursts. The wind bursts force swift, intraseasonal (20–50 day) eastward equatorial jets in spring, summer, and fall. In agreement with direct observations in the east, the spring jet is a single intraseasonal event, there are intraseasonal jets in summer, and the fall jet is long lived but strongly modulated on an intraseasonal scale (Fig. 40).

The model allowed analysing the momentum balance associated with this intraseasonal current response. The zonal pressure force is almost always westward in the upper 120 m. The zonal momentum balance is between local acceleration, stress, and pressure, while nonlinearity deepens and strengthens the eastward current. The westward pressure force associated with the thermocline deepening toward the east rapidly arrests eastward jets and, subsequently, generates (weak) westward flow.

3.2.1.2. Northern Indian Ocean coastal waveguide

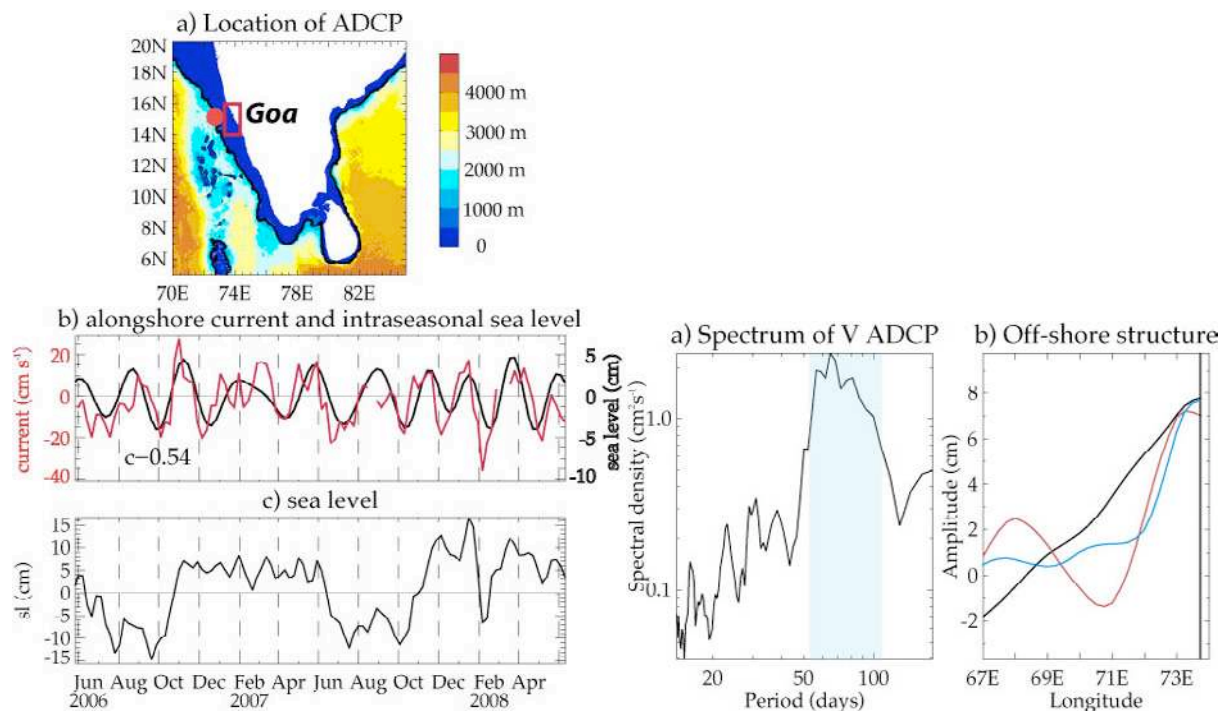


Figure 41. From Vialard et al. (2009b). (Left) a) Map of peninsular India and bathymetry. A red circle indicates the location of the ADCP on the shelf break off the state of Goa, on the western Coast of India. The red box (73°E to 74°E, 14°N to 16°N) indicates the averaging region for sea level plotted in panels b and c. b) Weekly alongshore current at 50m measured by the ADCP (red curve) and 55–110 day filtered sea level. c) Sea level. (Right) a) Power spectrum of the ADCP alongshore current at 50m. Shading highlights the 55–110 day band. b) Intraseasonal (55–110 day, red curve and 30-60 day, blue curve) and seasonal (110 day low-passed, black curve) typical offshore sea-level structure. The 55-110 day (30-60 day) structure functions have been multiplied by 3.5 (5) in order to be more easily compared with the stronger signal at seasonal scale. Intraseasonal currents dominate the WICC variability because of the trapping of intraseasonal energy at the coast, while seasonal signals radiate away.

As mentioned above, intraseasonal wind variability drives a significant surface current response in the equatorial waveguide (e.g. Reppin et al., 1999, Masumoto et al., 2005, Han et al., 2001, Sengupta et al., 2007). While equatorial intraseasonal variability of currents and sea level has been addressed in several studies, studies focusing on the northern Indian Ocean are scarce. Sengupta et al. (2001) concluded that current fluctuations south of Sri Lanka are largely driven by instabilities phase locked to the intraseasonal wind forcing. Durand et al. (2009) used along-track satellite data to describe the variability of currents and sea level along the east coast of India, finding significant intraseasonal variability superimposed on the seasonal cycle. Shetye et al. (2008) found that remote forcing makes a significant contribution to the variability of observed currents at 15°N on the west coast of India at periods longer than 10 days.

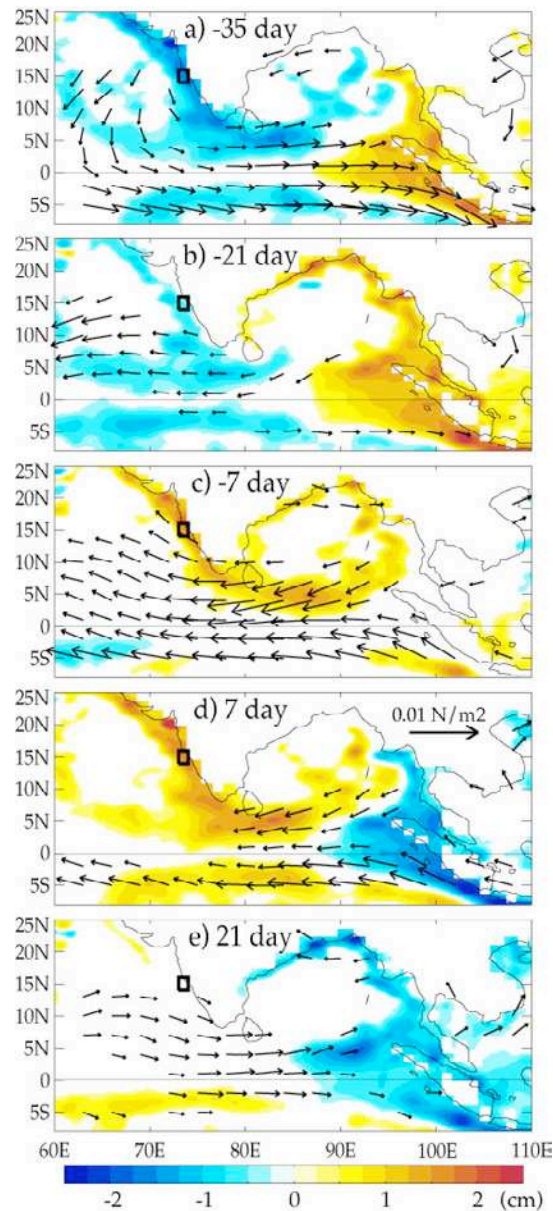


Figure 42. From [Vialard et al. \(2009b\)](#). Regression of 55–110 day filtered sea level (cm) and ERS-Quickscat winds ($N.m^{-2}$) to normalized 55–110 day filtered sea level within the black box ($73^{\circ}E$ to $74^{\circ}E$, $14^{\circ}N$ to $16^{\circ}N$). Patterns leading by 35 day (a), 21 day (b), 7 day (c) and lagging by 7 day (d), 21 day (e) with respect to the intraseasonal sea level off Goa. The 35-day lag pattern is quite similar to the pattern shown in panel (a) and has not been plotted. Values that are not significant at the 95% confidence level have been masked. Intraseasonal sea level variations in the northern Indian ocean coastal waveguide are part of a basin scale pattern.

In [Vialard et al. \(2009b\)](#) (draft provided at the end of this document), we have thus described intraseasonal current and sea-level variations in the coastal waveguide of the northern Indian Ocean, with emphasis on the forcing that drives them. Toward that end, we used a combination of satellite observations (sea level and wind stress), as well as a newly acquired current dataset at 15°N on the west coast of India, off Goa (see Fig 41 for location).

The wind associated with the Madden Julian oscillation forces a basin-scale pattern, involving equatorial waves, reflection at the eastern coast and propagation of coastal Kelvin waves into the Bay of Bengal and along the western coast of India (Fig. 42). Although the amplitude of intraseasonal sea level variations are much smaller than the seasonal cycle (typically 6–8 cm against 15–20 cm peak-to-through), intraseasonal (55–110 day) variations dominate the record of alongshore upper-ocean currents at 15°N on the western coast of India (Fig. 41). These observations can be interpreted within the framework of linear wave theory. At 15°N, the minimum period for planetary waves is ~90 day. As a result, intraseasonal energy is largely trapped at the coast (Fig. 41) in the form of poleward-propagating Kelvin waves, while lower-frequency signals associated with the annual cycle can radiate away westward as planetary waves. This dynamical difference results in a steeper offshore slope of sea level at intraseasonal timescale (Fig. 41), and thus stronger geostrophic alongshore currents. A consequence is that the alongshore currents are in-phase with intraseasonally-filtered sea level near the coast, and a gridded satellite product is shown to reproduce the current variations reasonably well (Fig. 41). This work thus underlines the importance of intraseasonal signals for coastal current variations on western continental margins, and opens potential applications for near real-time coastal currents monitoring.

3.2.2. Thermodynamic response and air sea coupling

3.2.2.1. Northern Indian Ocean

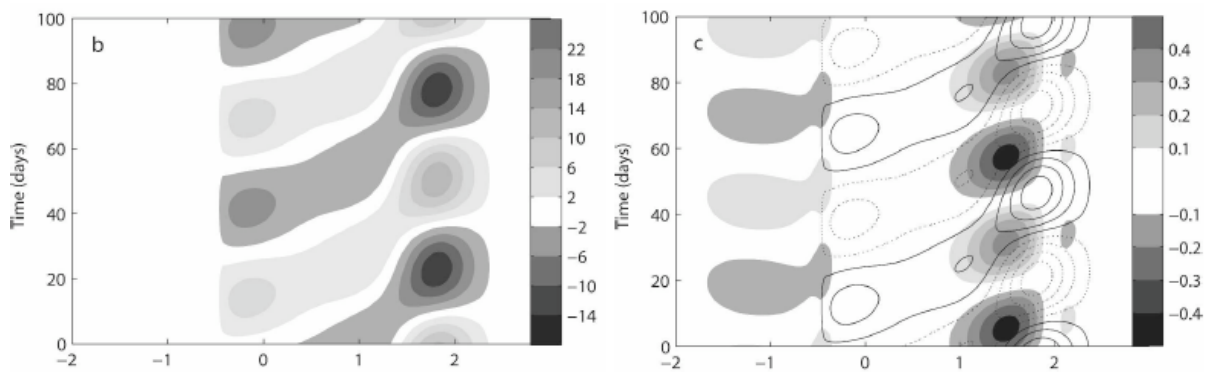


Figure 43. From [Bellon et al. \(2008\)](#). Precipitation anomaly (mm day^{-1}) in (b) the linear, uncoupled, atmospheric mode; (c) SST anomaly ($^{\circ}\text{C}$, shaded) and precipitation anomaly (solid/dotted contours for positive/negative values) in the coupled mode. Coupling impacts little the stability or spatial structure of the forced mode, but reduces its period by 25%.

In order to investigate the potential influence of coupling on the boreal summer intraseasonal oscillation, we used a simple coupled model in a zonally symmetric aquaplanet configuration ([Bellon et al. 2008](#)). The model consists of a linear atmospheric model of intermediate complexity based on quasi-equilibrium theory coupled to a simple, linear model of the upper ocean. This model has one unstable eigenmode with a period in the 30–60-day range and a structure similar to the observed northward-propagating intraseasonal oscillation in the Bay of Bengal/west Pacific sector (Fig. 43). The ocean–atmosphere coupling is shown to have little impact on either the growth rate or latitudinal structure of the atmospheric oscillation, but it reduces the oscillation’s period by a quarter. At latitudes corresponding to the north of the Indian Ocean, the sea surface temperature (SST) anomalies lead the

precipitation anomalies by a quarter of a period (Fig. 43), similarly to what has been observed in the Bay of Bengal (e.g. Sengupta and Ravichandran 2001, Vecchi and Harrison 2002). The mixed layer depth is in phase opposition to the SST: a monsoon break corresponds to both a warming and a shoaling of the mixed layer. This behaviour results from the similarity between the patterns of the predominant processes: wind-induced surface heat flux and wind stirring. The instability of the seasonal monsoon flow is sensitive to the seasonal mixed layer depth: the oscillation is damped when the oceanic mixed layer is thin (about 10 m deep or thinner), as in previous experiments with several models aimed at addressing the boreal winter Madden–Julian oscillation. This suggests that the weak thermal inertia of land might explain the minima of intraseasonal variance observed over the Asian continent (Fig. 8).

3.2.2.2. Thermocline ridge

As shown in Fig. 44, the SCTR region frequently witnesses strong convection and surface wind fluctuations associated with the MJO. In many instances, this forcing induces a large-scale SST cooling in this region. This SST cooling often exceeds 1°C in amplitude (up to 3°C more locally, Duvel et al 2004) and lasts about 20–40 days. Large intraseasonal SST cooling in response to the MJO does not happen every year, and was absent during 2003–2007, for reasons that I will discuss below.

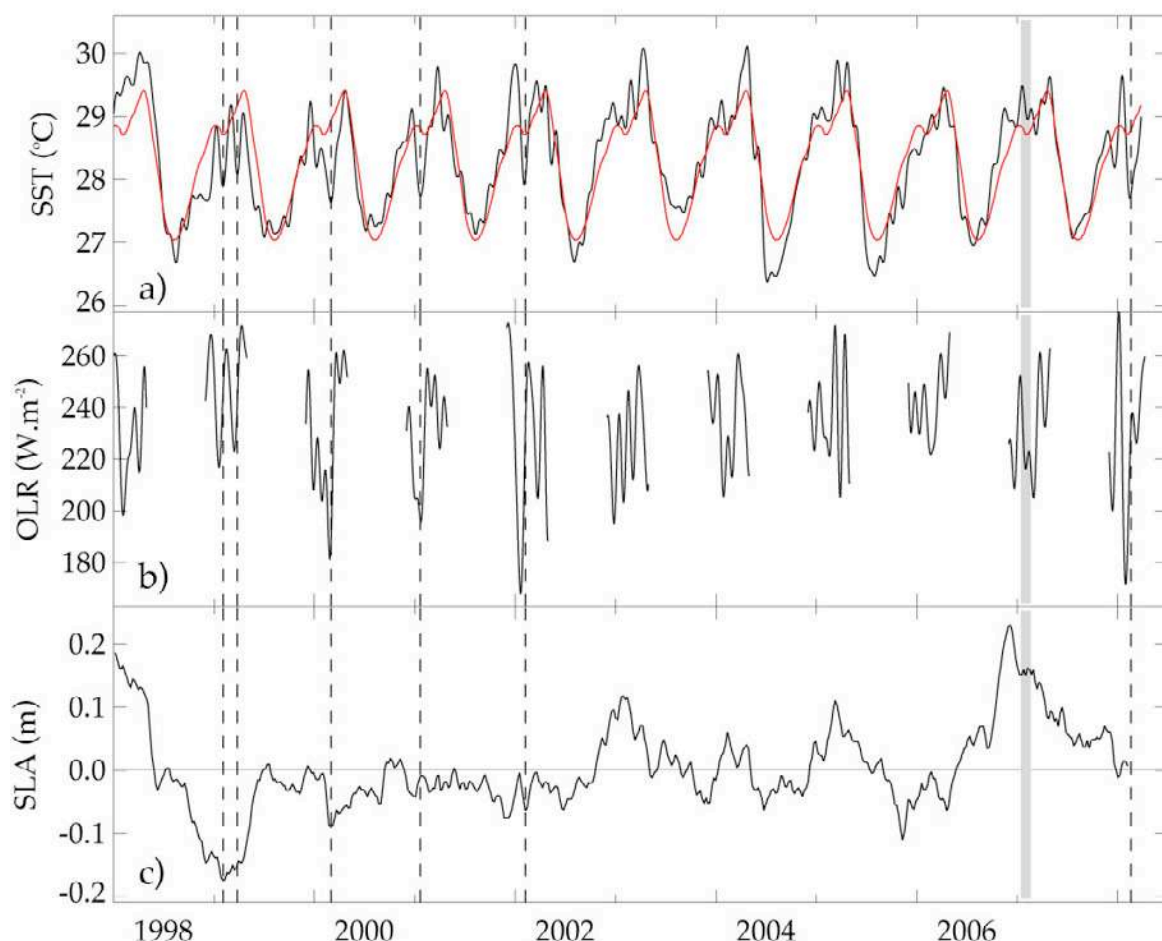


Figure 44. From Vialard et al. (2009a). Time series of average a) SST, b) Outgoing longwave radiation (OLR, a proxy for convection, low values indicating intense convection) and c) sea level interannual anomaly over the SCTR region (60°E–80°E, 5°S–10°S). In a) and b) a 30-day low pass filter has been applied and the climatology is shown in red. Only austral summer OLR are shown to improve readability. The grey bar indicates the timing of the Vasco-Cirene experiment. Dashed lines indicate the strongest intraseasonal SST cooling events.

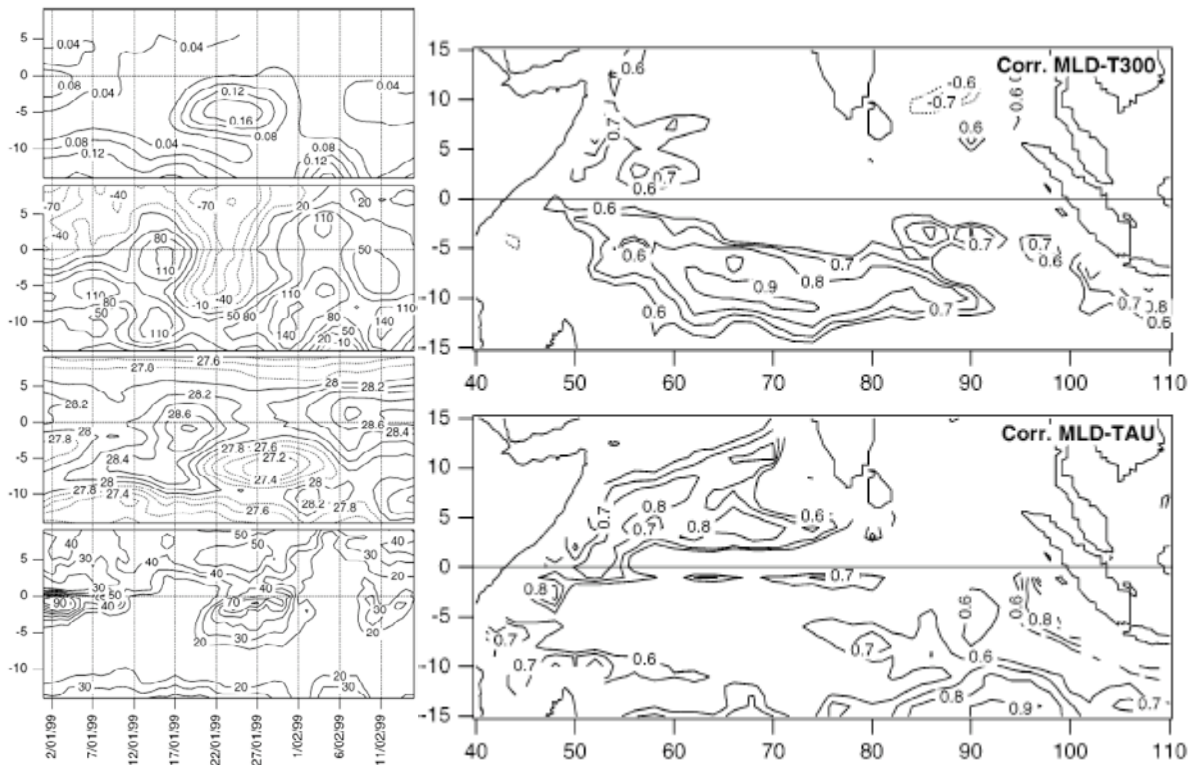


Figure 45. From Duvel et al. (2004). (Left) Time–latitude diagrams of the evolution of (top) wind stress in Pa, (middle top) net surface flux in $W m^2$, (middle bottom) temperature of the mixed layer in $^{\circ}C$, and (bottom) mixed layer depth in m for the OGCM. Values are averaged between 80° and $90^{\circ}E$. (Right) Correlation between the JFM average mixed layer depth of each year from an OGCM simulation (1990–2000) with (top) the average upper-300-m ocean temperature, (bottom) the wind stress. (Left) The strong deepening of the MLD near the equator prevents a strong SST signature there. (Right) The mixed layer depth in the SCTR is modulated by the thermocline depth at interannual timescale.

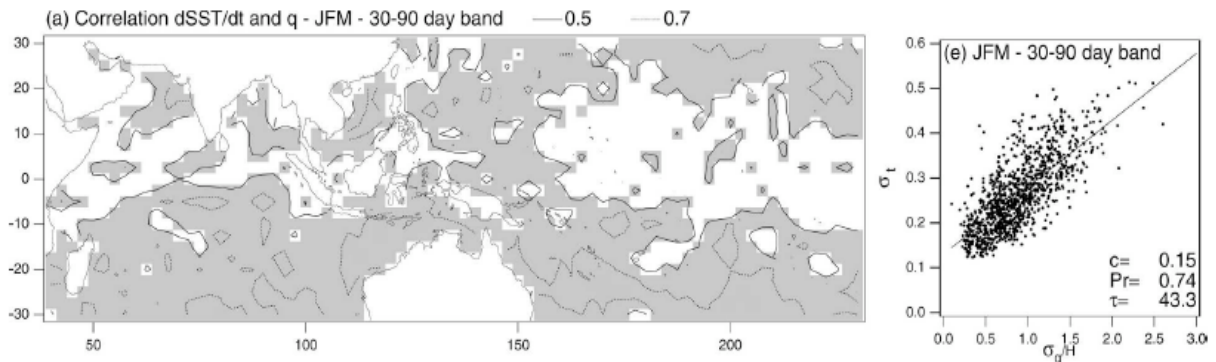


Figure 46. From Duvel and Vialard (2007). (left) Correlation between the derivative of the TMI SST and the NCEP net surface fluxes for the 30–90-day band in JFM. Solid contours represent a correlation of 0.5 and dashed contours one of 0.7. (right) Scatter diagrams for regions with a correlation coefficient larger than 0.5 between the amplitude of 30-90 day SST variability and the amplitude of flux variability scaled by the mixed layer depth. The value of the line slope c , the corresponding time scale τ , and the linear correlation coefficient (Pr) are also indicated. SST intraseasonal variations seem to be driven by fluxes in large region of the tropics, and the SST spectrum is reddened compared with the atmospheric forcing.

Role of the thermocline ridge. The spatial distribution of the SST response to the MJO matches the elongated structure of the thermocline ridge very well (Figs. 36 and 6a). Thanks to OGCM simulations that reproduced correctly the spatial structure of the SST signature of the MJO (albeit with smaller amplitude), we could understand the reason of the spatial

distribution of the SST response (Duvel et al 2004). Although the surface flux perturbation associated with the MJO spans a wider latitudinal range (roughly 8°S to 5°N in the case of Fig. 45 left), the surface response is largest in the SCTR region. This is because the shallow thermocline in the SCTR region prevents mixed layer deepening, whereas the mixed layer deepens strongly north of the SCTR because of the combined effect of wind stirring and negative buoyancy forcing.

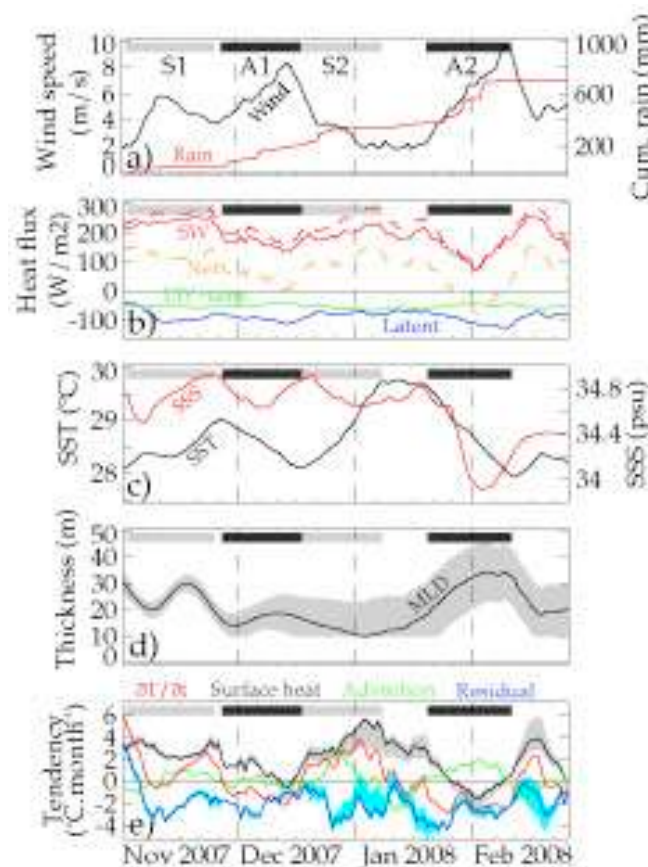


Figure 47. From Vialard et al. (2008). November 2007-February 2008 time series from the ATLAS mooring at 8°S, 67°E. a) Wind speed ($m s^{-1}$, black) and accumulated TRMM rainfall (mm, red); b) Surface heat fluxes ($W m^{-2}$): surface shortwave flux (net: red dashed; absorbed by the mixed layer: red), latent heat flux (blue), sensible + longwave flux (green) and net heat flux (dashed orange); c) SST ($^{\circ}C$, black) and SSS (psu, red); d) mixed layer depth (m) with one standard-deviation error bar (shading); e) Mixed layer heat budget in $^{\circ}C month^{-1}$ as in equation (1): mixed layer temperature tendency (red), atmospheric forcing heating rate (black), horizontal advection (green) and residual (blue), with shading indicating the one standard-deviation error bar. The grey (black) overbars indicate warming (cooling) periods corresponding to suppressed (active) convection that are used to indicate average values in the text. For this event, air-sea fluxes are the primary drivers of the SST signature of the MJO.

Mechanisms: fluxes or entrainment? In the modelling results of Duvel et al. (2004), analysis of the mixed layer budget suggested that the SST response in the SCTR was almost entirely driven by air-sea fluxes (latent and shortwave anomalies linked to the convective perturbation). In an analysis using satellite SST data and re-analysed fluxes, Duvel and Vialard (2007) found that over large regions of the tropics, there's a strong correlation between between air-sea fluxes and SST variability at intraseasonal timescale (Fig. 46). They further demonstrated that there is a reddening of intraseasonal SST variability spectrum compared to the heat flux spectrum, as expected from an ocean integrating atmospheric fluxes (e.g. Hasselman 1976). This behaviour explains the larger response of SST to MJO forcing

(~30-80 day timescale) than to quasi-biweekly intraseasonal oscillations (e.g. Chatterjee, and Goswami 2004). It is only after the Cirene cruise that in situ data became available in the region and allowed to compute the mixed-layer heat budget in the region from observations. Once again, the observational results suggested that the upper ocean SST changes were largely controlled by air-sea fluxes. Lateral advection and entrainment, while making a significant contribution to the surface layer heat budget, do not have systematic variations at the MJO timescale (Fig. 47).

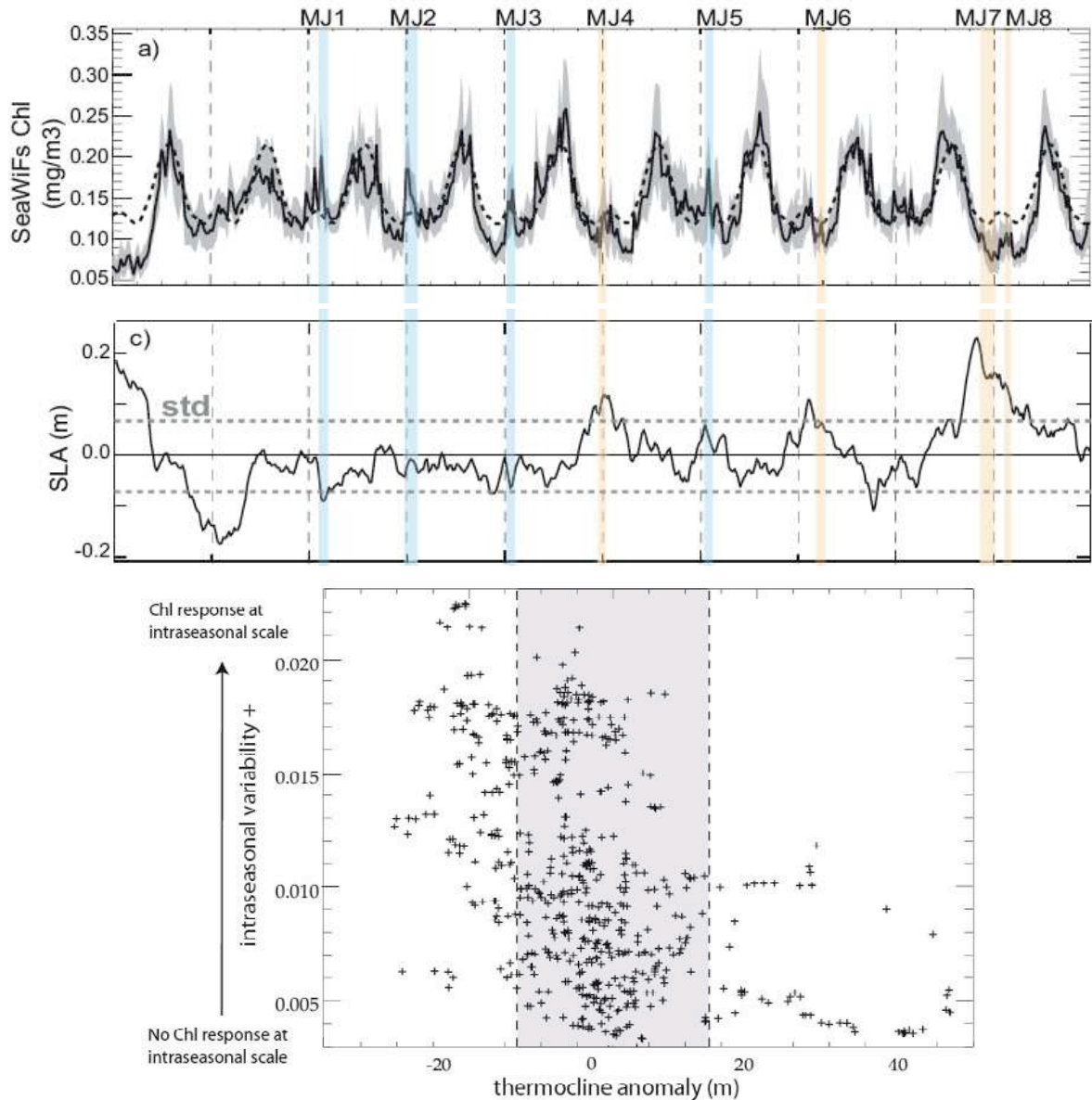


Figure 48. Adapted from [Resplandy et al. \(2009\)](#). January 1998-December 2007 time series averaged over the SCTR region. a) Surface SeaWiFS Chl median (black line) over the domain superimposed with 98-05 SeaWiFS climatological values (dashed line) and first to third quartile interval (grey shading). c) Sea Level Anomaly (SLA) (m). Highlighted MJOs correspond to active MJO phase over the Indian Ocean with amplitude greater than 1 and wind speed greater than (from Wheeler and Hendon 2004 index): blue indicates events with a response in Chl while orange indicates events with no response in Chl. The last panel shows a scatterplot between the amplitude of the Chlorophyll intraseasonal variability in the SCTR region and the thermocline depth anomaly in a forty years coupled biogeochemical-ocean general circulation model simulation. Larger intraseasonal Chl response to the MJO occurs when the thermocline is shallow.

Modulation of the MJO oceanic signature by interannual variability. The results we obtained seem to be at odds with other studies suggesting a significant contribution from either mixing/entrainment or Ekman pumping at intraseasonal timescale (Harrison and Vecchi 2001, Saji et al. 2006, Vinayachandran and Saji 2008, Lloyd and Vecchi 2009). In fact, this contradiction is only apparent. The importance of subsurface processes (mixing/entrainment and/or Ekman pumping) seems itself to be modulated by the interannual variability, as illustrated by a study of the biogeochemical response to the MJO in the SCTR region (Resplandy et al. 2009). This study shows that some MJO events are associated with surface chlorophyll blooms, while some others aren't. In observations, all the blooms happen during year of anomalously shallow thermocline associated with a negative IOD or La Niña, suggesting a control of intraseasonal blooms in response to the MJO by interannual variability (Fig. 48). This can be tested in a 40 years coupled ocean – biogeochemical model simulation (Fig. 48). Positive anomalies of thermocline are associated with very low values of Chl intraseasonal variability. On the contrary negative anomalies are mainly associated with relatively high intraseasonal variability of Chl. The spread of Chl intraseasonal response for anomalously shallow thermocline can be explained by the fact that shallow thermocline is a necessary but not sufficient condition for having a surface Chl response. I.e there can be a shallow thermocline associated with a shallow nutricline favourable to phytoplankton growth at the surface, but the biological response will occur only in cases where active MJO over the Indian Ocean induces strong winds over the SCTR.

Since a bloom is indicative of subsurface nutrient rich input water to the surface, this demonstrates that mixing with subsurface occurred and that it consequently probably played a role in cooling the SST (as also suggested by Vinayachandran and Saji, 2008). However, we demonstrate in Resplandy et al. (2009) that Chl intraseasonal events, and hence the contribution of mixing/upwelling, are modulated by the thermocline depth, with larger events when the thermocline is shallow in the SCTR, but weaker events otherwise. For example, the weak positive SLAs during the december 2007-January 2008 event directly observed by Vialard et al. (2008) might explain the relative weak contribution of the mixing and upwelling for this event. When the thermocline is anomalously shallow, on the other hand, the atmospheric forcing will combine with vertical processes to produce stronger cooling, and also a strong Chl response. It is also this modulation of the response by interannual variability which explains the relatively modest amount of significant Chl intraseasonal events in the SCTR (only 4 in 10 years, see figure 8), while significant MJO-related atmospheric forcing events occur almost every year.

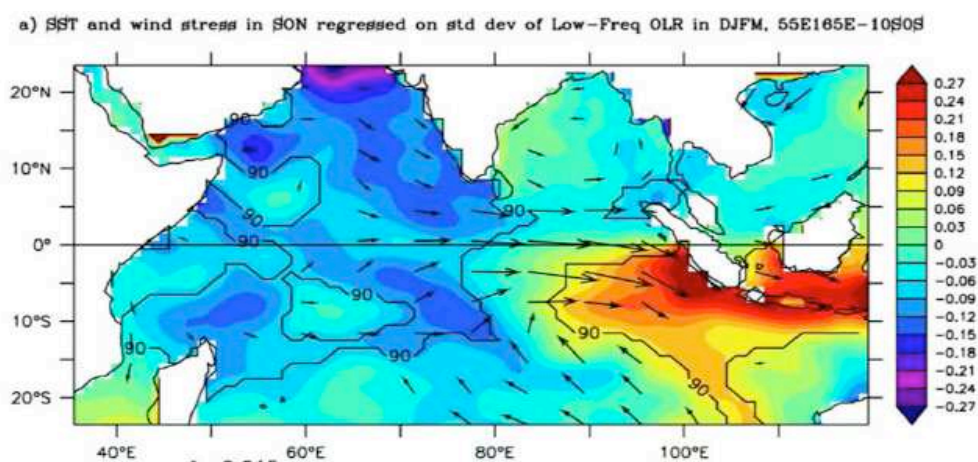


Figure 49. From Izumo et al. (2009). Regression between SST (colour, °C), wind stress (vector, $N m^{-2}$) interannual anomalies in September-November and an index of the MJO activity in December-March. The 90% confidence interval is indicated. Positive IOD years are followed by a decrease in MJO activity over the Indian Ocean and western Pacific.

Modulation of the MJO at interannual timescale. The fact that thermocline depth variability could modulate the SST signature of the MJO was first suggested by Harrison and Vecchi (2001) and Duvel et al (2004). Duvel et al (2004) further suggested that this change of the SST response could feedback on the MJO itself and modulate its activity. In a study currently in revision (Izumo et al 2009), we demonstrated that there is indeed a modulation of the MJO activity at interannual timescale. Fig. 49 shows that increased MJO activity in boreal winter tends to be preceded by a negative IOD. There are two possible explanations for that. The first one is that shallow thermocline following the IOD in the SCTR region (Fig. 32) induces a shallow, more reactive mixed layer (Fig. 45 right) and hence a larger SST signature of the MJO. This SST signature might feedback on the MJO, increasing its amplitude. However, this hypothesis does not explain the increase of the MJO activity in the western Pacific after an negative IOD (Izumo et al 2009), since the SST response to the MJO is much weaker in the western Pacific than in the Indian Ocean (Fig. 36). Another hypothesis to explain the modulation of the MJO at interannual timescale is the change in the atmospheric background state. The subsurface thermal anomalies in the SCTR region persist until March-April after and IOD, and induce changes in the convective and wind pattern over the Indian Ocean, and the western Pacific (e.g. Kug and Kang 2006, Annamalai et al 2005a). In particular the anomalous westerlies that develop over the Indian Ocean and western Pacific after a negative IOD have been suggested to be favourable breeding ground for the MJO (e.g. Inness et al. 2003b, Zhang and Dong 2004, Watterson and Syktus 2007). Understanding this interannual modulation of the MJO activity will require further research (section 4).

3.3. Results: the Indian Ocean dipole

3.3.1. Cirene: interannual anomalies in the thermocline ridge region

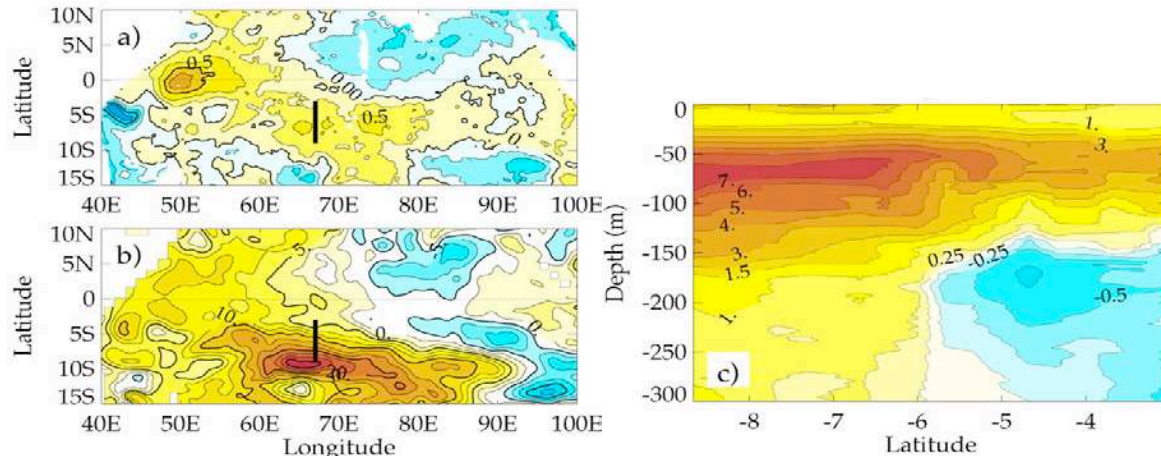


Figure 50. From Vialard et al. (2009a). Large scale situation during the Cirene cruise, in January-February 2007. a) SST interannual anomaly, b) Sea level interannual anomaly, c) Temperature difference between Cirene 67°E section and World Ocean Atlas 2005 climatology (Locarnini et al. 2006). The thick line on a) and b) shows the location of panel c) section. There was a large subsurface temperature anomaly during Cirene because of the 2006 IOD.

The large sea level anomaly in the SCTR region after an IOD (or further south after an ENSO) has been documented in many modelling studies or studies using remote observations. The Cirene dataset is the first one to offer in situ observations in this climatologically sensitive region. This dataset is presently still being analysed, but I'll try to give a flavour of the first results that it produced in this section.

The Cirene cruise happened after a strong IOD in 2006 (e.g. Vinayachandran et al. 2007). The equatorial zonal wind anomaly associated to this IOD induced, as usual, strong

Ekman convergence within the 5-10°S band (Fig. 32) which induced a large positive sea level anomaly in the SCTR region from late 2006 to late 2007 (Figs. 31, 50b). Because of the strong correlation between thermocline depth and SST anomalies in this region (Fig. 33), this translated into a warm SST anomaly in early 2007 (Fig. 50a). The Cirene cruise, in January-February 2007, was crossing the regions of largest sea level anomaly, and recorded subsurface temperature anomalies up to 7°C at the thermocline level (Fig. 50c). The cold anomalies around 150 to 250m and 4°S-5°S in this region are probably linked to decadal subsurface cooling accompanying long-term surface warming in the tropical Indian Ocean (e.g. Trenary and Han 2008).

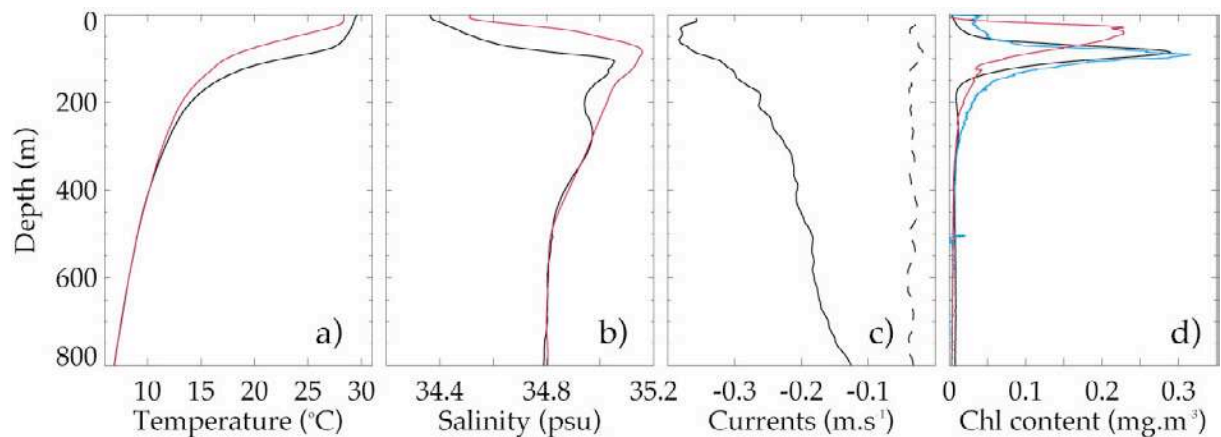


Figure 51. From [Vialard et al. \(2009a\)](#). Average profiles over whole cruise (14th January to 15th February) at 67°30'E, 8°S. a) Cirene Temperature (black) and climatology (red). b) Cirene Salinity (black) and climatology (red). c) Cirene zonal (continuous line) and meridional (dashed line) currents. d) Cirene chlorophyll content (estimated from the fluorescence profile, in black). On d) the vertical density gradients from Cirene (blue) and climatology (red) are also shown. In addition to the large temperature anomalies, the upper ocean was also unusually fresh during Cirene, and there was a significant westward current anomaly down to 800m.

The station data allowed to confirm the large subsurface temperature anomaly, but also indicated anomalous freshening of the upper 200m of the ocean, a depressed nutricline ([Wiggert et al. 2009](#)) and deeper than usual subsurface chlorophyll maximum (Fig. 51d). The zonal surface currents during the whole cruise were westward at $\sim 0.35 \text{ m s}^{-1}$, at a location where they are normally very weak (the thermocline ridge is normally the transition region between the SEC and SECC, Figs. 6-7). The surface current anomaly actually extends deep downward (Fig. 51) with 0.2 m s^{-1} currents at 600 m (comparison with geostrophic currents computed from climatology suggest that currents are normally near-zero at this depth). To understand the nature of the vertical distribution of current anomalies, we performed a normal mode decomposition of the currents (Fig. 52). The vertical structure of the Cirene currents is relatively well approximated by one vertical mode, but the second mode makes a contribution, especially near the surface. Two modes are sufficient to describe the Cirene currents. This has potential useful applications for understanding the large-scale patterns of sea level anomalies and transport in late 2006 and 2007 using a simplified projection model based on two vertical modes (work in progress).

Another ongoing work with my PhD student P. Kumar is the analysis of the causes of the warm and fresh mixed layer that prevailed in the mixed layer during Cirene. Understanding the causes of the SST anomalies in this region is particularly important in view of their multiple climatic consequences (cf end of section 3.1.1). To that end we developed a method to diagnose the mixed layer temperature and salinity budget from a combination of in situ (mostly Argo, which provides an estimate of the mixed layer depth) and satellite data (a

blend of several data is used to estimate air-sea fluxes and horizontal advection terms, the vertical processes being estimated as a residual).

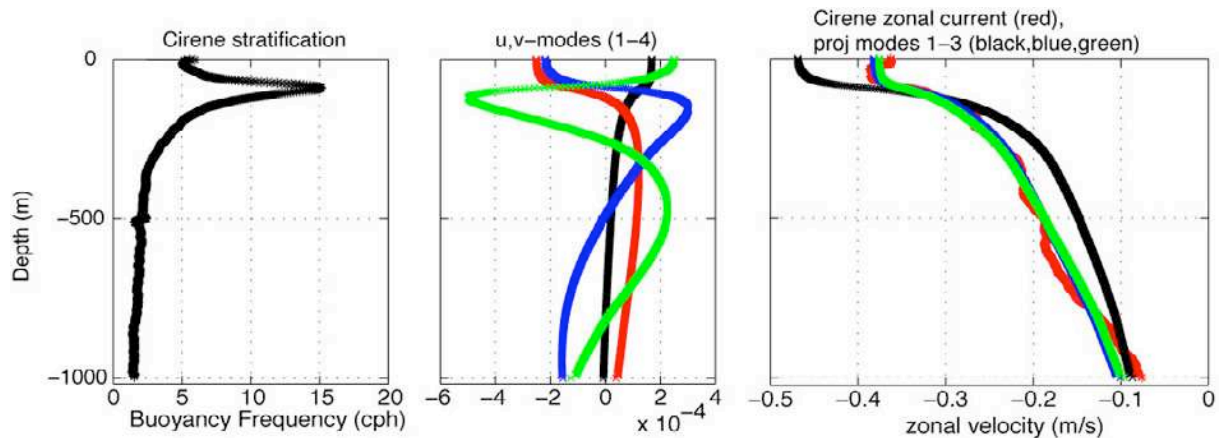


Figure 52. Courtesy of S. Kennan. (left) Cirene mean Brunt-Vaisala frequency. (Middle) Horizontal currents normal modes 1-4 (1 black, 2 red, 3 blue, 4 green). (Right) Cirene zonal current (red) and its projection on mode 1 (black), 1-2 (blue) and 1-2-3 (green). The Cire current vertical profile is very well approximated by a combination of the first two baroclinic modes.

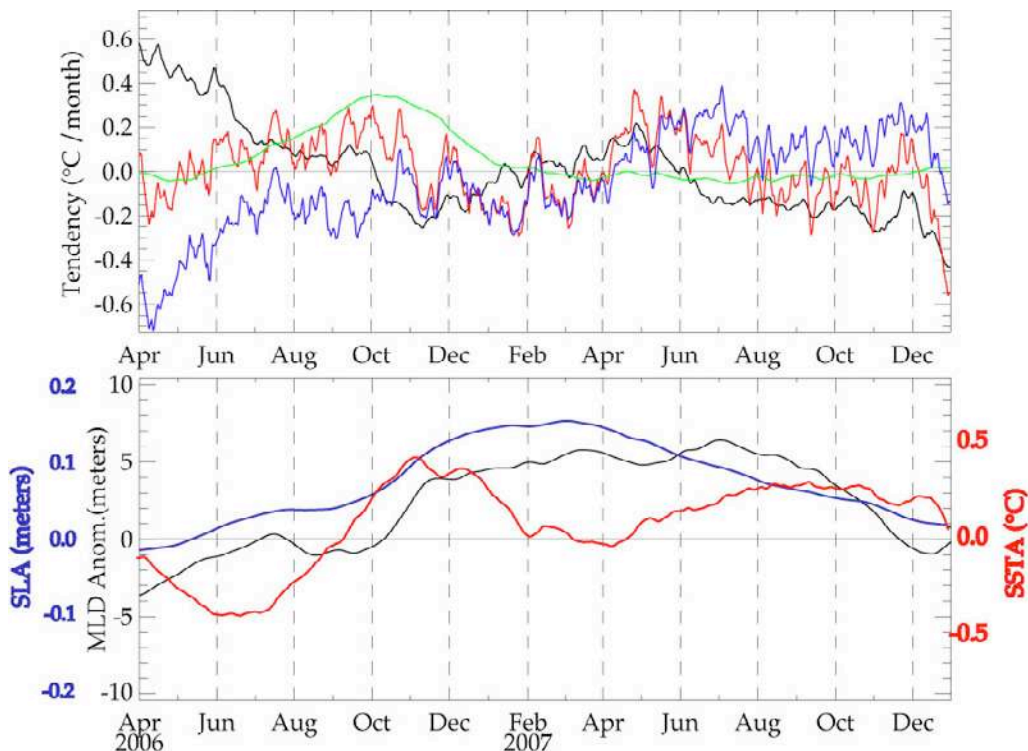


Figure 53. (Top) Estimates of interannual anomalies of tendency terms within the SCTR region (60–80°E, 10–5°S): mixed layer temperature tendency (red), air-sea fluxes (black), lateral advection (green) and subsurfaces processes (entrainment and upwelling, blue). (Bottom) Interannual anomalies of SST (red), mixed layer depth (black) and sea level (blue).

The analysis of this heat budget indicates that lateral advection contributed significantly to the initial warming in the SCTR region from August to November 2006 (Fig. 53). The breakup of the advective terms indicates that this advective warming was mostly contributed by zonal advection, consistent with the westward current anomalies observed during Cirene (Figs. 51, 52) and with the seasonal cycle of zonal SST gradients in this region (Fig. 5). Part of the high correlation between thermocline depth and SST anomalies in this region (Fig. 33)

could hence be explained by the zonal current anomalies in balance with the sea level anomaly, rather by than direct modulation of the subsurface cooling term. At a later stage (from April to December 2007), however, there is a decrease in subsurface cooling that maintains the positive SST anomaly throughout 2007 (Fig. 53). The influence of thermocline depth anomalies on the subsurface-surface connection hence seems to be seasonally dependent. We're currently trying to analyse this effect with a combination of in situ data analysis and modelling.

The analysis of the causes of the interannual upper ocean salinity anomaly also harvested interesting results. The time-series from the Argo mooring salinity (Fig. 39) showed a fast salinity change of ~ 0.5 psu over the upper 60 m in July 2007 and February 2008. Modelling experiments (not shown) displayed a similar quick salinity change and suggested the existence of a salinity front with large zonal displacements in the 5-10°S band. Analysis of Argo data confirmed the existence of this front (Fig. 54). Detailed analysis of mixed layer budget terms estimated from observations suggest that the zonal westward migration of this front occurs as a result of zonal advection by the South Equatorial Current, and that the rapid retreat around July is associated with meridional advection: the southward Ekman drift associated with the easterlies replaces the fresh water by saltier water originating from the equatorial band. Rainfall does not seem to play a strong role in controlling the front zonal movements, but is probably important in maintaining it at long timescales (most of the rainfall at this latitude occurs near the maritime continent and allows to maintain fresher water there). On the basis of this analysis, it is likely that the upper ocean freshwater anomaly in early 2007 was linked to anomalous zonal advection.

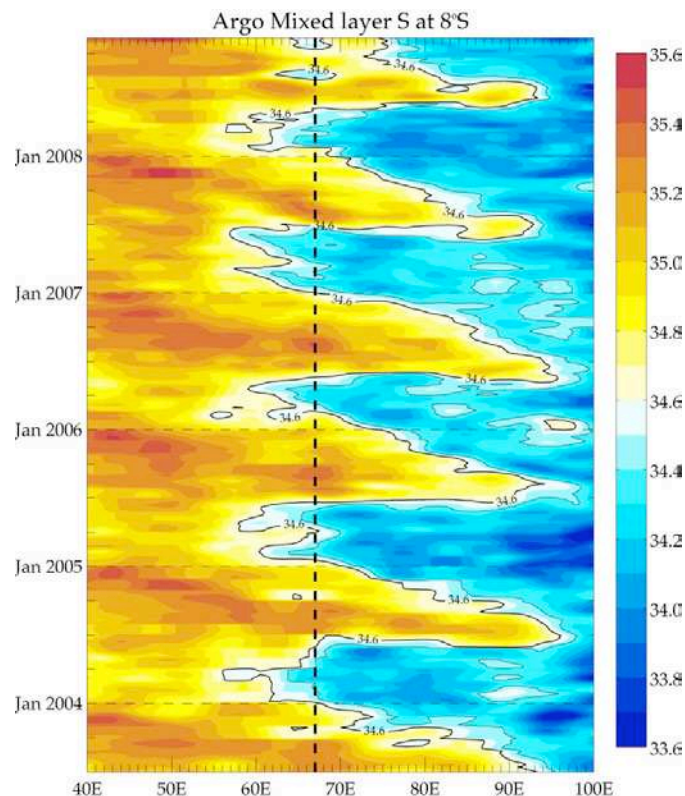


Figure 54. Time-longitude section of mixed layer salinity along 8°S in the Indian Ocean. The data is from the objective analysis of Argo data of Gaillard et al. (2009). There is a salinity front whose movements are primarily driven by advection in the SCTR latitude band.

3.3.2. The IOD: a trigger to El Niño?

Before moving to the next section, where I will discuss perspectives of my work, I would like to finish this result sections by very exciting and recent results that we are about to submit. This work has been done in collaboration with T. Izumo, M. Lengaigne, S. Cravatte, C. de Boyer Montegut, S. Masson, J-J. Luo, S. Behera and T. Yamagata.

We have discussed in section 3.1.1 some results of previous studies concerning interactions between ENSO and the IOD. It is for example known that ENSO is a possible trigger for the IOD: the easterly wind anomalies associated with change in Walker circulation pattern due to a developing ENSO in summer can start the Bjerknes interaction and result in an IOD (e.g. Annamalai et al 2003). But other studies suggest that the IOD and/or the Indian Ocean warming can also influence the termination of ENSO, because of the Pacific surface wind anomalies remotely induced by the changes in convection patterns over the Indian Ocean (e.g. Annamalai 2005a, Kug and Kang 2006, Behera and Yamagata 2003). I.e. up to now, most studies have focussed on the synchronous interaction between ENSO and the IOD. In our study, we go one step further and suggest that an IOD can influence the course of the ENSO in the Pacific during the *following* year.

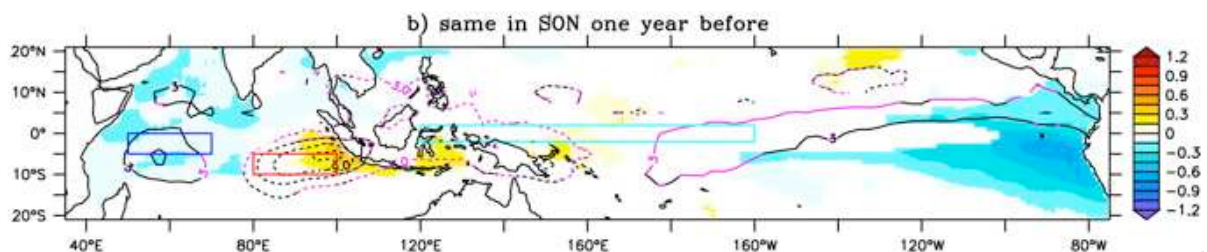


Figure 55. Anomalies of SST (colours) and OLR (contours) in September-November regressed with Niño3.4 index in December-February 14 months later. Only statistical significant signals at the 90% confidence level are plotted. A negative IOD tend to occur 14 months before an El Niño. Tests show that SST anomalies in the eastern Pacific are a much less performing predictor than the IOD index.

We show that El Niños (La Niñas) tend to be preceded by negative (positive) IODs peaking in October, 14 months before ENSO mature phase (Fig 55). We propose the following mechanism to explain the IOD influence on subsequent year's ENSO conditions, here discussed for the case of El Niño development. During a negative IOD, warm SST anomalies develop in the southeast Indian Ocean and maritime continent, increasing local convection, the ascending branch of the Walker circulation and inducing easterly wind anomalies in the western and central Pacific (Fig 56). Easterly wind anomalies favour the buildup of WWV (e.g. Meinen and McPhaden 2000), providing an efficient preconditioning for El Niño to develop. After November, the eastern pole of the IOD quickly recedes and induces a sudden collapse of these anomalous easterlies (Fig 56). The important role of wind anomalies in the western to central Pacific in ENSO transition has been noted before. We suggest here that it is more specifically the sudden relaxation of anomalous easterlies induced by the quick IOD demise that results in a sudden imbalance between zonal wind stress and pressure gradient. This imbalance propagates eastward as a Kelvin downwelling wave which pushes the western Pacific warm pool edge eastward and deepens the thermocline in the eastern Pacific (Fig. 56), thus triggering the Bjerknes feedback and leading to ENSO development.

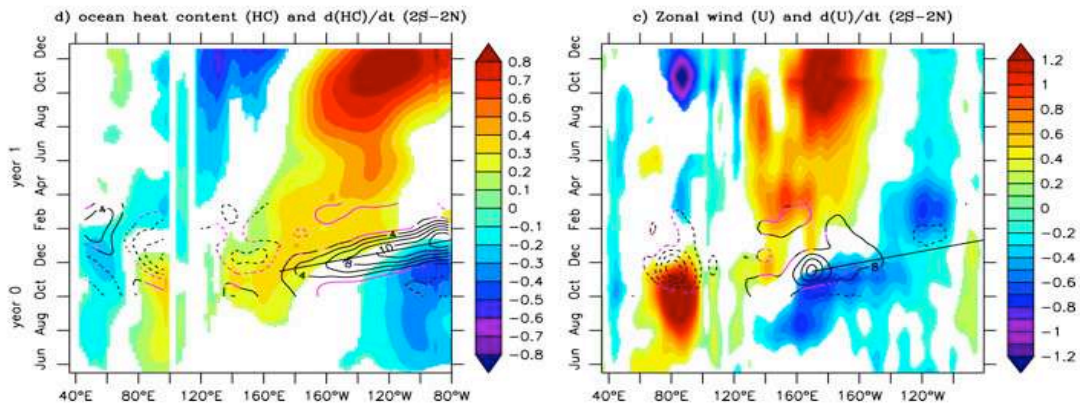


Figure 56. Heat content anomaly (left) and zonal wind anomaly (right) partially regressed on year 0 IOD index, with the influence of El Niño removed. The contours show the time-derivatives of the fields for October-March. The sudden demise of the positive IOD induces a switch from easterlies to westerlies and triggers a downwelling Kelvin wave.

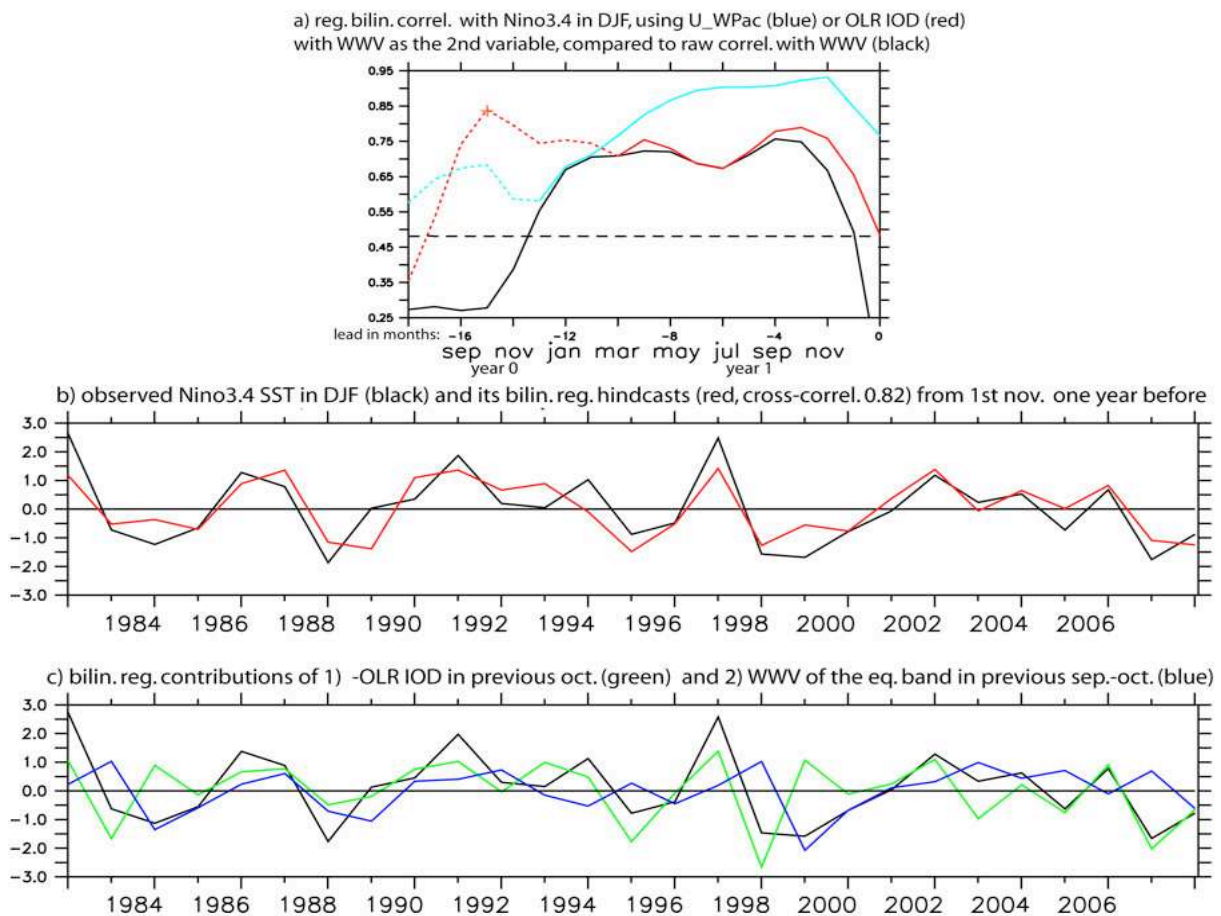


Figure 57. a) Correlation score of statistical forecast of ENSO peak using the Pacific WWV (black), the WWV and winds in the western Pacific (blue), the WWV and an IOD index (red). b) Observed (black) and predicted (red) SST anomaly at the peak of ENSO using the WWV/IOD bilinear regression model. c) Black curve as in b) and contributions of IOD (green) and WWV (blue) to the bilinear forecast shown in b).

The validity of this mechanism, and of the influence of the IOD on ENSO is supported by a simple statistical forecast of the ENSO peak. In agreement with the “recharge oscillator” theory for ENSO, the WWV provides an efficient predictor of the ENSO peak up to 9 months in advance (Fig. 55). While the predictive power of the WWV alone decreases steeply beyond 11 months of lead-time (correlation below 0.3), IOD indices are good predictors (correlation

of ~ 0.6) in autumn 13-15 months before the ENSO peak. The Indian Ocean contribution for example improves significantly the hindcasts of the 1997-98 El Niño, 1998 La Niña and 2007-08 La Niña (Fig. 57c). Over the whole 1981-2009 period the simple hindcast model results in a spectacular increase in skill score for leads of 13-15 months (Fig. 57a). This corresponds to a backward extension of the 0.8 skill score limit of more than 4 months. Whereas predictors of ENSO based on Indian Ocean variables had been suggested before, this study is the first one to identify clearly the IOD as an essential precursor/trigger of ENSO, and to provide a skill score above 0.8 before the so-called winter-spring predictability barrier (e.g. Jin et al. 2008). It highlights that the Indian Ocean is not completely slave to the powerful ENSO cycle from the neighbouring Pacific, but has degrees of freedom on its own and even partially controls ENSO state the following year.

A lot of studies have illustrated the potential role of intraseasonal wind anomalies in the western Pacific on ENSO development through the generation of Kelvin waves (e.g. Kessler 2000, McPhaden et al. 2006, [Vialard et al. 2001](#)). These anomalies include westerly wind bursts (WWBs) and the Madden-Julian Oscillation (MJO). The detailed evolution of WWBs and the MJO cannot be predicted beyond a couple of weeks. This sounds at odds with the present study, which shows that the ENSO peak is highly predictable as far as 14 months in advance. But it turns out that the envelope of the MJO itself is modulated by variability in the Indian Ocean, as discussed in section 3.2.2.2. Negative IODs are followed by more energetic MJOs in the Indian Ocean and western Pacific ([Izumo et al 2009](#)). The IOD index we use hence contains information on both interannual wind anomalies in the western-central Pacific and modulation of intraseasonal wind activity that precede El Niños. In this scenario, the changes in intraseasonal wind variability in the western Pacific could either be a consequence of interannual changes of the background state with no real role on the ENSO development, or alternatively contribute actively to the growth of ENSO together with the lower frequency wind anomaly.

This study claims for a better understanding of the links between the Indian and Pacific oceans. This is a necessary step to delineate the necessary physics to resolve in coupled ocean-atmosphere forecasting systems, which eventually represent the most complete way forward for seasonal forecasting. For achieving this improved understanding and a better constraint on dynamical forecasting systems, a necessary step forward is the achievement of a similar observing system in the Indian Ocean as those already established in the tropical Pacific and Atlantic oceans.

4. What's next?

Up to this point, I've presented my past or present areas of research and their context. In this last shorter section, I will present the main axes I have in mind for future (section 4.1). Those include brand new topics of research (like the climatic role of cyclones or processes in the North-Western Australian Basin), but also pursue of age-old science questions like processes of the MJO or the IOD-ENSO interactions. Observations are the drivers of science: in section 4.2, I'll give an overview on my projects in terms of observational programs. I'll finish with a few concluding words in section 4.3.

4.1. New areas to explore...

4.1.1. Tropical cyclones

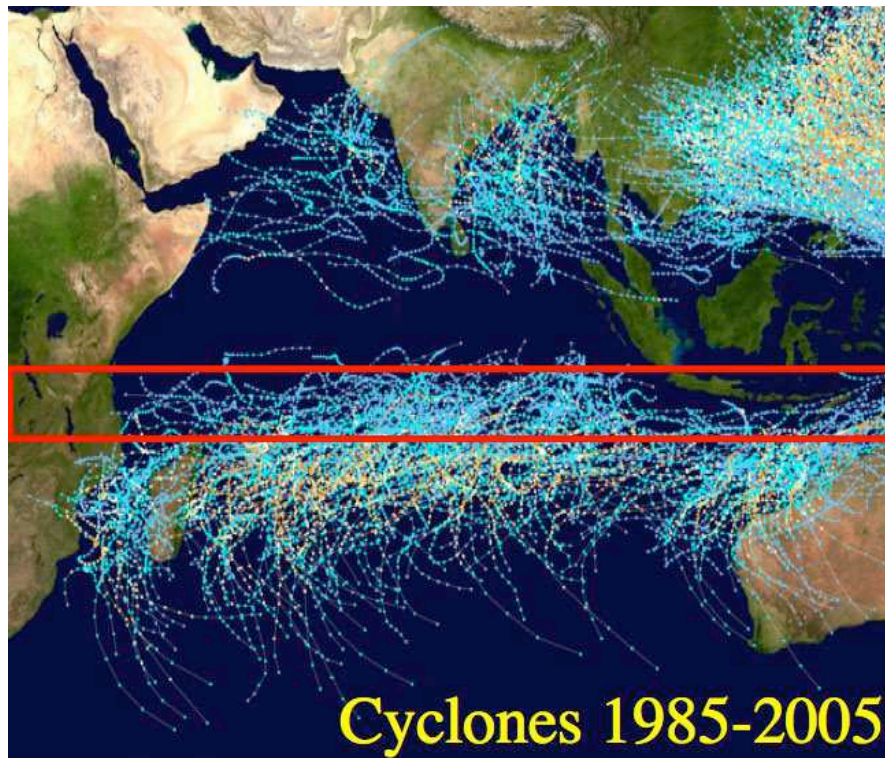


Figure 58. Trajectories of Tropical-Cyclones for 1985-2005. The red frame highlights the 5°S-12°S band. The SCTR is also a region of generation of tropical storms. Some of these tropical storms will become cyclones further south: do the oceanic stratification in the SCTR influence them during their early life?

Most of the cyclones that hit Australia or Madagascar / La Réunion were first developed as tropical storms in the 5-10°S band. It seems that air-sea interactions in this region can modify their future characteristics: an anomalous heat content in the SCTR region can influence the number of cyclone-days in the Madagascar-La Réunion sector (Xie et al 2002). In addition to this modulation of cyclonic activity by interannual variability, there's also a clear modulation of tropical cyclones in this region by the MJO (e.g. Liebmann et al. 1994, Bessafi and Wheeler 2006).

Cyclones can influence the ocean in mainly two ways: they are associated with heat uptake by evaporative cooling, and they induce additional mixing and Ekman pumping. On the other hand the upper ocean heat content along the cyclone track has long been known as an important parameter for controlling the evolution of the cyclone intensity (e.g. Goni and Trinanes 2003).

During the Cirene cruise, a tropical storm that would then become cyclone Dora passed almost exactly over the location of the long station and ATLAS mooring (Vialard et al 2009a). The detailed analysis of the upper ocean thermal response to the cyclone is underway in collaboration with G. Foltz and M. McPhaden. Similarly, the dynamic response to the cyclone (generation of near-inertial oscillations and associated mixing) is also ongoing (in collaboration with P. Bouruet-Aubertot, Y. Cuippers and X. Vaillant). But in addition to these punctual process studies, a more systematic study of the cyclone influence on the climate on this region and of the influence of the SCTR on cyclogenesis is underway, in collaboration with M. Lengaigne and C. Menkes. I am mostly interested by the following questions in this framework:

- Document better the oceanic response to tropical storms and cyclones in the Southern Indian Ocean from Cirene and RAMA data.
- Is the response to tropical cyclones in the SCTR region modulated at interannual timescales by ENSO / the IOD?
- How much do cyclones and tropical storms contribute to heat uptake and mean oceanic state in the Indian Ocean ?
- How much do tropical cyclones / storms contribute to the MJO induced cooling events in the SCTR and North Western Australian Basin regions?
- Is there an interannual modulation of the cyclone activity in the South Western Indian Ocean? Is rather related to large-scale atmospheric environment (e.g. vertical shear)? Is it related to change in the oceanic conditions?

I will try to address these questions in future, using both existing datasets (Cirene data and RAMA dataset) and modelling (both forced and coupled). The TRIO cruise and contribution to RAMA (section 4.2) also has some specific objectives in terms of cyclone observations.

4.1.2. Questions about the MJO

There is flourish of unresolved questions about MJO mechanisms (e.g. multi-scale nature of the MJO, interactions between the large scale subsidence and recharge of moisture in the planetary boundary layer, role of extra-tropical perturbations, cloud-radiation feedbacks, etc.; see Wang 2005 and Zhang 2005 for reviews). My objective here is not to summarize all these questions but to pinpoint those on which I would like to work on the coming years.

Role of coupling and diurnal cycle. There have been many studies of the role of coupling of the MJO. Most of these studies suggest that taking air-sea coupling into account result in a moderate improvement of the MJO simulated properties. However, existing coupled models largely underestimate the SST signature of the MJO in the SCTR and NWAB regions (Xavier et al 2008), and only a few studies did take into account the diurnal cycle of the SST (Woolnough et al 2007, Bernie et al 2008). There is a real need to re-assess the role of the coupling in the MJO in coupled models with a more realistic response in these two key regions. Analysis of a recent simulation with the Sintex-F model (Luo et al. 2003) that includes the diurnal cycle show a reasonable amplitude of the SST response in the SCTR and NWAB regions and can for example be used to re-assess the impact of coupling on the MJO.

Interannual modulation of the MJO. In Izumo et al (2009), we have demonstrated that the IOD modulates the amplitude of the MJO activity in the Indian Ocean and Western Pacific. But the mechanism explaining the control of the change in MJO activity by the mean state remains to be elucidated. As we discussed earlier, two possible tracks to follow are the modulation of intraseasonal air-sea coupling by the ocean subsurface interannual anomaly or the interannual changes in the Atmospheric basic state. I think that the second option is most likely, and it could be tested by examining composites of the MJO structure (and in particular

moisture convergence in the atmospheric boundary layer) from re-analyses after negative or positive IOD years. Sensitivity experiments with a coupled model are another possible route to follow to examine this issue.

The MJO as an off-equatorial process. The dominant MJO theory (frictional convergence feedback) is largely an equatorial theory (i.e. based on equatorial Kelvin and first meridional mode Rossby waves, which are symmetric and have maximum signature at the equator or within 10°N-10°S). Inclusion of mean state in the frictional convergence feedback theory has had some success in explaining the summer intra-seasonal oscillation (Wang 2005), but has not been applied to the boreal winter MJO. The MJO is largely shifted to the south of the equator in boreal winter. Friction in the boundary layer is much less efficient in producing convergence at around 10°S than in the equatorial beta-plane. Most of the analyses of the MJO structure and associated moisture convergence use an equatorial MJO index (e.g. Hendon and Salby 1994). It would be extremely useful to re-assess the three-dimensional patterns associated with the MJO without restricting the analysis to the equatorial band, in particular for the Boreal winter MJO. In the past, I have mostly concentrated on mechanisms of the oceanic response to the MJO, but I have become more and more familiar with the concepts of tropical meteorology over the years. In the coming years, I'm planning to get more involved in the analysis of the atmospheric structure of the MJO. I would like to start by examining the 4D structure of the MJO specifically for winter, and try to relate the observed features to the existing MJO theories.

4.1.3. The North-Western Australian basin (NWAB)

Duvel and Vialard (2007) demonstrated that the region with strongest SST signature of the MJO is found northwest of Australia, between Australia and Indonesia. This region is also a region of very strong diurnal cycle of the SST, and very strong modulation of this diurnal cycle by the MJO (Bellenger and Duvel 2009). The SST signature in this region is even stronger than in the SCTR region, possibly because of the intraseasonal SST response rectification by the diurnal cycle proposed by Bernie et al. (2005). To my knowledge, the impact of this large SST signal on the MJO characteristics over Australia and Indonesia has not been studied, and deserves such a study because of the strong modulation of rainfall by the MJO over northern Australia (Wheeler and Hendon 2004). The ocean response to the MJO in this region, and the potential feedback on the MJO properties thus deserves to be better studied, both from an observational and modelling point of view.

There is presently no mooring planned within the RAMA framework in this region. I proposed within the framework of the IOP to deploy an ATLAS mooring (in collaboration with PMEL) in this region in the framework of the TRIO cruise (see 4.2). This mooring will remain at this location for about two years in the framework of a process study dedicated to the study of the ocean signature of the MJO in this region. The potential inclusion of this mooring in the RAMA design will then be discussed within the IOP depending of the results harvested during this process experiment phase. This mooring data will allow to document better the surface flux signature of the MJO in this region, the contribution of the diurnal cycle to the total intraseasonal variability and the processes of the SST signature of the MJO.

This observational analysis will have to be completed by a modelling approach to evaluate the impact of coupling on the MJO in this region. I am also presently seeking collaborations in Australia to study the impact of the large SST signals in the North-Western Australian Basin region, in particular in terms of potential predictability of the rainfall.

4.1.4. Indo-Pacific as a single basin

Some of our recent work suggests a potential influence of the IOD on next year's evolution of the ENSO cycle in the Pacific basin (section 3.3.2). Although the suggestion of

this impact from the statistical forecast approach is very strong (including an IOD index spectacularly increases forecasts of the ENSO peak in the 11-15 months lead time range), the exact mechanism by which the IOD could influence El Niño still has to be studied in more detail. A few examples of questions, which have to be addressed through a mix of observational analysis and GCM experiments follow:

- Does a negative (positive) IOD induce an increase (decrease) of Easterlies over the Pacific during July-November? Observations seem to show that (section 3.3.2) but some previous modelling studies suggest otherwise (e.g. Annamalai et al. 2005a).
- How much does such increased easterlies contribute to WWV recharge (and ENSO preconditioning) in the Pacific Ocean? Does the delayed-oscillator mechanism also contribute to ENSO triggering by the IOD? (Anomalous easterlies force downwelling Rossby waves in October-November, which come back as downwelling Kelvin Waves 3-6 months later; the zonal current anomalies associated with these waves can help initiating an eastward movement of the warm pool).
- What is the forced oceanic response to easterlies relaxation such as those documented in figure 56? By how much does the resulting eastward advection push the warm pool eastward?
- What are the respective roles of the low frequency wind perturbations and of the modulation of MJO / WWB activity in the eastward extension of the warm pool (although they seem to be difficult to separate: Marshall et al. 2009)?

Investigating these questions will help confirming or infirming the mechanism proposed in section 3.3.2 and to ascertain the influence of the IOD on the ENSO cycle. All in all, the Pacific and Indian oceans appear as highly interactive systems. Indeed, El Niño induces an overall long-lasting warming of the Indian ocean and sometimes triggers an IOD (section 3.1.1). An IOD or basin-wide Indian ocean warming seem to influence the synchronous ENSO, in particular during its decaying phase (e.g. Annamalai et al. 2005a, Kug and Kang 2006). And our results now suggest that an IOD can influence the following year ENSO. This “closing of the loop” is a potential explanation to the biannual tendency of the western Pacific and Indian Ocean (e.g. Clarke et al. 1998, Meehl 1997): an ENSO tends to induce a synchronous IOD, which tend to favour an opposite phase ENSO the following year, etc... In this respect, it seems to be advisable to study the Indian and Pacific oceans as one, rather as separate systems.

Another strong argument for studying Pacific and Indian Oceans together is the fact the MJO develops in the Indian ocean and propagates in the Pacific. The results in this document also show that interannual anomalies in the Indian Ocean can modify the MJO characteristics both in the Indian Ocean and Western Pacific, making one more case to consider to study these two basins together. In fact, this is a rather obvious case, considering the fact that these two basins share the area of warm water responsible for the ascending part of the Walker circulation, one of the fundamental ingredients of our Earth’s climate.

4.2. Observational programs

4.2.1. The TRIO program

TRIO can be seen of a follow-up to Vasco-Cirene, with extended science goals. I won’t describe the TRIO project in detail here, but just give an overview. The reader craving for more details can access the TRIO science plan and ship time proposal from my webpage (<http://www.locean-ipsl.upmc.fr/~jv>).

The TRIO (Thermocline ridge of the Indian Ocean) project aims at analysing the coupled processes associated with prominent phenomena in the 5°S-12°S band of the Indian Ocean (i.e. cyclones, MJO, IOD), their scale interactions and their predictability. TRIO is an integrated project that continues and expands the Vasco-Cirene programme. TRIO will combine modelling, analysis of past observations and a new field experiment. The field experiment is mostly based on a cruise in the 5°S-12°S band and will interact with three satellite programs (Altika, SMOS and Megha-tropiques) and with the development of a mooring Array in the Indian Ocean (the RAMA array). The TRIO cruise will cover the 5°S-10°S band in the Indian Ocean and the northwestern Australian basin. These two regions have recently been identified as the two regions with the strongest surface temperature signals associated with the MJO. The TRIO cruise plans include a deployment of a mooring in the NWAB region (cf 4.1.3), study of strong intraseasonal Rossby waves along 12°S (see TRIO science plan), study of the salinity front, study of ocean mixing at selected sites, and a long-term station to complete the SWICE measurement network, and more targeted on the MJO and cyclones.

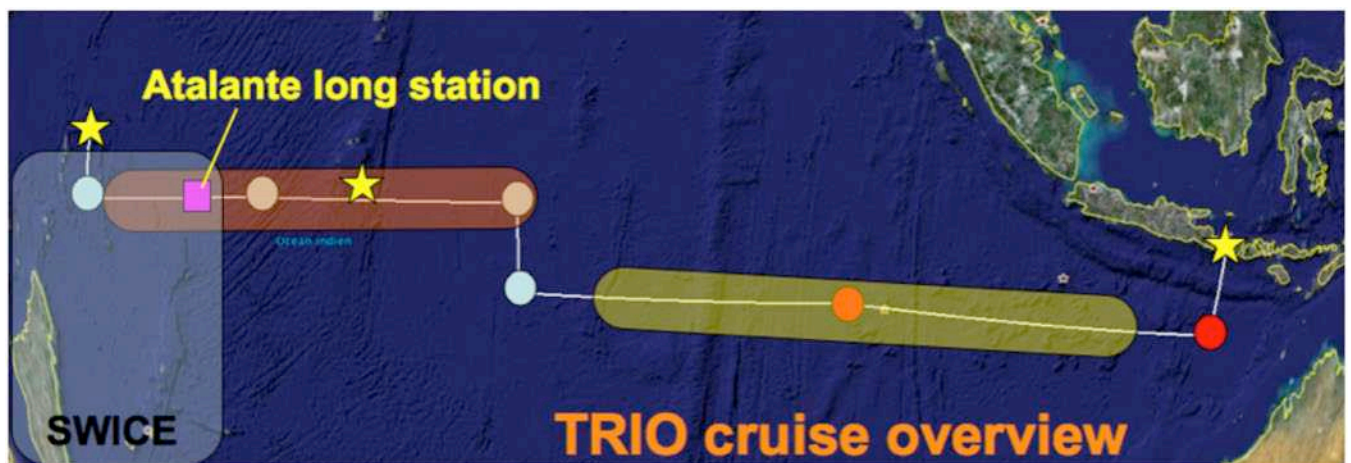


Figure 59. Overview of the TRIO cruise. The cruise starts from Padang Bai in Bali (Indonesia), deploys two new moorings in collaboration with PMEL (red circles) and services up to 4 more RAMA moorings, depending on the state of the network. There is strong intraseasonal variability of the sea level along 12°S, and TRIO will sample one Rossby wave oceanic structure (within the region highlighted in yellow). TRIO will repeat partially one WOCE section (region highlighted in red), allowing for an estimate of interannual to decadal variability in this region, and allowing sampling the salinity front in this region. The main process study of TRIO, in collaboration with SWICE follows: the Atalante, located at the magenta square, will perform a ~25-day long station with intense atmospheric, surface, and oceanic measurements. Autonomous profiling instruments (ASIP, Glider, microstructure measurements) will be deployed during that station. All along the cruise, Argo profilers will be deployed to fill gaps in the Argo network, and continuous measurements will be acquired (TSG, S-ADCP, Flux mast, Radiosondes, WBTs, XCTDs). The stars indicate the departure port (Padang Bai in Bali) and the arrival port (Victoria in Seychelles). The last star indicates the Diego Garcia Island, where a port call might be organized.

The initial plan was to coordinate TRIO with SWICE (South West Indian Ocean Cyclone Experiment, a French project targeting Cyclone analysis in the southwestern Indian Ocean). The SWICE project targets the period in early 2011. Unfortunately, the TRIO ship time proposal has not been selected in late 2009 and it seems now unlikely that the TRIO cruise will happen in early 2011, but rather in late 2011 or early 2012. We will explore the following option with the SWICE investigators: SWICE could be rescheduled one year later. This would have several advantages: TRIO could thus contribute and benefit from the intensive radiosonde network set up during SWICE. In addition, TRIO and SWICE could join

an international effort to study the MJO in late 2011 / early 2012 (the Japanese CINDY cruise by K. Yoneyama, the US lead DYNAMO cruise by C. Zhang and the Australian cruise). If this synchronization happens, this international effort would lead to an intensive meteorological and oceanographic effort during the convection / cyclonic season in the Indian Ocean with an intensive radiosonde network (from Island and ships), one plane (SWICE) and up to 4 oceanographic ships (Japanese, US, Australian and French with TRIO). This will be discussed among the main players of this proposal at the next IOP meeting in June.

4.2.2. French contribution to the RAMA array

The RAMA array is an international effort. Up to now, the largest contributions have been from US (PMEL), Japan (JAMSTEC), India (Ministry of Earth Sciences and INCOIS), China, Indonesia and South Africa. The French contribution has only been punctual (deployment of the 8°S, 67°E mooring during the Cirene cruise in January 2007; re-deployment of this mooring during a transit of the Marion Dufresne in August 2008). The TRIO cruise will also contribute to RAMA, but again in a punctual way. I'm now trying to organise a more permanent contribution of France to the RAMA array, by taking opportunity of the presence of the Marion Dufresne in the Indian Ocean. Making reasonable assumptions based on previous years port calls and routes, the minimum number of days that seem necessary to perform sufficient interventions on the array every year is 15 days of ship time (either as dedicated cruises or as piggyback-cruises).

This has several incentives. First, there is mounting evidence that suggests that climatic anomalies in the Indian Ocean not only have impact locally around the Indian Ocean, but also at the global scale (see Schott et al. 2009 for a review). Second, France (through Météo France) is responsible of the cyclone forecasts in the southwest Indian Ocean sector. The cyclones that develop over the thermocline ridge can indeed affect French territories like La Réunion. In this respect, data from the RAMA array have two strong potential benefits: 1) they will contribute to the improved understanding of air-sea interactions associated with tropical storm and cyclones; 2) surface meteorological data from the RAMA array can contribute to improved forecast by assimilation of surface wind and pressure data in weather forecast models.

I have thus started a dialog with the potential parties involved in setting up this contribution to RAMA: IPEV (who owns the Marion Dufresne), INSU (the French coordinating organism for this kind of action), Météo France (responsible of cyclone forecasts over the south-western Indian Ocean sector) and IRD (who has historically contributed to TAO and PIRATA arrays and has the expertise to help in such deployments). All the parties sounded interested by the project. IPEV could contribute some dedicated ship time from the Marion Dufresne. Météo France has proposed to fund extra pressure sensors on all the RAMA moorings at 5°S and southward. INSU and IRD could contribute with manpower to second the PMEL personnel with deployments. The next step is now for me to compile a formal proposal for this plan (maybe as an "ORE"), aiming at a memorandum of understanding between NOAA, IPEV, IRD, Météo France and INSU.

4.3. Concluding remarks

For my first steps in climate science, I worked on the tropical Pacific, mostly from an oceanographic perspective, and using mostly modelling tools. After a parenthesis in data assimilation and seasonal forecasting at ECMWF, my work as an IRD researcher has been attracted more towards tropical meteorology, focussed on the Indian Ocean, and largely based on observational analysis. This involvement in observations culminated in the Cirene cruise. Now, it seems to me that instead of this thematic movement I had over the last few years (from ocean to atmosphere, from modelling to observations and from the Pacific to the Indian

Ocean), I need to try to take more height in order to combine both perspectives at the same time (ocean and atmosphere, modelling and observations, Pacific and Indian, cheese and dessert). I tried to illustrate this in section 4.1.4: when it comes to interannual variability, the Indian and Pacific Oceans probably cannot be studied as separate basins... In this respect, it also seems quite important to remain curious and read a lot, about one's research topics, but also about connected ones. There is a permanent flow of ideas within climate research: for example, the wind evaporation feedback idea was initially developed to explain the MJO, but does not really apply to it. On the other hand, a slight alteration of this idea (wind-evaporation-SST feedback) is quite successful in explaining meridional dipole anomalies that sometime occur in the Atlantic Ocean (Xie and Philander 1994).

The synergy between observations and modelling is also very important. Observations are the drivers of science. This is particularly true in the poorly observed Indian Ocean where every new type of observation seems to allow the discovery of a new and potentially important feature. The TMI satellite data allowed discovering that the MJO SST signature was much larger than previously thought, thanks to the ability of this instrument to "see" below convective clouds (section 3.1.2). The Argo data allowed to discover a zonally moving salinity front at 10°S in the Indian Ocean (section 3.3.1). Even revisiting old datasets (like altimetry dataset) allow the discovery of new features, like the basin scale intraseasonal circulation discussed in section 3.2.1. The models then take their full dimension when it comes to analyse the processes responsible for these features. For example, I am now using a modelling approach (combination of linear continuously stratified model and OGCM) to investigate the details of the intraseasonal response of the Northern Indian Ocean coastal waveguide to winds variations associated with the MJO. This modelling approach makes it much easier to e.g. distinguish the respective contributions of local and remote forcing than a purely observational analysis.

I will thus try to adopt this synergistic approach combining observations and modelling in the next few years. But observations, and in particular oceanographic cruise, will probably be my main emphasis. I enjoyed tremendously being the chief scientist on Cirene and can't wait to be back on the deck of a research vessel for TRIO. Organizing an oceanographic campaign is a long and hazardous task, especially in those times where funding becomes sparse. This is especially the case in the Indian Ocean, where French R/Vs are difficult to bring. But in the end, it is such a rewarding feeling to be at the heart of the problem: there, somewhere in the Indian Ocean, floating at the interface between the ocean and the atmosphere, listening to their secret conversation and dreaming about what happens above and below...

Abbreviations

AGCM. Atmospheric General Circulation Model. A model constructed from primitive equations.

Argo. Array for Real-Time Geostrophic Oceanography. This program has led to the deployment of ~3000 autonomous profilers in the world ocean, that nominally provide a 0-2000m profile of conductivity, temperature, pressure every 10 days.

CLIVAR. Climate variability and predictability. One of the WCRP programs.

ECMWF. European Centre of Medium-Range Weather Forecast. European organization based in Reading (United Kingdom) and performing routinely ensemble long lead forecasts at several lead times, up to 6 months seasonal forecasts.

EICC. East Indian Coastal Current. Seasonally reversing current flowing along the East Coast of India.

ENSO. El Niño Southern Oscillation. The leading mode of climate variability at interannual timescales.

EUC. Equatorial Under-Current. Eastward flowing subsurface current at the thermocline level found in the Atlantic and Pacific oceans. A transient EUC can also form in the Indian Ocean (Sengupta et al 2007).

GCM. General Circulation Model. A model constructed from primitive equations. See OGCM and AGCM.

IOD. Indian Ocean Dipole. The little brother of El Niño. Air-Sea coupled interannual phenomenon in the Indian Ocean Basin.

IOP. Indian Ocean Panel. One of the expert panels from CLIVAR.

ITCZ. Inter Tropical Convergence Zone. The seasonally migrating region of maximum deep atmospheric convection in the tropics.

MJO. The Madden-Julian Oscillation, named after its discoverers, is the leading mode of Atmospheric variability at intraseasonal timescale, and involves coupling between deep atmospheric convection and dynamics.

MLD. Mixed layer depth. The upper ocean layer that exchange properties with the atmosphere.

NCEP. U.S. National Centers for Environmental Prediction. The NCEP has produced a widely used re-analysis of the atmospheric conditions over the last 50 years.

NEC. North Equatorial Current. The westward current that flows at ~10°N in the Pacific ocean, on the northern flank of the thermocline ridge associated with ITCZ wind convergence.

NECC. North Equatorial Counter-Current. The eastward current that flows at ~6°N in the Pacific ocean, on the southern flank of the thermocline ridge associated with ITCZ wind convergence.

NOAA. The National Oceanic and Atmospheric Administration is US a federal agency focused on the condition of the oceans and the atmosphere. They are the main contributors to the TAO, RAMA and PIRATA programs.

NWAB. North Western Australian Basin. The region of strongest signature of the ocean to the MJO (Duvel and Vialard 2007), located between Australia and Indonesia.

OLR. Outgoing longwave radiation at the top of the Atmosphere (in $W m^{-2}$). Indicates the temperature of the surface (clear sky) or cloud top (cloudy scenes) and is hence a proxy of atmospheric convection.

OGCM. Ocean General Circulation Model. A model constructed from primitive equations.

- PIRATA. *Prediction and Research Moored Array in the Atlantic. A basin-scale moored array monitoring in near real time the state of the Atlantic Ocean subsurface ocean and surface meteorological parameters.*
- PMEL. *Pacific-Marine Environment Laboratory. A NOAA laboratory in Seattle (US) that has played a key role in the three tropical mooring arrays (TAO, PIRATA, RAMA) development.*
- RAMA. *Research Moored Array for African-Asian-Australian Monsoon Analysis and Prediction. A basin-scale moored array monitoring in near real time the state of the Indian Ocean subsurface ocean and surface meteorological parameters. The Indian Ocean counterpart to TAO and PIRATA.*
- SCTR. *Seychelles-Chagos Thermocline Ridge. A thermocline ridge within 5-10°S in the Indian ocean, induced by climatological Ekman pumping. It has strong climatic impacts, and variability at several timescales (cyclones / MJO / IOD).*
- SEC. *South Equatorial Current. In the Pacific, the South equatorial current has two branches (one slightly north of the equator, one between 2°S and 10°S). In the Indian Ocean, the South Equatorial current is on the southern Flank Of the SCTR, southward of 10°S. There's also a SEC in the Atlantic ocean.*
- SL or SLA. *Sea level or sea level anomaly. Elevation of the sea surface due to ocean dynamics. In this manuscript, SL always refer to anomalies / mean circulation and SLA to anomalies / mean seasonal cycle.*
- SST or SSTA. *Sea Surface temperature or Sea Surface Temperature anomaly. In this manuscript, SSTA refers to anomalies / mean seasonal cycle.*
- TAO. *Tropical Atmosphere Ocean array. A basin-scale moored array monitoring in near real time the state of the Pacific Ocean subsurface ocean and surface meteorological parameters.*
- TIWs and TIVs. *Tropical Instability Waves or Vortices. Vortices and associated undulations of the SST front north of the equatorial tongue in the Eastern Atlantic and Pacific oceans.*
- TOGA. *Tropical Ocean Global Atmosphere. The precursor to the CLIVAR program. The TAO array was built during the TOGA decade.*
- WCRP. *World Climate Research Program.*
- WICC. *West Indian Coastal Current. Current flowing along the East Coast of India. The WICC was though to be seasonally reversing but we demonstrated that it is in fact dominated by intraseasonal fluctuations (Vialard et al. 2009b).*
- WJ. *Wyrтки Jet. Named after its discoverer Klaus Wyrтки. Strong westward jet (often more than 1 m s⁻¹) that occurs in the equatorial Indian Ocean during the Inter-monsoons (May and October-November).*
- WWB. *Westerly Wind Bursts. Synoptic to intraseasonal wind events in the Indian Ocean and Western Pacific. WWBs occur more frequently (but not always) during the active phase of the MJO. In the western Pacific, they can contribute to trigger an El Niño.*
- WWV. *Warm water volume. The volume of water above 20°C within 5°N-5°S, 120°E-80°W in the Pacific Ocean. The WWV is an efficient predictor of El Niño.*

References

- Allen, M. R., S. P. Lawrence, M. J. Murray, C. T. Mutlow, T. N. Stockdale, D. T. Llewellyn-Jones, and D. L. T. Anderson, 1995: Control of tropical instability waves in the Pacific. *Geophys. Res. Lett.*, **22**, 2581–2584.
- An, S.-I., 2008: Interannual Variations of the Tropical Ocean Instability Wave and ENSO, *J. Climate*, **21**, 3680–3686.
- Annamalai, H., H. Okajima and M. Watanabe, 2007: Possible impact of the Indian Ocean SST on the northern hemisphere circulation during El Niño, *J. Climate*, **20**, 3164–3189.
- Annamalai, H., P. Liu and S.-P. Xie, 2005b: Southwest Indian Ocean SST variability: its local effect and remote influence on Asian monsoons, *J. Climate*, **18**, 4150–4167.
- Annamalai, H., R. Murtugudde, J. Potemra, S.P. Xie, P. Liu, and B. Wang, 2003: Coupled dynamics over the Indian Ocean: Spring initiation of the zonal mode. *Deep Sea Research II*, **50**, 2305–2330.
- Annamalai, H., S.-P. Xie, J.-P. McCreary, and R. Murtugudde, 2005a: Impact of Indian Ocean sea surface temperature on developing El Niño, *J. Clim.*, **18**, 302–319.
- Baturin, N. G. and P. P. Niiler, 1997: Effects of instability waves in the mixed layer of the equatorial Pacific. *J. Geophys. Res.*, **102**, 27771–27793.
- Behera, S.K. and T. Yamagata, 2003: Influence of the Indian Ocean Dipole on the Southern Oscillation, *J. Meteorol. Soc. Jap.*, **81**, 169–177.
- Bellenger, H. and J.-P. Duvel, 2009: An Analysis of Ocean Diurnal Warm Layers over Tropical Oceans, *J. Clim.*, **in press**.
- Bellon, G., A.H. Sobel and J. Vialard, 2008, Ocean-atmosphere coupling in the monsoon intraseasonal oscillation: a simple model study, *Journal of Climate*, **21**, 5254–5270.
- Benestad, R. E., R. T. Sutton, M. R. Allen, and D. L. T. Anderson, 2001: The influence of subseasonal wind variability on tropical instability waves in the Pacific. *Geophys. Res. Lett.*, **28**, 2041–2044.
- Bernie, D.J., E. Guilyardi, G. Madec, J.M. Slingo and S.J. Woolnough, 2005: Impact of resolving the diurnal cycle in an ocean–atmosphere GCM. Part 2: A diurnally coupled CGCM, *Clim. Dyn.*, **31**, 901–925.
- Bernie, D.J., S.J. Woolnough, J.M. Slingo and E. Guilyardi, 2005: Modeling diurnal and intraseasonal variability of the ocean mixed layer, *J. Climate*, **18**, 1190–1202.
- Bessafi, M. and M.C. Wheeler, 2006: Modulation of south Indian Ocean tropical cyclones by the Madden-Julian oscillation and convectively coupled equatorial waves, *Mon. Wea. Rev.*, **134**, 638–656.
- Bjerknes, J. 1966: A possible response of the atmospheric Hadley circulation to anomalies of ocean temperature. *Tellus* **18**, 820–829.
- Bladé, I., and D. Hartmann, 1993: Tropical intraseasonal oscillations in a simple nonlinear model. *J. Atmos. Sci.*, **50**, 2922–2939.
- Bonjean F. and G.S.E. Lagerloef, 2002: Diagnostic Model and Analysis of the Surface Currents in the Tropical Pacific Ocean, *J. Phys. Oceanogr.*, **32**, 2938–2954.
- Boulanger, J.-P., and C. Menkes, The TRIDENT Pacific model. Part II: The thermodynamical model and the role of long equatorial wave reflection during the 1993–1998 TOPEX/POSEIDON period, *Clim. Dyn.*, **17**, 175–186, 2001.
- Boulanger, J.-P., S. Cravatte, and C. Menkes, Reflected and locally wind-forced interannual equatorial Kelvin waves in the western Pacific Ocean, *J. Geophys. Res.*, **108**, 3311, doi:10.1029/2002JC001760, 2003.
- Busalacchi A. J., M. J. McPhaden, and J. Picaut, 1994: Variability in equatorial Pacific sea surface topography during verification phase of the TOPEX/POSEIDON mission, *J. Geophys. Res.*, **99**, 24 725–24 738.
- Chatterjee, P., and B. N. Goswami, 2004: Structure, genesis and scale selection of the tropical quasi-biweekly mode, *Q. J. R. Meteorol. Soc.*, **130**, 1171–1194.
- Chavez, F. P., P. G. Strutton, G. E. Friederich, R. A. Feely, G. C. Feldman, D. G. Foley, M. J. McPhaden, 1999: Biological and Chemical Response of the Equatorial Pacific Ocean to the 1997–1998 El Niño, *Science*, **286**, 2126–2131.
- Chelton D. B., Wentz F. J., Gentemann C. L., De Szoeko R. A. and Schlax M. G., 2000: Satellite microwave SST observations of transequatorial tropical instability waves., *Geophys. Res. Letters.*, **27**, 1239–1242.
- Chelton D.B., Esbesen S. K., Schlax M. G., Thum N., Freilich M. H., Wentz F. J., Gentemann C. L., McPhaden M. J., Schopf P. S., 2001: Observations of coupling between surface wind stress and sea surface temperature in the eastern equatorial Pacific, *J. Climate*, **14**, 1479–1498.
- Clarke, A. J., X. Liu and S. Van Gorder, 1998: Dynamics of the Biennial Oscillation in the Equatorial Indian and Far Western Pacific Oceans, *J. Clim.*, **11**, 987–1001.
- CLIVAR/GOOS Indian Ocean Panel, and Collaborators, 2006: Understanding the role of the Indian Ocean in the climate system—Implementation plan for sustained observations. *ICPO Publication Series No. 100*, *GOOS Rep.* **152**, International CLIVAR Project Office, 76 pp.
- Cox, M.D., 1980: Generation and propagation of 30-day waves in a numerical model of the Pacific, *J. Phys. Oceanogr.*, **10**, 1168–1186.

- De Boyer Montégut, C., J. Vialard, S.S.C. Shenoi, D. Shankar, F. Durand, C. Ethé and G. Madec, 2007, Simulated seasonal and interannual variability of mixed layer heat budget in the northern Indian Ocean, *Journal of Climate*, **20**, 3249-3268.
- Dupuis, H., C. Guérin, D. Hauser, A. Weill, P. Nacass, W. Drennan, S. Cloché, and H. Graber, 2003: Impact of low distortion corrections on turbulent fluxes estimated by the inertial-dissipative method during FETCH experiment on R/V L'Atalante. *J. Geophys. Res.*, **108**, doi:10.1029/2001JC001075.
- Durand, F., D. Shankar, F. Birol, and S. S. C. Shenoi, 2009: Spatiotemporal structure of the East India Coastal Current from satellite altimetry, *J. Geophys. Res.*, **114**, C02013, doi:10.1029/2008JC004807.
- Durand, F., S. R. Shetye, J. Vialard, D. Shankar, D., S. S. C. Shenoi, C. Ethé, and G. Madec, 2004: Impact of temperature inversions on SST evolution in the South-Eastern Arabian Sea during the pre-summer monsoon season. *Geophys. Res. Lett.*, **31**, L01305, 10.1029/2003GL018906.
- Dutrieux, P., C. Menkes, J. Vialard, P. Flament and B. Blanke, 2008, Lagrangian study of Tropical Instability Vortices in the Atlantic ocean, *J. Phys. Oceanogr.*, **38**, 400-417.
- Duvel, J-P. and J. Vialard, 2007, Indo-Pacific Sea Surface Temperature Perturbations Associated with Intraseasonal Oscillations of the Tropical Convection, *Journal of Climate*, **20**, 3056-3082.
- Duvel, J-P., C. Basdevant, H. Bellenger, G. Reverdin, A. Vargas and J. Vialard, 2009, The Aeroclipper: A New Device to Explore Convective Systems and Cyclones, *Bull. Am. Met. Soc.*, **90**, 63-71.
- Duvel, J-P., R. Roca and J. Vialard, 2004, Ocean Mixed Layer Temperature Variations induced by Intraseasonal Convective Perturbations over the Indian Ocean. *J. Atm. Sciences*, **61**, 1004-1023.
- Emanuel, K. A., 1987: An air-sea interaction model of intraseasonal oscillations in the tropics, *J. Atmos. Sci.*, **44**, 2324-2340.
- Fairall, C. W., E. F. Bradley, J. E. Hare, A. A. Grachev, and J. B. Edson, 2003: Bulk parameterization of air-sea fluxes: Updates and verification for the COARE algorithm. *J. Climate*, **16**, 571-591.
- Farrel, B., and P. Ioannou, 1996a: Generalized stability theory. Part I: Autonomous operators. *J. Atmos. Sci.*, **53**, 2025-2040.
- Farrel, B., and P. Ioannou: Generalized stability theory. Part II: Nonautonomous operators. *J. Atmos. Sci.*, **53**, 2041-2053.
- Fischer, A., P. Terray, E. Guilyardi, S. Gualdi and P. Delecluse, 2005: Two independent triggers for the Indian Ocean Dipole/Zonal mode in a coupled GCM, *J. Clim.*, **18**, 3428-3449.
- Flament, P., S. C. Kennan, R. Knox, P. P. Niiler and R. Bernstein, 1996: The three-dimensional structure of an upper vortex in the tropical Pacific. *Nature*, **382**, 610-613.
- Foltz, G. R., J. A. Carton, and E. P. Chassignet, 2004: Tropical instability vortices in the Atlantic Ocean. *J. Geophys. Res.*, **109**, C03029, doi:10.1029/2003JC001942.
- Gadgil, S. and S. Gadgil, 2006, The Indian Monsoon, GDP, and Agriculture, *Economic and Political Weekly (India)*, **November 25, 2006**.
- Gaillard, F., E. Autret, V. Thierry, P. Galaup, C. Coatanoean, and T. Loubrieu, 2009 : Quality Control of Large Argo Datasets, *J. Atm. Oceanic Tech.*, **26**, 337-351.
- Gill, A. E., Some simple solutions for heat-induced tropical circulation, *Q. J. R. Meteorol. Soc.*, **106**, 447-462, 1980.
- Gill, A.E., 1982: Atmosphere-Ocean Dynamics. *International Geophysics series, vol 30, Academic Press (eds)*, 662 pp.
- Goni, G. J., and J. A. Trinanes, 2003: Ocean thermal structure monitoring could aid in the intensity forecast of tropical cyclones, *Eos Trans. AGU*, **84**, 577-580.
- Gorgues, T., C. Menkes, O. Aumont, J. Vialard, Y. Dandoneau and L. Bopp, 2005, Biogeochemical impact of Tropical Instability Waves in the Equatorial Pacific, *Geophys. Res. Lett.*, **32**, L24615, doi :10.1029/2005GL024110.
- Goswami, B.N., 2005: South Asian Monsoon. In *Intraseasonal Variability in the Atmosphere-Ocean Climate System*, W.K.M. Lau and D.E. Waliser (eds.), Praxis Springer, Berlin, 19-55.
- Gould, J., and Argo Steering Team, 2004: Argo profiling floats bring new era of in situ ocean observations. *Eos, Trans. Amer. Geophys. Union*, **85**, 179-191.
- Graham, N. E., and T. P. Barnett, 1987: Sea surface temperature, surface wind divergence, and convection over the tropical oceans. *Science*, **238**, 657-659.
- Han, W., D. M. Lawrence, and P. J. Webster, 2001: Dynamical response of equatorial Indian Ocean to intraseasonal winds: Zonal flow. *Geophys. Res. Lett.*, **28**, 4215-4218.
- Hansen, D. and C. Paul, 1984: Genesis and effect of long waves in the equatorial Pacific. *J. Geophys. Res.*, **89**, 10341-10440.
- Harrison D. E., and N. K. Larkin, 1998: El Niño-Southern oscillation sea surface temperature and wind anomalies, 1946-1993, *Rev. Geophys.*, **36**, 353-399.
- Harrison, D. E., and A. Vecchi, 2001: January 1999 Indian Ocean cooling event. *Geophys. Res. Lett.*, **28**, 3717-3720.

- Hashizume, H., S. P. Xie, M. Fujiwara, M. Shiotani, T. Watanabe, Y. Tanimoto, W. T. Liu, and K. Takeuchi, 2002: Direct observations of atmospheric boundary layer response to SST variations associated with tropical instability waves over the eastern equatorial Pacific, *J. Clim.*, **15**, 3379–3393.
- Hashizume, H., S.-P. Xie, W. T. Liu, and K. Takeuchi, 2001: Local and remote atmospheric response to tropical instability waves: A global view from space, *J. Geophys. Res.*, **106**, 10,173–10,186.
- Hasselmann, K., 1976: Stochastic climate models. 1: Theory. *Tellus*, **28**, 473–485.
- Hastenrath, S., A. Nicklis and L. Greishar, 1993: Atmospheric-hydrospheric mechanisms of climate anomalies in the western equatorial Indian Ocean, *J. Geophys. Res.*, **98**, 20819–20235.
- Hayes, S. P., M. J. McPhaden, and J. M. Wallace, 1989: The influence of sea surface temperature on surface wind in the eastern equatorial Pacific: Weekly to monthly variability, *J. Clim.*, **2**, 1500–1506.
- Hendon, H. H. and M.L. Salby, 1994: The life cycle of the Madden-Julian Oscillation, *J. Atmos. Sci.*, **51**, 2225–2237.
- Hendon, H. H., B. Liebmann, and J. D. Glick, 1998: Oceanic Kelvin waves and the Madden-Julian Oscillation, *J. Atmos. Sci.*, **55**, 88–101.
- Hu Q., and D. A. Randall, 1994: Low-frequency oscillations in radiative–convective systems. *J. Atmos. Sci.*, **51**, 1089–1099.
- Ingram, K. T., M.C. Roncoli and P. H. Kirshen, 2002: Opportunities and constraints for farmers of west Africa to use seasonal precipitation forecasts with Burkina Faso as a case study, *Agr. Syst.*, **74**, 331–349.
- Inness, P. M., and J. M. Slingo, 2003a: Simulation of the Madden–Julian oscillation in a coupled general circulation model. Part I: Comparison with observations and an atmosphere-only GCM. *J. Climate*, **16**, 345–364.
- Inness, P.M., J.M. Slingo, E. Guilyardi, and J. Cole, 2003b: Simulation of the Madden–Julian Oscillation in a Coupled General Circulation Model. Part II: The Role of the Basic State. *J. Climate*, **16**, 365–382.
- Izumo, T., C. de Boyer Montégut, J.-J. Luo, S.K. Behera, S. Masson and T. Yamagata, 2008: The role of the western Arabian Sea upwelling in Indian monsoon rainfall variability, *J. Climate*, **21**, 5603–5623.
- Izumo, T., S. Masson, J. Vialard, G. Madec, C. de Boyer Montégut, S.K. Behera, J.-J. Luo, K. Takahashi and T. Yamagata, 2009: Interannual variations of low-frequency Madden-Julian Oscillation in Austral Summer: Observations, *Clim. Dyn.*, **in revision**.
- Jin, F.-F., 1997: An equatorial ocean recharge paradigm for ENSO. Part I: Conceptual model. *J. Atmos. Sci.*, **54**, 811–829.
- Jones, C., D. E. Waliser, and C. Gautier, 1998: The influence of the Madden–Julian oscillation on ocean surface heat fluxes and sea surface temperature. *J. Climate*, **11**, 1057–1072.
- Jury, M., B. Pathack and B. Parker, 1999: Climatic determinants and statistical prediction of tropical cyclone days in the Southwest Indian Ocean, *J. Clim.*, **12**, 1738–1755.
- Kennan, S. C., P. Flament, 2000: Observations of a tropical instability vortex, *J. Phys. Oceanogr.*, **30**, 2277–2301.
- Kessler, W. S., M. J. McPhaden, and K. M. Weickmann, 1995: Forcing of intraseasonal Kelvin waves in the equatorial Pacific, *J. Geophys. Res.*, **100**, 10,613–10,632.
- Klein, S. A., B. J. Soden, and N.-C. Lau, 1999: Remote sea surface temperature variations during ENSO: Evidence for a tropical atmospheric bridge. *J. Climate*, **12**, 917–932.
- Kug, J.-S., and I.-S. Kang, 2006: Interactive feedback between ENSO and the Indian Ocean, *J. Clim.*, **19**, 1784–1801.
- Lau, K.-M., and L. Peng, 1987: Origin of low-frequency (intraseasonal) oscillations in the tropical atmosphere. Part I: Basic theory, *J. Atmos. Sci.*, **44**, 950–972.
- Lau, N.-C., and M. J. Nath, 2000: Impact of ENSO on the variability of the Asian–Australian monsoons as simulated in GCM experiments. *J. Climate*, **13**, 4287–4309.
- Lawrence, D. M. and P. J. Webster, 2002: The boreal summer intraseasonal oscillation: Relationship between eastward and northward movement of convection. *J. Atmos. Sci.*, **59**, 1593–1606.
- Legeckis, R., 1977: Long waves in the equatorial Pacific Ocean. A view from a geostationary satellite, *Science*, **197**, 1179–1181.
- Lehodey P., M. Bertignac, J. Hampton, A. Lewis, and J. Picaut, 1997, El Niño Southern Oscillation and tuna in the western Pacific, *Nature*, **389**, 715–718.
- Lengaigne, M., E. Guilyardi, J. P. Boulanger, C. Menkes, P. Delecluse, P. Inness, J. Cole, and J. Slingo, 2004: Triggering of El Niño by westerly wind events in a coupled general circulation model, *Clim. Dyn.*, **23**, 601–620.
- Liebmann, B., and C.A. Smith, 1996: Description of a complete (interpolated) outgoing longwave radiation dataset, *Bull. Amer. Meteor. Soc.*, **77**, 1275–1277.
- Liebmann, B., H.H. Hendon and J.D. Glick, 1994: The relationship between tropical cyclone of the Western Pacific and Indian Oceans and the Madden-Julian oscillation, *J. Met. Soc. Jap.*, **72**, 401–412.
- Lighthill, M. J., 1969: Dynamic response of the Indian Ocean to the onset of the southwest monsoon.

- Philosophical Transactions of the Royal Meteorological Society*, **A**, **A265**, 45–92.
- Lin, J. L. et al., 2006: Tropical intraseasonal variability in 14 IPRC AR4 climate models. Part I: Convective signals, *J. Clim.*, **19**, 2665-2690.
- Lindzen, R. S., and S. Nigam, 1987: On the role of sea surface temperature gradients in forcing low-level winds and convergence in the tropics, *J. Atmos. Sci.*, **44**, 2418– 2436.
- Liu, W., X. Xie, P. S. Polito, S. P. Xie, and H. Hashizume, 2000: Atmospheric manifestation of tropical instability wave observed by QuickSCAT and Tropical Rain Measuring Mission, *Geophys. Res. Lett.*, **27**, 2545– 2548.
- Lloyd, I. D. and G. A. Vecchi, 2009: Submonthly Indian Ocean Cooling Events and their Interaction with Large-Scale Conditions. *J. Climate*, **in revision**.
- Locarnini, R. A., A. V. Mishonov, J. I. Antonov, T. P. Boyer, and H. E. Garcia, 2006: World Ocean Atlas 2005, Volume 1: Temperature. S. Levitus, Ed. NOAA Atlas NESDIS 61, U.S. Government Printing Office, Washington, D.C., 182 pp.
- Luo, J.-J., S. Masson, S. K. Behera, P. Delecluse, S. Gualdi, A. Navarra, and T. Yamagata, 2003 : South Pacific Origin of the Decadal ENSO-like Variation as Simulated by a Coupled GCM. *Geophys. Res. Lett.*, **30**, doi:10.1029/2003GL018649.
- Luther, D.S. and E.S. Johnson, 1990: Eddy energetics in the upper equatorial Pacific during Hawaii-to-Tahiti Shuttle Experiment, *Journal of Physical Oceanography*, **20**, 913-944.
- Luyten, J.R. and D.H. Roemmich, 1982 : Equatorial currents at semi annual period in the Indian Ocean, *J. Phys. Oceanogr.*, **12**, 406-413.
- Lyman, J. M., D. B. Chelton, R. A. de Szoeke and R. M. Samelson, 2005: Tropical Instability Waves as a resonance between Rossby waves. *Journal of Physical Oceanography*, **35**, 232-254.
- Maloney, E. D., and A. H. Sobel, 2004: Surface fluxes and ocean coupling in the tropical intraseasonal oscillation. *J. Climate*, **17**, 4368–4386.
- Marsac, F., and J.-L. Le Blanc, 1999, Oceanographic changes during the 1997-1998 El Niño in the Indian Ocean and their impact on the purse seine fishery, *paper presented at First Session of the IOTC Working Party on Tropical Tunas, Victoria, Seychelles, 1-4 September 1999*.
- Marshall, A. G., O. Alves and H. H. Hendon, 2009: A Coupled GCM Analysis of MJO Activity at the Onset of El Niño, *J. Atm. Sci.*, **66**, 966-983.
- Masina, S., S.G.H. Philander and A.B.G. Bush, 1999: An analysis of tropical instability waves in a numerical model of the Pacific Ocean. 2. Generation and energetics of the waves, *J. Geophys. Res.*, **104**, 29637-29661.
- Masson, S., J.-J. Luo, G. Madec, J. Vialard, F. Durand, S. Gualdi, E. Guilyardi, S. Behera, P. Delecluse, A. Navarra and T. Yamagata, Impact of barrier layer on winter-spring variability of the South-Eastern Arabian Sea, *Geophys. Res. Lett.*, **32**, L07703 10.1029/2004GL021980
- Masumoto, Y., H. Hase, Y. Kuroda, H. Matsuura, and K. Takeuchi, 2005: Intraseasonal variability in the upper layer currents observed in the eastern equatorial Indian Ocean. *Geophys. Res. Lett.*, **32**, L02607, doi:10.1029/2004GL021896.
- McCreary, J. P., P. K. Kundu, and R. L. Molinari, 1993:A numerical investigation of dynamics, thermodynamics and mixed layer processes in the Indian Ocean. *Prog. Oceanogr.*, **31**, 181–244.
- McCreary, J. P., R. Murtugudde, J. Vialard, P. N. Vinayachandran, J. D. Wiggert, R. R. Hood, D. Shankar, and S. R. Shetye, 2009: Biophysical processes in the Indian Ocean, *In: Indian Ocean Biogeochemical Processes and Ecological Variability*, J.D. Wiggert, R.R. Hood, S.W.A. Naqvi, S.L. Smith, and K.H. Brink (ed.), American Geophysical Union, Washington, D. C, **accepted**.
- McCreary, J. P., W. Han, D. Shankar, and S. R. Shetye, 1996: Dynamics of the East India Coastal Current. 2. Numerical solutions. *J. Geophys. Res.*, **101**, 13993–14010.
- McCreary, J.P., P.K. Kundu and R.L. Molinari, 1993: A numerical investigation of dynamics, thermodynamics and mixed-layer processes in the Indian Ocean, *Prog. Oceanogr.*, **31**, 181-244.
- McPhaden, M. J. 1999. Genesis and evolution of the 1997-1998 El Niño. *Science* **283**, 950-954.
- McPhaden, M. J., A. J. Busalacchi, R. Cheney, J. R. Donguy, K. S. Gage, D. Halpern, M. Ji, P. Julian, G. Meyers, G. T. Mitchum, P. P. Niiler, J. Picaut, R. W. Reynolds, N. Smith, K. Takeuchi, 1998: The Tropical Ocean-Global Atmosphere (TOGA) observing system: A decade of progress. *J. Geophys. Res.*, **103**, 14169-14240.
- McPhaden, M. J., G. Meyers, K. Ando, Y. Masumoto, V. S. N. Murty, M. Ravichandran, F. Syamsudin, J. Vialard, W. Yu, L. Wu, 2009: RAMA: Research Moored Array for African-Asian-Australian Monsoon Analysis and Prediction. *Bull. Am. Meteor. Soc.*, **accepted**.
- McPhaden, M., J., G. R. Foltz, V. S. N. Murty, M. Ravichandran, G. A. Vecchi, J. Vialard, J. D.. Wiggert and L. Tu, 2009: Ocean-Atmosphere Interactions During Cyclone Nargis, *Eos Trans. AGU*, **90**, 53-54.
- McPhaden, M.J., X. Zhang, H.H. Hendon, and M.C. Wheeler, 2006: Large Scale Dynamics and MJO Forcing of ENSO Variability. *Geophys. Res. Lett.*, **33**, L16702, doi:10.1029/2006GL026786.

- Meehl, G.A., 1997: The south Asian monsoon and the tropospheric biennial oscillation *J. Climate*, **10**, 1921–1943.
- Meinen, C.S. and M.J. McPhaden, 2000: Observations of warm water volume changes in the equatorial Pacific and their relationship to El Niño and La Niña. *J. Clim.*, **13**, 3551–3559.
- Menkes C., S. C. Kennan, P. Flament., Y. Dandonneau, S. Masson, B. Biessy, E. Marchal, G. Eldin, J. Grelet, Y. Montel, A. Morlière, A. Lebourges, C. Moulin, G. Champalbert., Alain herbland, 2002: A whirling ecosystem in the equatorial Atlantic, *Geophys. Res. Letters*, **29**.
- Menkes, C., J. Vialard, S.C. Kennan, J-P. Boulanger, G. Madec and K. Rodgers, 2006, A modelling study of the three-dimensional heat budget of Tropical Instability Waves in the Equatorial Pacific, *Journal of Physical Oceanography*, **36**, 847–865.
- Minnett, P. J., R. O. Knuteson, F. A. Best, B. J. Osborne, J. A. Hanafin, and O. B. Brown, 2001: The Marine-Atmosphere Emitted Radiance Interferometer: A high-accuracy, seagoing infrared spectroradiometer. *J. Atmos. Oceanic Technol.*, **18**, 994–1013.
- Molteni, F., R. Buizza, T.N. Palmer and T. Petroliagis, 1996: The ECMWF ensemble prediction system: methodology and validation. *Q. J. R. Meteorol. Soc.*, **122**, 73–119.
- Moore, A. and R. Kleeman, 1996: The dynamics of error growth and predictability in a coupled model of ENSO. *Quart. J. Roy. Meteor. Soc.*, **122**, 1405–1446.
- Moore, A., J. Vialard, A.T. Weaver, D.L.T Anderson, R. Kleeman and J.R. Johnson, 2003 : The role of air-sea interaction in controlling the optimal perturbations of low-frequency ocean atmosphere modes, *Journal of Climate*, **16**, 951–968.
- Moore, A., J. Zavala-Garay, Y. Tang, R. Kleeman, A.T. Weaver, J. Vialard, K. Sahami, D.L.T. Anderson and M. Fisher, 2006, On the low-dimensionality of ENSO as evidenced by the optimal forcing patterns of coupled models, *Journal of Climate*, **19**, 4683–4699, doi : 10.1175/JCLI3870.1
- Murtugudde, R., J. P. McCreary, and A. J. Busalacchi, 2000: Oceanic processes associated with anomalous events in the Indian Ocean with relevance to 1997–1998. *J. Geophys. Res.*, **105**, 3295–3306.
- Neelin, J. D., I. M. Held, and K. H. Cook, 1987 : Evaporationwind feedback and low-frequency variability in the tropical atmosphere, *J. Atmos. Sci.*, **44**, 2341–2348.
- Palmer, T., and D. Mansfield, 1984: Response of two atmospheric general circulation models to sea surface temperature anomalies in the tropical east and west Pacific, *Nature*, **310**, 483–485.
- Palmer, T.N. and D. L. T. Anderson, 1994: The prospects for seasonal forecasting—A review paper. *Quart. J. Roy. Meteor. Soc.*, **120**, 755–793.
- Perigaud C., 1990: Sea level oscillations observed with GEOSAT along the two shear fronts of the North Equatorial Countercurrents, *J. Geophys. Res.*, **95**, 7239–7248.
- Perigaud, C. and P. Delecluse, 1993: Interannual sea level variations in the tropical Indian Ocean from Geosat and shallow water simulations, *J. Phys. Oceanogr.*, **23**, 1916–1934.
- Peter, A., M. Le Hénaff, Y. du Penhoat, C. E. Menkes, F. Marin, J. Vialard, G. Caniaux, and A. Lazar, 2006: A model study of the seasonal mixed layer heat budget in the equatorial Atlantic, *J. Geophys. Res.*, **111**, C06014, doi:10.1029/2005JC003157.
- Pezzi, L. P., J. Vialard, K. J. Richards, C. Menkes, and D. Anderson, 2004: Influence of ocean-atmosphere coupling on the properties of tropical instability waves, *Geophys. Res. Lett.*, **31**, L16306, doi:10.1029/2004GL019995.
- Picaut, J., F. Masia, and Y. du Penhoat, 1997: An advective-reflective conceptual model for the oscillatory nature of the ENSO, *Science*, **277**, 663–666.
- Picaut, J., M. Ioualalen, T. Delcroix, F. Masia, R. Murtugudde and J. Vialard, 2001 : Displacements of an Oceanic Zone of Convergence on the Eastern Edge of the Pacific Warm Pool : Consequences for ENSO and Bio-chemical Phenomena. *Journal of Geophysical Research*, **106**, 2363–2386.
- Qiao, L., and R. H. Weisberg, 1995: Tropical instability wave kinematics: Observations from the Tropical Instability Wave Experiment (TIWE). *J. Geophys. Res.*, **100**, 8677–8693.
- Radenac, M-H., C. Menkes, J. Vialard, C. Moulin, Y. Dandonneau, T. Delcroix, C. Dupouy, A. Stoens, and P-Y. Deschamps, 2001 : Modeled and observed impacts of the 1997-1998 El Niño on nitrate and new production in the equatorial Pacific. *Journal of Geophysical Research*, **106**, 26879–26889.
- Rao, S. A., and T. Yamagata, 2004: Abrupt termination of Indian Ocean dipole events in response to intraseasonal disturbances. *Geophys. Res. Lett.*, **31**, L19306, doi:10.1029/2004GL020842.
- Rao, S. A., S. Masson, J-J. Luo, S. K. Behera, and T. Yamagata 2007: Termination of Indian Ocean Dipole events in a coupled general circulation model. *J. Climate*, **20**, 3018–3035, doi:10.1175/JCLI4164.1.
- Reppin, J., F. A. Schott, J. Fischer, and D. Quadfasel, 1999: Equatorial currents and transports in the upper central Indian Ocean: annual cycle and interannual variability. *J. Geophys. Res.*, **104**, 15495–15514.
- Resplandy, L., J. Vialard, Y. Dandonneau, O. Aumont, M. Levy, 2009: Seasonal and intraseasonal biogeochemical variability in the thermocline ridge of the Indian Ocean, *J. Geophys. Res.*, **in revision**.
- Reverdin, G., and J. Luyten, 1986 : Near-surface meanders in the equatorial Indian Ocean, *J. Phys. Oceanogr.*,

- 16**, 1088-1100.
- Reverdin, G., D. L. Cadet, and D. Gutzler, 1986 : Interannual displacements of convection and surface circulation over the Indian Ocean, *Q. Jour. Roy. Met. Soc.*, **112**, 43-67.
- Ricci, S., A.T. Weaver, J. Vialard and P. Rogel, 2005: Incorporating State-Dependent Temperature–Salinity Constraints in the Background Error Covariance of Variational Ocean Data Assimilation. *Mon. Wea. Rev.*, **133**, 317-338, doi: 10.1175/MWR2872.1.
- Rui, H. and B. Wang, 1990: Development characteristics and dynamic structure of tropical intraseasonal convection anomalies, *J. Atm. Sci.*, **47**, 357-379.
- Saji, N. H., and . Yamagata, 2003: A Structure of SST and surface wind variability during Indian Ocean Dipole mode events: COADS observations. *J. Clim.*, **16**, 2735-2751.
- Saji, N. H., B. N. Goswami, P. N. Vinayachandran and T. Yamagata, 1999: A dipole mode in the tropical Indian Ocean. *Nature*, **401**, 360-363.
- Saji, N. H., S.-P. Xie and C. Y. Tam, 2006: Satellite observations of intense intraseasonal cooling events in the tropical south Indian Ocean. *Geophys. Res. Lett.*, **33**, L14704, doi:10.1029/2006GL026525.
- Schott, F. A., S.-P. Xie, and J. P. McCreary Jr., 2009, Indian Ocean circulation and climate variability, *Rev. Geophys.*, **47**, doi:10.1029/2007RG000245.
- Schott, F., and J.P. McCreary, 2001: *The monsoon circulation of the Indian Ocean*. *Prog. Oceanogr.*, **51**, 1-123.
- Segschneider, J., D.L.T. Anderson, J. Vialard, M. Balmaseda, T.N. Stockdale, A. Troccoli, and K. Haines, 2001 : Initialization of seasonal forecasts assimilating sea level and temperature observations. *J. Climate*, **14**, 4292-4307.
- Seiki, A., and Y.N. Takayabu, 2007: Westerly Wind Bursts and Their Relationship with Intraseasonal Variations and ENSO. Part I: Statistics. *Mon. Wea. Rev.*, **135**, 3325–3345.
- Sengupta, D., R. Senan, and B. N. Goswami, 2001: Origin of intraseasonal variability of circulation in the tropical central Indian Ocean. *Geophys. Res. Lett.*, **28**, 1267–1270.
- Sengupta, D., and M. Ravichandran, 2001: Oscillations of Bay of Bengal sea surface temperature during the 1998 summer monsoon. *Geophys. Res. Lett.*, **28**, 2033–2036.
- Sengupta, D., R. Senan, B.N. Goswami and J. Vialard, 2007, Intraseasonal variability of equatorial Indian Ocean zonal currents, *Journal of Climate*, **20**, 3036-3055.
- Sévellec, F., T. Huck, M. Ben Jelloul and J. Vialard, 2009, Non-normal multidecadal response of the thermohaline circulation induced by optimal surface salinity perturbations, *J. Phys. Oceanogr.*, **39**, 852-872.
- Sévellec, F., T. Huck, M. Ben Jelloul, N. Grima J. Vialard and A.T Weaver, 2008, Optimal surface salinity perturbations of the meridional overturning and heat transport in a global ocean general circulation model. *J. Phys. Oceanogr.*, **38**, 2739-2754.
- Shankar, D., and S. R. Shetye, 1997 : On the dynamics of the Lakshadweep high and low in the southeastern Arabian Sea. *J. Geophys. Res.*, **102**, 12551–12562.
- Shenoi, S. S. C., D. Shankar, and S. R. Shetye, 2002: Differences in heat budgets of the near-surface Arabian Sea and Bay of Bengal: Implications for the summer monsoon. *J. Geophys. Res.*, **107**, 3052, doi:10.1029/2000JC000679.
- Shetye, S. R., I. Suresh, D. Shankar, D. Sundar, S. Jayakumar, P. Mehra, R. G. Prabhudesai, and P. S. Pednekar 2008: Observational evidence for remote forcing of the West India Coastal Current, *J. Geophys. Res.*, **113**, C11001, doi:10.1029/2008JC004874.
- Shinoda, T., and H. H. Hendon, 1998: Mixed layer modeling of intraseasonal variability in the tropical western Pacific and Indian Oceans. *J. Climate*, **11**, 2668–2685.
- Slingo, J. M. et al., 1996 : Intraseasonal oscillation in 15 atmospheric general circulation models : Results from an AMIP diagnostic subproject, *Clim. Dyn.*, **12**, 325-357.
- Small, R. J., K. Richards, S.-P. Xie, P. Dutrieux and T. Miyama, 2009, Damping of Tropical Instability waves caused by the action of surface currents on stress, *J. Geophys. Res.*, **accepted**.
- Small, R. J., S.-P. Xie, and Y. Wang, 2003: Numerical simulation of atmospheric response to pacific tropical instability waves, *J. Clim.*, **16**, 3722– 3740.
- Stevenson, J. W. and P. P. Niiler, 1983: Upper ocean heat budget during the Hawaii-to-Tahiti shuttle experiment. *J. Phys. Oceanogr.*, **13**, 1894-1907.
- Swenson M. S. and D. V. Hansen, 1999: Tropical pacific ocean mixed layer heat budget: the pacific cold tongue. *J. Phys. Oceanogr.*, **29**, 83-91.
- Tang, Y., R. Kleeman, A. M. Moore, J. Vialard, and A. Weaver, 2004, An off-line, numerically efficient initialization scheme in an oceanic general circulation model for El Niño–Southern Oscillation prediction, *J. Geophys. Res.*, **109**, C05014, doi:10.1029/2003JC002159.
- Tang, Y., R. Kleeman, A.M. Moore, A. Weaver, J. Vialard: The use of ocean reanalysis products to initialize ENSO predictions, *Geophys. Res. Lett.* **30**, 1694, 10.1029/2003GL017664

- Trenary, L. L., and W. Han, 2008: Causes of decadal subsurface cooling in the tropical Indian Ocean during 1961–2000, *Geophys. Res. Lett.*, **35**, L17602, doi:10.1029/2008GL034687.
- Troccoli A., M. Balmaseda, J. Segsneider, J. Vialard, D.L.T. Anderson, K. Haines, T. Stockdale, F. Vitart and A.D. Fox, 2002 :Salinity adjustments in the presence of temperature data assimilation, *Monthly Weather Review*, **130**, 89-102.
- Tsai, P.T.H., J.J. O'Brien, M.E. Luther, 1992: The 26-day oscillation observed in the satellite sea surface temperature measurements in the equatorial western Indian Ocean. *J. Geophys. Res.*, **31**, 9605-9618.
- Vecchi, G.A. and D.E. Harrison, 2002: Monsoon breaks and subseasonal temperature variability in the Bay of Bengal, *J. Clim.*, **15**, 1485-1493.
- Vecchi, G.A. and D.E. Harrison, 2004: Interannual Indian rainfall variability and Indian Ocean sea surface temperature anomalies. In *Earth Climate: The Ocean-Atmosphere Interaction*, C. Wang, S.-P. Xie, and J.A. Carton (eds.), American Geophysical Union, Geophysical Monograph 147, Washington D.C., 247-260.
- Vialard, J. and P. Delecluse, 1998a: An OGCM Study for the TOGA Decade. Part I : Role of Salinity in the Physics of the Western Pacific Fresh Pool. *Journal of Physical Oceanography*, **28**, 1071 - 1088.
- Vialard, J. and P. Delecluse, 1998b: An OGCM Study for the TOGA Decade. Part II : Barrier Layer Formation and Variability. *Journal of Physical Oceanography*, **28**, 1089 - 1106.
- Vialard, J., A.T. Weaver, D.L.T. Anderson and P. Delecluse, 2003a: Three- and four-dimensional variational assimilation with a general circulation model of the tropical Pacific Ocean, Part 2 : physical validation. *Monthly Weather Review*, **131**, 1379-1395.
- Vialard, J., C. Menkes, D.L.T. Anderson and M. Balmaseda, 2003b: Sensitivity of Pacific Ocean Tropical Instability Waves to Initial Conditions. *Journal of Physical Oceanography*, **33**, 105-121.
- Vialard, J., C. Menkes, J-P. Boulanger, P. Delecluse, E. Guilyardi and M. McPhaden, 2001: A model study of the oceanic mechanisms affecting the equatorial SST during the 1997-98 El Niño. *Journal of Physical Oceanography*, **31**, 1649-1675.
- Vialard, J., F. Vitart, M.A. Balmaseda, T.N. Stockdale, D.L.T. Anderson, 2005, An ensemble generation method for seasonal forecasting with an ocean-atmosphere coupled model. *Mon. Wea. Rev.*, **133**, 441-453, doi: 10.1175/MWR-2863.1
- Vialard, J., G. Foltz, M. McPhaden , J-P. Duvel and C. de Boyer Montégut, 2008, Strong Indian Ocean sea surface temperature signals associated with the Madden-Julian Oscillation in late 2007 and early 2008, *Geophys. Res. Lett.*, **35**, L19608, doi:10.1029/2008GL035238.
- Vialard, J., J-P. Duvel, M. McPhaden, P. Bouruet-Aubertot, B. Ward, E. Key, D. Bourras, R. Weller, P. Minnett, A. Weill, C. Cassou, L. Eymard, T. Fristedt, C. Basdevant, Y. Dandoneau, O. Duteil, T. Izumo, C. de Boyer Montégut, S. Masson, F. Marsac, C. Menkes, S. Kennan, 2009a, Cirene: Air Sea Interactions in the Seychelles-Chagos thermocline ridge region, *Bull. Am. Met. Soc.*, **90**, 45-61.
- Vialard, J., P. Delecluse, and C. Menkes, 2002, A modeling study of salinity variability and its effects in the tropical Pacific Ocean during the 1993–1999 period, *J. Geophys. Res.*, **107**, 8005, doi:10.1029/2000JC000758.
- Vialard, J., S.S.C. Shenoi, J.P. McCreary, D. Shankar, F. Durand, V. Fernando and S.R. Shetye, 2009b: Intraseasonal response of Northern Indian Ocean coastal waveguide to the Madden-Julian Oscillation, *Geophys. Res. Lett.*, **submitted**.
- Vinayachandran P. N., J. Kurian, C. P. Neema, 2007: Indian Ocean response to anomalous conditions in 2006, *Geophys. Res. Lett.*, **34**, doi:10.1029/2007GL030194.
- Vinayachandran, P. N., and N. H. Saji, 2008: Mechanisms of South Indian Ocean intraseasonal cooling. *Geophys. Res. Lett.*, **35**, L23607, doi:10.1029/2008GL035733.
- Vossepoel, F., A.T. Weaver, J. Vialard and P. Delecluse, 2004, Adjustment of near-equatorial wind stress with four-dimensional variational data assimilation in a model of the Pacific Ocean, *Mon. Wea. Rev.*, **132**, 2070-2083.
- Waliser, D. E., K. M. Lau, and J.-H. Kim, 1999: The influence of coupled sea surface temperatures on the Madden-Julian oscillation: A model perturbation experiment. *J. Atmos. Sci.*, **56**, 333–358.
- Wang W. and M. J. McPhaden, 1999: The surface layer heat balance in the equatorial Pacific ocean. Part I: mean seasonal cycle, *J. Phys. Oceanogr.*, **29**, 1812-1831.
- Wang, B. and H. Rui, 1990: Dynamics of the coupled moist Kelvin-Rossby wave on an equatorial beta-plane, *J. Atm. Sci.*, **47**, 397-413.
- Wang, B., 1988: Dynamics of tropical low-frequency waves: An analysis of the moist Kelvin wave, *J. Atmos. Sci.*, **45**, 2051–2065.
- Wang, B., 2005: Theory. In *Intraseasonal Variability in the Atmosphere-Ocean Climate System*, W.K.M. Lau and D.E. Waliser (eds.), Praxis Springer, Berlin, 307–360.
- Wang, C. and Picaut, J. 2004: Understanding ENSO Physics - A Review. In: *Earth's climate: the ocean-atmosphere interaction*. AGU, Washington D.C., C. Wang, S.-P. Xie and J.A. Carton Eds., 21-48.

- Wang, C., R. H. Weisberg, and J. I. Virmani, Western Pacific interannual variability associated with the El Niño–Southern Oscillation, *J. Geophys. Res.*, **104**, 5131–5149, 1999.
- Wang, L., C. J. Kobalinsky, and S. Howden, 2001: Annual Rossby wave in the Southern Indian Ocean: Why does it “appear” to break down in the middle ocean?, *J. Phys. Oceanogr.*, **31**, 54–74.
- Ward, B., R. Wanninkhof, P. J. Minnett, and M. Head, 2004: SkinDeEp: A profiling instrument for upper decameter sea surface measurements. *J. Atmos. Oceanic Technol.*, **21**, 207–222.
- Watterson, I.G. and Syktus, J., 2007: The influence of air–sea interaction on the Madden-Julian Oscillation: the role of the seasonal mean state. *Climate Dynamics*, **28**, 703–722.
- Weaver, A.T., J. Vialard, and D.L.T. Anderson, 2003: Three- and four-dimensional variational assimilation with a general circulation model of the tropical Pacific Ocean, Part 1 : formulation, internal diagnostics and consistency checks. *Monthly Weather Review*, **131**, 1360–1378.
- Webster, P. J., 2008, Myanmar’s deadly “daffodil,” *Nat. Geosci.*, **1**, 488–490.
- Webster, P. J., A. M. Moore, J. P. Loschnigg, and R. R. Leben, 1999: Coupled oceanic–atmospheric dynamics in the Indian Ocean during 1997–98. *Nature*, **401**, 356–360.
- Weidman P.D., D.L. Mickler, B. Dayyani Et G.H. Born, 1999: Analysis of Legeckis eddies in the near-equatorial Pacific, *J. Geophys. Res.*, **104**, 7865–7887.
- Weisberg, R. H., and C. Wang 1997: A western Pacific oscillator paradigm for the El Niño–Southern Oscillation. *Geophys. Res. Lett.*, **24**, 779–782.
- Wentz, F.J., C. Gentemann, D. Smith, D. Chelton, 2000: Satellite measurements of sea-surface temperature through clouds. *Science*, **288**, 847–850.
- Wheeler, M., and G. Kiladis, 1999: Convectively coupled equatorial waves: Analysis of clouds and temperature in the wavenumber–frequency domain. *J. Atmos. Sci.*, **56**, 374–399.
- Wheeler, M.C., and H. H. Hendon, 2004: An All-Season Real-Time Multivariate MJO Index: Development of an Index for Monitoring and Prediction. *Mon. Wea. Rev.*, **132**, 1917–1932.
- Woolnough, S. J., F. Vitart, and M. A. Balmaseda, 2007: The role of the ocean in the Madden–Julian oscillation: Implications for MJO prediction. *Quart. J. Roy. Meteor. Soc.*, **133**, 117–128.
- Woolnough, S. J., J. M. Slingo, and B. J. Hoskins, 2000: The relationship between convection and sea surface temperature on intraseasonal timescales. *J. Climate*, **13**, 2086–2104.
- Wyrtki, K., 1973: An equatorial jet in the Indian Ocean. *Science*, **181**, 262–264.
- Xavier, P. K., J-P. Duvel and F. Doblas-Reyes, 2008: Boreal Summer Intraseasonal Variability in Coupled Seasonal Hindcasts, *J. Clim.*, **21**, 4477–4497.
- Xie, S.-P., and S. G. H. Philander, 1994 : A coupled ocean-atmosphere model of relevance to the ITCZ in the eastern Pacific, *Tellus, Ser. A*, **46**, 340–350.
- Xie, S.-P., H. Annamalai, F.A. Schott and J.P. McCreary, 2002: Structure and mechanisms of south Indian climate variability, *J. Climate*, **9**, 840–858.
- Xie, S.-P., K. Hu, J. Hafne, H. Tokinaga, Y. Du, G. Duang and T. Sampe, 2009 : Indian Ocean capacitor effect on Indo-western Pacific climate during the summer following El Niño. *J. Clim.*, **in press**.
- Xie, S.-P., M. Ishiwatari, H. Hashizume, and K. Takeuchi, 1998: Coupled ocean–atmospheric waves on the equatorial front. *Geophys. Res. Lett.*, **25**, 3863–3866.
- Yamagata, T., S. K. Behera, J.-J. Luo, S. Masson, M. Jury, and S. A. Rao, 2004: Coupled ocean-atmosphere variability in the tropical Indian Ocean, in *Earth Climate: The Ocean-Atmosphere Interaction*, *Geophys. Monogr. Ser.*, **147**, edited by C. Wang, S.-P. Xie, and J. A. Carton, pp. 189–212, AGU, Washington, D. C.
- Yu, W., B. Xiang, L. Liu, and N. Liu, 2005: Understanding the origins of interannual thermocline variations in the tropical Indian Ocean, *Geophys. Res. Lett.*, **32**, L24706, doi:10.1029/2005GL024327.
- Zavala-Garay J., C. Zhang, A.M. Moore, A.T. Wittenberg, M.J. Harrison, A. Rosati, J. Vialard and R. Kleeman, 2008, Sensitivity of hybrid ENSO models to unresolved atmospheric variability, *Journal of Climate*, **21**, 3704–3721.
- Zhang, C., 2005: Madden-Julian Oscillation, *Rev. Geophys.*, **43**, RG2003, doi:10.1029/2004RG000158.
- Zhang, C., and M. Dong, 2004: Seasonality of the Madden-Julian Oscillation, *J. Clim.*, **17**, 3169–3180.

Appendix A. Scientific output and training

A.1 Publications

40 accepted/published papers refereed papers (9 as a first author)

The blue number in brackets after each paper is the number of citations at the end of May 2009 obtained from Web of Science or Scopus (highest of the two), when available. A summary of citations with h-index from Web of science is also available at the end of the publication list.

The publications which have been co-signed with PhD students are highlighted in grey (see detail in Appendix A2).

Accepted / in press

- McCreary, J. P., R. Murtugudde, J. Vialard, P. N. Vinayachandran, J. D. Wiggert, R. R. Hood, D. Shankar, and S. R. Shetye, 2009: Biophysical processes in the Indian Ocean, *In: Indian Ocean Biogeochemical Processes and Ecological Variability*, J.D.Wiggert, R.R. Hood, S.W.A. Naqvi, S.L. Smith, and K.H. Brink (ed.), American Geophysical Union, Washington, D. C, **accepted**.
- McPhaden, M. J., G. Meyers, K. Ando, Y. Masumoto, V. S. N. Murty, M. Ravichandran, F. Syamsudin, J. Vialard, W. Yu, L. Wu, 2009: RAMA: Research Moored Array for African-Asian-Australian Monsoon Analysis and Prediction. *Bull. Am. Meteor. Soc.*, **accepted**.
- Wiggert, J.D., J. Vialard, and M.J. Behrenfeld, 2009: Basin-wide modification of dynamical and biogeochemical processes by the Indian Ocean Dipole. *In: Indian Ocean Biogeochemical Processes and Ecological Variability*, J.D.Wiggert, R.R. Hood, S.W.A. Naqvi, S.L. Smith, and K.H. Brink (ed.), American Geophysical Union, Washington, D. C, **accepted**.

2009

- Duvel, J-P., C. Basdevant, H. Bellenger, G. Reverdin, A. Vargas and J. Vialard, 2009, The Aeroclipper: A New Device to Explore Convective Systems and Cyclones, *Bull. Am. Met. Soc.*, **90**, 63-71. [2]
- McPhaden, M., J., G. R. Foltz, V. S. N. Murty, M. Ravichandran, G. A. Vecchi, J. Vialard, J. D.. Wiggert and L. Tu, 2009: Ocean-Atmosphere Interactions During Cyclone Nargis, *Eos Trans. AGU*, **90**, 53-54.
- Sévellec, F., T. Huck, M. Ben Jelloul and J. Vialard, 2009, Non-normal multidecadal response of the thermohaline circulation induced by optimal surface salinity perturbations, *J. Phys. Oceanogr.*, **39**, 852-872.
- Vialard, J., J-P. Duvel, M. McPhaden, P. Bouruet-Aubertot, B. Ward, E. Key, D. Bourras, R. Weller, P. Minnett, A. Weill, C. Cassou, L. Eymard, T. Fristedt, C. Basdevant, Y. Dandoneau, O. Duteil, T. Izumo, C. de Boyer Montégut, S. Masson, F. Marsac, C. Menkes, S. Kennan, 2009, Cirene: Air Sea Interactions in the Seychelles-Chagos thermocline ridge region, *Bull. Am. Met. Soc.*, **90**, 45-61. [1]

2008

- Bellon, G., A.H. Sobel and J. Vialard, 2008, Ocean-atmosphere coupling in the monsoon intraseasonal oscillation: a simple model study, *Journal of Climate*, **21**, 5254-5270. [1]
- Dutrieux, P., C. Menkes, J. Vialard, P. Flament and B. Blanke, 2008, Lagrangian study of Tropical Instability Vortices in the Atlantic ocean, *J. Phys. Oceanogr.*, **38**, 400-417. [1]
- Sévellec, F., T. Huck, M. Ben Jelloul, N. Grima J. Vialard and A.T Weaver, 2008, Optimal surface salinity perturbations of the meridional overturning and heat transport in a global ocean general circulation model. *J. Phys. Oceanogr.*, **38**, 2739-2754. [0]
- Vialard, J., G. Foltz, M. McPhaden, J-P. Duvel and C. de Boyer Montégut, 2008, Strong Indian Ocean sea surface temperature signals associated with the Madden-Julian Oscillation in late 2007 and early 2008, *Geophys. Res. Lett.*, **35**, L19608, doi:10.1029/2008GL035238. [1]
- Zavala-Garay J., C. Zhang, A.M. Moore, A.T. Wittenberg, M.J. Harrison, A. Rosati, J. Vialard and R. Kleeman, 2008, Sensitivity of hybrid ENSO models to unresolved atmospheric variability, *Journal of Climate*, **21**, 3704-3721. [1]

2007

- De Boyer Montégut, C., J. Vialard, S.S.C. Shenoi, D. Shankar, F. Durand, C. Ethé and G. Madec, 2007, Simulated seasonal and interannual variability of mixed layer heat budget in the northern Indian Ocean, *Journal of Climate*, **20**, 3249-3268. [9]

- Duvel, J-P. and J. Vialard, 2007, Indo-Pacific Sea Surface Temperature Perturbations Associated with Intraseasonal Oscillations of the Tropical Convection, *Journal of Climate*, **20**, 3056-3082. [7]
- Sengupta, D., R. Senan, B.N. Goswami and J. Vialard, 2007, Intraseasonal variability of equatorial Indian Ocean zonal currents, *Journal of Climate*, **20**, 3036-3055. [2]

2006

- Menkes, C., J. Vialard, S.C. Kennan, J-P. Boulanger, G. Madec and K. Rodgers, 2006, A modelling study of the three-dimensional heat budget of Tropical Instability Waves in the Equatorial Pacific, *Journal of Physical Oceanography*, **36** (5), 847–865. [10]
- Moore, A., J. Zavala-Garay, Y. Tang, R. Kleeman, A.T. Weaver, J. Vialard, K. Sahami, D.L.T. Anderson and M. Fisher, 2006, On the low-dimensionality of ENSO as evidenced by the optimal forcing patterns of coupled models, *Journal of Climate*, **19** (18), 4683-4699, doi : 10.1175/JCLI3870.1 [10]
- Peter, A., M. Le Hénaff, Y. du Penhoat, C. E. Menkes, F. Marin, J. Vialard, G. Caniaux, and A. Lazar (2006), A model study of the seasonal mixed layer heat budget in the equatorial Atlantic, *J. Geophys. Res.*, **111**, C06014, doi:10.1029/2005JC003157. [5]

2005

- Gorgues, T., C. Menkes, O. Aumont, J. Vialard, Y. Dandoneau and L. Bopp, 2005, Biogeochemical impact of Tropical Instability Waves in the Equatorial Pacific, *Geophys. Res. Lett.*, **32**, L24615, doi :10.1029/2005GL024110. [10]
- Masson, S., J.-J. Luo, G. Madec, J. Vialard, F. Durand, S. Gualdi, E. Guilyardi, S. Behera, P. Delecluse, A. Navarra and T. Yamagata, Impact of barrier layer on winter-spring variability of the South-Eastern Arabian Sea, *Geophys. Res. Lett.*, **32** (7), L07703 10.1029/2004GL021980 [20]
- Ricci, S., A.T. Weaver, J. Vialard and P. Rogel, 2005: Incorporating State-Dependent Temperature–Salinity Constraints in the Background Error Covariance of Variational Ocean Data Assimilation. *Mon. Wea. Rev.*, **133** (1), 317-338, doi: 10.1175/MWR2872.1. [15]
- Vialard, J., F. Vitart, M.A. Balmaseda, T.N. Stockdale, D.L.T. Anderson, 2005, An ensemble generation method for seasonal forecasting with an ocean-atmosphere coupled model. *Mon. Wea. Rev.*, **133** (2), 441-453, doi: 10.1175/MWR-2863.1 [14]

2004

- Durand, F., S. R. Shetye, J. Vialard, D. Shankar, D., S. S. C. Shenoi, C. Ethe, and G. Madec, 2004: Impact of temperature inversions on SST evolution in the South-Eastern Arabian Sea during the pre-summer monsoon season. *Geophys. Res. Lett.*, **31** (1), L01305, 10.1029/2003GL018906. [24]
- Duvel, J-P., R. Roca and J. Vialard, 2004, Ocean Mixed Layer Temperature Variations induced by Intraseasonal Convective Perturbations over the Indian Ocean. *J. Atm. Sciences*, **61**, 1004-1023. [24]
- Pezzi, L. P., J. Vialard, K. J. Richards, C. Menkes, and D. Anderson (2004), Influence of ocean-atmosphere coupling on the properties of tropical instability waves, *Geophys. Res. Lett.*, **31**, L16306, doi:10.1029/2004GL019995. [11]
- Tang, Y., R. Kleeman, A. M. Moore, J. Vialard, and A. Weaver, 2004, An off-line, numerically efficient initialization scheme in an oceanic general circulation model for El Niño–Southern Oscillation prediction, *J. Geophys. Res.*, **109**, C05014, doi:10.1029/2003JC002159. [3]
- Vossepoel, F., A.T. Weaver, J. Vialard and P. Delecluse, 2004, Adjustment of near-equatorial wind stress with four-dimensional variational data assimilation in a model of the Pacific Ocean, *Mon. Wea. Rev.*, **132**, 2070-2083. [4]

2003

- Vialard, J., A.T. Weaver, D.L.T. Anderson and P. Delecluse, 2003a: Three- and four-dimensional variational assimilation with a general circulation model of the tropical Pacific Ocean, Part 2 : physical validation. *Monthly Weather Review*, **131**, 1379-1395. [29]
- Moore, A., J. Vialard, A.T. Weaver, D.L.T. Anderson, R. Kleeman and J.R. Johnson, 2003 : The role of air-sea interaction in controlling the optimal perturbations of low-frequency ocean atmosphere modes, *Journal of Climate*, **16**, 951-968. [15]
- Weaver, A.T., J. Vialard, and D.L.T. Anderson, 2003: Three- and four-dimensional variational assimilation with a general circulation model of the tropical Pacific Ocean, Part 1 : formulation, internal diagnostics and consistency checks. *Monthly Weather Review*, **131**, 1360-1378. [51]
- Tang, Y., R. Kleeman, A.M. Moore, A. Weaver, J. Vialard: The use of ocean reanalysis products to initialize ENSO predictions, *Geophys. Res. Lett.*, **30**, 1694, 10.1029/2003GL017664 [6]

Vialard, J., C. Menkes, D.L.T Anderson and M. Balmaseda, 2003b: Sensitivity of Pacific Ocean Tropical Instability Waves to Initial Conditions. *Journal of Physical Oceanography*, **33**, 105-121. [8]

2002

Troccoli A., M. Balmaseda, J. Segschneider, J. Vialard, D.L.T. Anderson, K. Haines, T. Stockdale, F. Vitart and A.D. Fox, 2002 :Salinity adjustments in the presence of temperature data assimilation, *Monthly Weather Review*, **130**, 89-102. [28]

Vialard, J., P. Delecluse, and C. Menkes, 2002, A modeling study of salinity variability and its effects in the tropical Pacific Ocean during the 1993–1999 period, *J. Geophys. Res.*, **107**, 8005, doi:10.1029/2000JC000758. [21]

2001

Vialard, J., C. Menkes, J-P. Boulanger, P. Delecluse, E. Guilyardi and M. McPhaden, 2001: A model study of the oceanic mechanisms affecting the equatorial SST during the 1997-98 El Niño. *Journal of Physical Oceanography*, **31**, 1649-1675. [77]

Radenac, M-H., C. Menkes, J. Vialard, C. Moulin, Y. Dandonneau, T. Delcroix, C. Dupouy, A. Stoens, and P-Y. Deschamps, 2001 : Modeled and observed impacts of the 1997-1998 El Niño on nitrate and new production in the equatorial Pacific. *Journal of Geophysical Research*, **106**, 26879-26889. [13]

Segschneider, J., D.L.T. Anderson, J. Vialard, M. Balmaseda, T.N. Stockdale, A. Troccoli, and K. Haines, 2001 : Initialization of seasonal forecasts assimilating sea level and temperature observations. *J. Climate*, **14**, 4292-4307. [11]

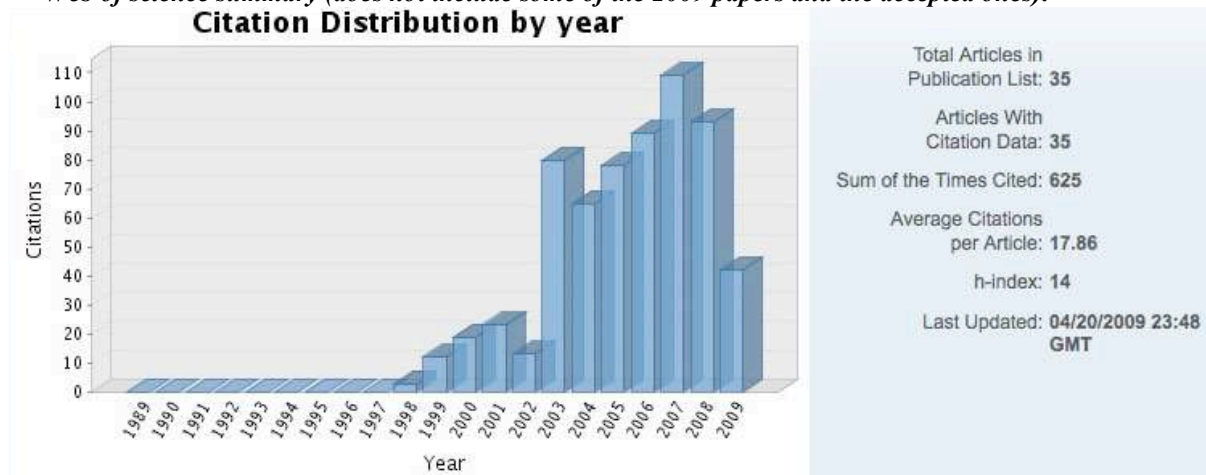
Picaut, J., M. Ioualalen, T. Delcroix, F. Masia, R. Murtugudde and J. Vialard, 2001 : Displacements of an Oceanic Zone of Convergence on the Eastern Edge of the Pacific Warm Pool : Consequences for ENSO and Bio-chemical Phenomena. *Journal of Geophysical Research*, **106**, 2363-2386. [30]

1998

Vialard, J. and P. Delecluse, 1998a: An OGCM Study for the TOGA Decade. Part I : Role of Salinity in the Physics of the Western Pacific Fresh Pool. *Journal of Physical Oceanography*, **28**, 1071 - 1088. [84]

Vialard, J. and P. Delecluse, 1998b: An OGCM Study for the TOGA Decade. Part II : Barrier Layer Formation and Variability. *Journal of Physical Oceanography*, **28**, 1089 - 1106. [91]

Web of science summary (does not include some of the 2009 papers and the accepted ones):



A.2 Scientific advisory and training activities

PhDs:

Luciano Pezzi (Brazil) (University of Southampton, 2001-2003, Advisor: K. Richards)

- Topic: «Equatorial Pacific dynamics: Lateral mixing and tropical instability waves.»
- Role: 4-months visit to LOCEAN to work with me on the effect of coupling on TIWs
- Co-signed publications: 1

Sophie Ricci (Université Toulouse 3, 2002-2004, Advisor: A. Weaver)

- Topic: «Assimilation variationnelle océanique : modélisation multivariée de la matrice de covariance d'erreur d'ébauche.»
- Role: Thesis committee, contribution to PhD tutorship.
- Co-signed publications: 1

Clément de Boyer Montégut (Université Paris 6, 2003-2005, Advisor: G. Madec)

- Topic: «Couche mélangée océanique et bilan de chaleur et de sel dans le Nord de l'Océan Indien.»
- Role: Contribution to PhD tutorship.
- Co-signed publications during the PhD: 1 (+ 2 since)

Thomas Gorgues (Université Paris 6, 2003-2006, Advisor: Y. Dandonneau)

- Topic: «Modélisation biogéochimique du Pacifique tropical.»
- Role: Contribution to PhD tutorship.
- Co-signed publications: 1

Florian Sévellec (Université de Bretagne Occidentale, 2004-2007, Advisor: T. Huck)

- Topic: «Variabilité basse fréquence endogène et exogène de la circulation thermohaline.»
- Role: Contribution to PhD tutorship.
- Co-signed publications: 2

Anne-Charlotte Peter (Université Toulouse 3, 2005-2007, Advisor: Y. duPenhoat)

- Topic: «Variabilité de la température de la couche de mélange en Atlantique équatorial aux échelles saisonnières à interannuelles.»
- Role: Collaborative work on tropical Atlantic seasonal heat budget.
- Co-signed publications: 1

Laure Resplandy (Université Paris 6, 2006+, Advisor: M. Lévy)

- Topic: «Biogeochemical processes in the Arabian Sea»
- Role: Contribution to PhD tutorship.
- Co-signed publications: 1 publication currently in revision.

I. Suresh (Inde) (Indian Institute of Science, 2007+, Advisor: P.N. Vinayachandran)

- Topic: «Intraseasonal variability in the Arabian Sea»
- Role: Contribution to PhD tutorship.
- Co-signed publications: not yet.

Praveen Kumar (Inde) (Andhra University, 2008+, Advisor: V.S.N. Murty)

- Topic: «Intraseasonal to interannual heat budget of the tropical Indian Ocean»
- Role: Main PhD advisor.
- Co-signed publications: not yet.

Thesis committees:

Arthur Vidard (Université Joseph Fourier, Grenoble, Décembre 2001)

- Topic: «Vers une prise en compte de l'erreur modèle en assimilation 4D-Variationnelle - Application à un modèle réaliste d'océan »

Sophie Ricci (Université Paul Sabatier, Toulouse, Mars 2004)

- Topic: «Assimilation variationnelle océanique : modélisation multivariée de la matrice de covariance d'erreur d'ébauche.»

Hugo Bellenger (Ecole Polytechnique, Palaiseau, Mars 2007)

- Topic: «Rôle de l'interaction océan-atmosphère dans la variabilité intrasaisonnière de la convection tropicale.»

Masters training period that lead to publications:

Pierre Dutrieux (LOCEAN, 2002)

- Topic: «Lagrangian analysis of Atlantic ocean Tropical Instability Vortices»
- Co-signed publication: 1

Post-docs & other :

Fabien Durand

- Topic: «Barrier layer formation in the Southeastern Arabian Sea»
- Postdoc in NIO, Goa (2003)
- Co-signed publications during the postdoc: 1 (+ 1 since)

Retish Senan (Inde)

- Topic: «Intraseasonal to interannual variability of the tropical Indian Ocean»
- Postdoc (2004-2005)
- Co-signed publications: 1 (+ 1 in preparation)

Florian Sévellec

- Topic: «Generalised stability analysis of the tropical Pacific Ocean»
- Postdoc in the framework of the ENSEMBLES European project (2007)
- Co-signed publications: 2 (+ 1 in preparation)

Charles Deltel and then Bruno Luong

- Development of the altimetry assimilation into the OPAVAR system
- Engineers (CNES funding; May 2002-May 2004 and June 2004-May 2005)
- Delivered: the system is now able to assimilate altimeter observations.

A.3 Research projects / cruises

Research projects

Funded :

- ENACT (FP5 2002-2004) «Enhanced ocean data assimilation and climate prediction», co-I
- ENSEMBLES (FP6 2004-2009) «Ensemble seasonal to multi-decadal predictions», co-I
- Projet CNES «Climate variability and altimeter data : toward a global approach of seasonal-to-interannual climate predictability and ocean variability», financement d'un poste d'ingénieur sur 2002-2005.
- Co-I des projets PNEDC puis LEFE sur la variabilité de l'Océan Indien (LOTI, OCTAVIE) 2004-2008
- PI du projet TRIO soumis à LEFE (projet d'accompagnement de la campagne en mer TRIO)

Oceanographic cruises

Past:

- Valorisation de transit Cirene, Marion Dufresne, 10 jours en Octobre 2005, chef de mission.
- Campagne Cirene, Suroît, 44 jours en Janvier-Février 2007, chef de mission
- Valorisation de transit Cirene, Marion Dufresne, 12 jours en Août 2008 (remplacement d'un mouillage ATLAS du réseau RAMA), chef de projet

Future:

- Le projet TRIO de campagne dans l'Océan Indien en fin 2010 ou début 2011 a été positivement évalué par le comité inter-organismes LEFE. Le projet de campagne a été soumis à la commission flotte et est en cours d'évaluation.

A.4 Curriculum Vitæ

Jérôme VIALARD

Born the 04th of June, 1972 in Cahors (France), French nationality
Married with Marie-Luce Vernay (26th of May, 2007), one child (Capucine Vialard, born 6th December, 2008 in Assagao, Goa)

22, rue Nicolas Berthot, 21000 Dijon, France
Phone: +33 3 80 43 84 66
E-mail: jv@locean-ipsl.upmc.fr

Sagar Society plot 4, Dona Paula, Goa 403004, India
+91 96 57 89 73 31
vialardj@nio.org

Education

- 1997 PhD in Physical Oceanography
 LODYC, University of Paris VI, Paris
 Dissertation title: “Influence of salinity on ocean-atmosphere interactions in the Tropical Pacific Ocean”
- 1994 **M. Sc.** in physical oceanography and meteorology
 Engineer diploma from Ecole Nationale Supérieure de Technique Avancées (ENSTA)

Research experience

- 2002+ IRD scientist at LODYC (Laboratoire d’Océanographie Dynamique et de Climatologie, Paris)
 Research interests: Mechanisms and predictability of intraseasonal to interannual variability of the ocean-atmosphere system in the Indo-Pacific Region. Madden-Julian oscillation. Tropical instability waves. Ocean-atmosphere coupling at intraseasonal timescale in the Indian Ocean. Ocean data assimilation.
- 1999-2001 Scientist in charge of the oceanic data assimilation system at ECMWF, in the seasonal forecasting group
 Topic: Improve the quality of ocean re-analyses and the skill of seasonal forecasts.
- Nominated member of the CLIVAR Indian Ocean Panel since 2006.
- Reviewer for *Journal of Physical Oceanography*, *Journal of Atmospheric Sciences*, *Journal of Geophysical Research (Oceans)*, *Quarterly Journal of the Royal Meteorological Society*, *Journal of the Meteorological Society of Japan*, *Annales Geophysicae*, *Geophysical Research letters*, *Ocean Modelling*, *Current Science (Indian Academy of Sciences Bangalore)*

Publications (refereed papers)

A total of 40 accepted or published refereed papers. Visit <http://www.researcherid.com/rid/C-2809-2008> for citation metrics and h-index. A complete publication list is available earlier in this manuscript.

Appendix B. Selection of articles

The following selection of articles is representative of some of the studies I have undertaken since my PhD on the following subjects:

TIWs

Menkes, C., J. Vialard, S.C. Kennan, J-P. Boulanger, G. Madec and K. Rodgers, 2006, A modelling study of the three-dimensional heat budget of Tropical Instability Waves in the Equatorial Pacific, *Journal of Physical Oceanography*, **36**, 847–865.

El Niño

Vialard, J., C. Menkes, J-P. Boulanger, P. Delecluse, E. Guilyardi and M. McPhaden, 2001: A model study of the oceanic mechanisms affecting the equatorial SST during the 1997-98 El Niño. *Journal of Physical Oceanography*, **31**, 1649-1675.

Oceanic signature of the MJO

Vialard, J., S.S.C. Shenoi, J.P. McCreary, D. Shankar, F. Durand, V. Fernando and S.R. Shetye, 2009: Intraseasonal response of Northern Indian Ocean coastal waveguide to the Madden-Julian Oscillation, *Geophys. Res. Lett.*, **in revision**.

Vialard, J., G. Foltz, M. McPhaden, J-P. Duvel and C. de Boyer Montégut, 2008, Strong Indian Ocean sea surface temperature signals associated with the Madden-Julian Oscillation in late 2007 and early 2008, *Geophys. Res. Lett.*, **35**, L19608, doi:10.1029/2008GL035238.

Interannual variability in the Indian Ocean

Vialard, J., et al., 2009, Cirene: Air Sea Interactions in the Seychelles-Chagos thermocline ridge region, *Bull. Am. Met. Soc.*, **90**, 45-61.